NANOSCALE PATTERNING WITH DNA NANOSTRUCTURES

by

Hyojeong Kim

B.A. in Chemistry, Whitman College, 2011

Submitted to the Graduate Faculty of the

Kenneth P. Dietrich School of Arts and Sciences in partial fulfillment

of the requirements for the degree of

Doctor of Philosophy

University of Pittsburgh

2018

UNIVERSITY OF PITTSBURGH

KENNETH P. DIETRICH SCHOOL OF ARTS AND SCIENCES

This dissertation was presented

by

Hyojeong Kim

It was defended on

April 3rd, 2018

and approved by

Tara Meyer, Ph.D., Professor, Department of Chemistry

Geoffrey Hutchison, Ph.D., Associate Professor, Department of Chemistry

Lei Li, Ph.D., Associate Professor, Department of Chemical and Petroleum Engineering

Dissertation Advisor: Haitao Liu, Ph.D., Associate Professor, Department of Chemistry

Copyright © by Hyojeong Kim

2018

NANOSCALE PATTERNING WITH DNA NANOSTRUCTURES

Hyojeong Kim, PhD

University of Pittsburgh, 2018

Predictable and programmable Watson-Crick base pairing between DNA strands makes DNA not only a hereditary material, but also an ideal building block for designing nanometer-scale structures. Since Seeman opened the door to the era of DNA nanotechnology in 1982 by introducing the idea of utilizing DNA to build a mechanically robust four-arm junction structure to the scientific community, there has been an explosive growth in both structural DNA nanotechnology and DNA-based nanofabrication in the past few decades.

This dissertation focuses on the nanoscale patterning of soft and hard materials with DNA nanostructures. Chapter two specifically presents an advanced nanoimprint lithography method to construct polymer stamps with negative tone patterns using one- to three-dimensional DNA nanostructures to transfer patterns with high fidelity. The resulting polymer stamps further serve as molds to transfer the patterns to positive imprints on other polymer films. Chapter three presents a method to increase the stability of DNA nanostructure templates through conformal coating with a nanometer-thin protective inorganic oxide layer created using atomic layer deposition. Chapter four presents a new method of direct high contrast pattern transfer from DNA nanostructures to a silicon substrate by reactive ion etching with the help of calcium chloride. This study is the first report on high contrast pattern transfer from unmodified DNA nanostructures to silicon. We hope this dissertation could encourage future work to reveal the true power of DNA-based nanofabrication.

TABLE OF CONTENTS

1.0 INTRODUCTION 1

1.1 STATE-OF-THE-ART LITHOGRAPHIC TECHNOLOGY 1

1.2 DNA NANOTECHNOLOGY 6

1.2.1 DNA Nanostructures 9

1.2.2 Current Limitations on DNA Nanostructures 13

1.2.3 DNA Nanostructure based Nanofabrication 17

1.2.4 Nanoscale Patterning of Soft and Hard Materials with DNA Nanostructures 20

2.0 DNA NANOSTRUCTURE-MEDIATED MOLECULAR IMPRINTING LITHOGRAPHY 22

2.1 CHAPTER PREFACE 22

2.2 INTRODUCTION 23

2.3 EXPERIMENTAL SECTION 27

2.3.1 Materials 27

2.3.2 Preparation of a Silicon Wafer 28

2.3.3 Preparation of a PDMS Backing Film 28

2.3.4 DNA Nanostructures 29

2.3.5 Fabrication of a PMMA or PLLA Stamp by Replication over DNA Nanostructures 31
2.3.6 Fabrication of an a-PFPE Stamp by Replication over DNA Nanostructures 32
2.3.7 Replica Molding of Pattern on a PMMA or PLLA Stamp into an a-PFPE Stamp 32
2.3.8 Characterization 33
2.4 RESULTS AND DISCUSSION 34
2.4.1 General Fabrication Process of a Polymer Stamp using a DNA Nanostructure Master Template 34
2.4.2 Fabrication of a PMMA Stamp by Replication over DNA Nanostructures 35
2.4.3 Fabrication of a PLLA Stamp by Replication over DNA Nanostructures49
2.4.4 Yield of Replication Process and Stability of a DNA Nanostructure Master Template for Pattern Replication Process to a PMMA or PLLA Stamp 51
2.4.5 Fabrication of an a-PFPE Stamp by Replication over DNA Nanostructures 54
2.4.6 Long-term Stability of Nanoscale Features on a Polymer Stamp 57
2.4.7 Application of a Polymer Stamp to Replica Molding................................ 58
2.5 CONCLUSIONS 62
3.0 INCREASING THE STABILITY OF DNA NANOSTRUCTURE TEMPLATE BY ATOMIC LAYER DEPOSITION OF ALUMINIUM OXIDE AND ITS APPLICATION IN IMPRINTING LITHOGRAPHY 64

3.1 CHAPTER PREFACE ... **64**

3.2 INTRODUCTION ... **65**

3.3 EXPERIMENTAL SECTION ... **69**

3.3.1 Materials ... **69**

3.3.2 Preparation of a Silicon Wafer ... **70**

3.3.3 Preparation of a PDMS Backing Film ... **70**

3.3.4 Preparation and Deposition of DNA Nanostructures on a Silicon Wafer 71

3.3.5 Atomic Layer Deposition (ALD) of Al_2O_3 as a Protective Inorganic Film on a DNA Master Template ... **72**

3.3.6 Fabrication of a PLLA Stamp by Replication over DNA Nanostructures with a Protective Al_2O_3 Film ... **73**

3.3.7 UV/Ozone Treatment ... **73**

3.3.8 Characterization ... **74**

3.4 RESULTS AND DISCUSSION ... **75**

3.4.1 General Fabrication Process of a Polymer Stamp using a DNA Nanostructure Master Template with a Protective Al_2O_3 Film ... **75**

3.4.2 Fabrication of a PLLA Stamp by Replication over a DNA Nanotube Master Template with a 2 nm or 5 nm Al_2O_3 Film ... **76**

3.4.3 Fabrication of a PLLA Stamp by Replication over a DNA Origami Triangle Master Template with a 2 nm or 5 nm Al_2O_3 Film ... **91**

3.4.4 Investigation of Surface Morphology of a DNA Nanostructure Master Template with a 20 nm Al_2O_3 Film ... **98**

3.5 CONCLUSIONS ... **100**

4.0 CALCIUM INTERFERENCE IN REACTIVE ION ETCHING FOR NANOSCALE PATTERNING OF HIGH ASPECT RATIO 101
4.1 CHAPTER PREFACE 101
4.2 INTRODUCTION 102
4.3 EXPERIMENTAL 104
4.3.1 Materials 104
4.3.2 Preparation of a Silicon Wafer 104
4.3.3 Preparation and Deposition of DNA Nanotubes on a Silicon Wafer with an Additional Divalent Cation 105
4.3.4 Reactive Ion Etching (RIE) of a DNA Nanotube Substrate 106
4.3.5 UV/Ozone Treatment 106
4.3.6 Characterization 107
4.4 RESULTS AND DISCUSSION 108
4.4.1 General Preparation Process of a DNA Nanotube Substrate with an Additional Divalent Cation 108
4.4.2 Pattern Transfer from DNA Nanotubes to a Silicon Substrate with RIE 109
4.4.3 Removal of Polymer Residues on an Etched DNA Nanotube Substrate with UV/O_3 Treatment 113
4.4.4 Effect of Calcium Concentration on a DNA Nanotube Substrate 115
4.4.5 Effects of Calcium-Containing Crystals and Their Concentration on a Silicon Substrate without DNA Nanotubes 119
4.4.6 XPS Analysis of Calcium Coverage on a Silicon Substrate 123

4.4.7 Relationship between the Height of DNA Nanotubes to the Depth of Trenches **124**

4.4.8 Proposed Mechanism **125**

4.5 CONCLUSION **127**

5.0 CONCLUSION **128**

5.1 DNA NANOSTRUCTURES-MEDIATED MOLECULAR IMPRINTING LITHOGRAPHY **129**

5.2 INCREASING THE STABILITY OF DNA NANOSTRUCTURE TEMPLATES BY ATOMIC LAYER DEPOSITION OF AL_2O_3 AND ITS APPLICATION IN IMPRINTING LITHGRAPHY **130**

5.3 CALCIUM INTERFERENCE IN REACTIVE ION ETCHING FOR NANOSCALE PATTERNING OF HIGH ASPECT RATIO **132**

5.4 FINAL REMARKS **133**

APPENDIX **134**

BIBLIOGRAPHY **136**

LIST OF TABLES

Table 1. Statistical analysis of degrees of etching. Silicon wafers were incubated with 250 mM $CaCl_2$ and 10 × TAE/Mg^{2+} buffer solutions to which 62.5 mM, 125 mM, and 250 mM $CaCl_2$ solutions were added. The AFM images were classified as (a) completely etched (E), islands with flat top (I), moderately etched (M), and completely flat, unetched (F). 122

Table 2. XPS analysis of calcium and silicon coverage on a silicon substrate. Silicon wafers were incubated with 250 mM $CaCl_2$ and 10 × TAE/Mg^{2+} buffer solutions to which 62.5 mM, 125 mM, and 250 mM $CaCl_2$ solutions were added. The silicon wafers used for XPS analysis were different from the wafers used for statistical analysis of degrees of etching in Table 1............ 123

LIST OF FIGURES

Figure 1. Schematic representation of extreme ultraviolet lithography. Reprinted with permission from: reference 20 Copyright © 2010, Springer Nature. 5

Figure 2. DNA nanostructures. (a) Schematic representation of a four-arm branched DNA molecule with sticky end tails to form larger arrangements (left). AFM images of crystalline hexagonal DNA 2D array self-assembled from three-point-star motifs with sticky ends (middle, top) and its zoomed-in view (middle, bottom). Individual raw cryo-electron microscopic images and corresponding projections of 3D DNA dodecahedron structure reconstructed from the cryo-electron microscopic images (right). (b) AFM images of DNA origami shapes (left). AFM (top) and TEM (bottom) images of a nanoflask (middle). AFM image of origami checkerboard lattices on a single mica surface (right) (c) Complex shapes designed using a molecular canvas made of DNA single stranded tiles (left). Computer-generated models and TEM images of shapes made from a 3D molecular canvas made of DNA bricks (middle). One- and two-dimensional DNA crystals made of DNA bricks (right). Reprinted with permission from: reference 51 Copyright © 2010 Annual Reviews, Inc (a, left), reference 59 Copyright © 2005, American Chemical Society (a, middle), reference 65 Copyright © 2008, Springer Nature (a, right), reference 39 Copyright © 2006, Springer Nature (b, left), reference 43 Copyright © 2011, American Association for the Advancement of Science (b, middle), reference 71 Copyright © 2014, Springer Nature (b, right),

reference 44 Copyright © 2012, Springer Nature (c, left), reference 73 Copyright © 2012, American Association for the Advancement of Science (c, middle), reference 74 Copyright © 2014, Springer Nature (c, right). 8

Figure 3. Limited stability of DNA origami nanostructures under diverse environments. AFM height images of DNA origami triangles deposited on silicon wafers after (a) heated at 300 °C for 10 minutes, (b) 20 minutes of UV/O_3 treatment, and immersed in (c) hexane for 24 hours, (d) pH 1.88, (e) pH 12.00, and (f) 0.2 M NaCl solution for 10 seconds. Scale bars represent (a,d–f) 250 nm and (b,c) 50 nm. Reprinted with permission from: reference 76 Copyright © 2014, American Chemical Society. 15

Figure 4. Deterministic assembly of DNA nanostructures. AFM images of DNA origami nanostructures assembled (a) on *ca.* 110 nm patterned triangles on a diamond-like carbon/diamond-like carbon on silicon surface and (b) on patterned nitrogen-doped reduced graphene oxide film. Scale bars represent (a) 500 nm and (b) 2 µm. Reprinted with permission from: reference 78 Copyright © 2009, Springer Nature (a), reference 79 Copyright © 2012 WILEY-VCH Verlag GmbH & Co. KGaA, Weinheim (b)... 16

Figure 5. DNA Nanostructure based Nanofabrication. AFM images of (a) H-shaped Au nanoparticle assemblies on DNA origami rectangles on a mica, (b) continuous Au nanoparticle assemblies on T-shaped DNA origami on a SiO_2 wafer, (c) final etched graphene shapes after Au metallized DNA masks were removed, (d) triangular trenches produced upon the exposure of DNA origami triangles on a SiO_2 wafer to HF vapor under high-moisture condition, (e) carbonized DNA origami triangles, and (f) triangular trenches on a PMMA stamp. Reprinted with permission from: reference 94 Copyright © 2011, American Chemical Society (a), reference 96 Copyright © 2012, American Chemical Society (b), reference 97 Copyright ©

2013, Springer Nature (c), reference 102 Copyright © 2011, American Chemical Society (d), reference 105 Copyright © 2016, American Chemical Society (e), reference 106 Copyright © 2015, Springer Nature (f). 19

Figure 6. General fabrication process of a polymer stamp using a DNA nanostructure master template. (a) A silicon wafer. (b) DNA nanostructures are deposited on the silicon wafer. (c) A polymer film (*e.g.*, PMMA) is spin-coated onto the silicon wafer. (d) The surface perimeter of the polymer film (*ca.* 1 mm wide) is removed from the four edges of the film. (e) A PDMS backing stamp is adhered to the polymer film as a flexible support. (f) Droplets of water are added to one edge of the exposed silicon wafer and the PDMS/polymer film is peeled off. 35

Figure 7. Fabrication of a PMMA stamp by replication over DNA nanotubes. AFM height (left) and phase (right) images with corresponding cross-sectional analysis of (a,c) DNA nanotubes deposited on silicon wafers and (b,d) negative replicas of the DNA nanotubes on PMMA stamps. White lines on the AFM images indicate where the cross-sections were determined. Scale bars represent (a,b) 300 nm and (c,d) 3 μm. 36

Figure 8. Fabrication of a PMMA stamp by replication over 2D DNA brick crystals. (a) Scheme of 2D DNA brick crystal. The repeating units are represented as the blue and orange blocks. (b) Cross-sectional view of the scheme of 2D DNA brick crystal. (c) TEM image of 2D DNA brick crystal. AFM height (left) and phase (right) images with corresponding cross-sectional analysis of (d,f) 2D DNA brick crystals deposited on silicon wafers and (e,g) negative replicas of the 2D DNA brick crystals on PMMA stamps. White lines on the AFM images indicate where the cross-sections were determined. Scale bars represent (c) 500 nm and (d–g) 300 nm. 38

Figure 9. Fabrication of a PMMA stamp by replication over hexagonal DNA 2D arrays. (a) Scheme of hexagonal DNA 2D array assembled from 3-point-star motifs. (b) AFM height (left)

and phase (right) images with corresponding cross-sectional analysis of DNA 2D arrays assembled on a silicon wafer. (c) Zoomed-in view of the area in the white dashed box in image b. The inset is the Fourier transform of image c. (d) AFM height (left) and phase (right) images with corresponding cross-sectional analysis of negative replicas of the arrays on a PMMA stamp. (e) Zoomed-in view of the area in the white dashed box in image d. The inset is the Fourier transform of image e. White arrows indicate the replicated patterns on the PMMA stamp. White lines on the AFM images indicate where the cross-sections were determined. Scale bars represent (b,d) 400 nm and (c,e) 50 nm. 41

Figure 10. Fabrication of a PMMA stamp by replication over λ-DNAs. AFM height (left) and phase (right) images with corresponding cross-sectional analysis of (a,c) λ-DNAs deposited on silicon wafers and (b,d) negative replicas of the λ-DNAs on PMMA stamps. White lines on the AFM images indicate where the cross-sections were determined. Scale bars represent 200 nm. 43

Figure 11. Fabrication of a PMMA stamp by replication over DNA origami triangles. (a) Folding path of DNA scaffold strand in DNA origami triangle. Red lines represent staple strands bridging trapezoidal sides. Reprinted with permission from: reference 39 Copyright © 2006, Springer Nature. AFM height (left) and phase (right) images with corresponding cross-sectional analysis of (b) DNA origami triangles deposited on a silicon wafer and (c) negative replicas of the DNA origami triangles on a PMMA stamp. Zoomed-in images are to the left of the corresponding images. White lines on the AFM images indicate where the cross-sections were determined. Scale bars represent (zoomed-in images) 50 nm and (zoomed-out images) 200 nm. 45

Figure 12. Analysis of dangling loops of a DNA origami triangle master template and a PMMA stamp. AFM height images of (a) DNA origami triangles deposited on a silicon wafer and (b) negative replicas of the DNA origami triangles on a PMMA stamp. The dangling loops of the

DNA triangles and the corresponding patterns of the triangular trenches are indicated by the red arrows. Scale bars represent 200 nm.. 46

Figure 13. Analysis of vertices of triangular trenches on a PMMA stamp. (a–c) AFM height images with corresponding cross-sectional analysis of negative replicas of DNA origami triangles on a PMMA stamp. White lines on the AFM images indicate where the cross-sections were determined. Red cursors in the AFM images and corresponding cross-sections define the outer sides of the vertices that are measured. Dashed green circles (middle) highlight the curve valleys that correspond to the trenches at the vertices. In images a and b, the bump appears in the zoomed-in curve valley of the cross-section (bottom), confirming the presence of the bump at the vertex. In image c, the bump does not appear at the curve valley, indicating that no bump exists in the vertex. Scale bars represent 200 nm. Note: Images a–c are identical................................ 48

Figure 14. Fabrication of a PLLA stamp by replication over DNA nanotubes. AFM height (left) and phase (right) images with corresponding cross-sectional analysis of (a) DNA nanotubes deposited on a silicon wafer and (b) negative replicas of the DNA nanotubes on a PLLA stamp. White lines on the AFM images indicate where the cross-sections were determined. Scale bars represent 300 nm.. 49

Figure 15. Fabrication of a PLLA stamp by replication over DNA origami triangles. AFM height (left) and phase (right) images with corresponding cross-sectional analysis of (a) DNA origami triangles deposited on a silicon wafer and (b) negative replicas of the DNA origami triangles on a PLLA stamp. White lines on the AFM images indicate where the cross-sections were determined. Scale bars represent 150 nm. 50

Figure 16. Analysis of dangling loops of a DNA origami triangle master template and a PLLA stamp. AFM height images of (a) DNA origami triangles deposited on a silicon wafer and (b)

negative replicas of the DNA origami triangles on a PLLA stamp. The dangling loops of the DNA triangles and the corresponding patterns of the triangular trenches are indicated by the red arrows. Scale bars represent 200 nm.. 50

Figure 17. Yield of replication process and stability of a DNA nanotube master template after pattern replication process to a PMMA stamp. AFM height (top and bottom) and phase images (middle) with corresponding cross-sectional analysis of DNA nanotubes deposited on silicon wafers before (left) and after (middle) replication to PMMA stamps, and PMMA replicas (right) of the same area. White lines on the AFM images indicate where the cross-sections were determined. Scale bars represent 300 nm. Note: The images of the PMMA stamps were flipped horizontally to match the orientation of those of the DNA master templates. 53

Figure 18. Stability of a DNA nanotube master template after pattern replication process to a PMMA stamp. AFM height images with corresponding cross-sectional analysis of DNA nanotubes on a silicon wafer in the same location (a) before and (b) after replication to a PMMA stamp. White lines on the AFM images indicate where the cross-sections were determined. Scale bars represent 300 nm. Compared to the results shown in Figure 12, this experiment used less water and decreased the incubation time (*i.e.*, the time between adding water to the master template and peeling off the polymer stamp). 54

Figure 19. Fabrication of an a-PFPE stamp by replication over DNA nanotubes. AFM height images with corresponding cross-sectional analysis of DNA nanotubes deposited on a silicon wafer (a) before and (b) after replication to an a-PFPE stamp, and (c) negative replicas of the DNA nanotubes on the a-PFPE stamp of the same area. White lines on the AFM images indicate where the cross-sections were determined. Scale bars represent 300 nm. Note: Image c is flipped horizontally to match the orientation of those of the DNA master template. 55

Figure 20. Stability of a DNA nanotube master template for multiple pattern replication process to a-PFPE stamps. AFM height images with corresponding cross-sectional analysis of DNA nanotubes in three different locations before (left) and after 5th (middle) and 10th (right) pattern transfer to a-PFPE stamps of the same area. White lines on the AFM images indicate where the cross-sections were determined. Scale bars represent (a–f) 300 nm and (g–i) 1.5 µm. 56

Figure 21. Long-term stability of nanoscale features on a polymer stamp. AFM height (left) and phase (right) images with corresponding cross-sectional analysis of a PMMA stamp (a) immediately after being peeled off and (b) after 10 days of aging in the air. White lines on the AFM images indicate where the cross-sections were determined. Scale bars represent 500 nm. 57

Figure 22. Application of a PMMA stamp to replica molding. AFM height images with corresponding cross-sectional analysis of (a) DNA nanotubes on a silicon wafer, (b) negative replicas of the DNA nanotubes on a PMMA stamp, and (c) positive replicas of the DNA nanotubes on an a-PFPE substrate transferred from the PMMA stamp by replica molding. White lines on the AFM images indicate where the cross-sections were determined. Scale bars represent 300 nm. Note: Images a and b are also shown in Figure 7. 59

Figure 23. Application of a PLLA stamp to replica molding. AFM height images with corresponding cross-sectional analysis of (a) DNA nanotubes on a silicon wafer, (b) negative replicas of the DNA nanotubes on a PLLA stamp, and (c) positive replicas of the DNA nanotubes on an a-PFPE substrate transferred from the PLLA stamp by replica molding. White lines on the AFM images indicate where the cross-sections were determined. Scale bars represent 300 nm. 60

Figure 24. Stability of nanoscale features on PMMA and PLLA stamps during replica molding. AFM height (left) and phase (right) images with corresponding cross-sectional analysis of (a)

PMMA and (b) PLLA stamps after transfer of pattern to a-PFPE. White lines on the AFM images indicate where the cross-sections were determined. Scale bars represent 300 nm........... 61

Figure 25. General fabrication process of a polymer stamp using a DNA nanostructure master template with a protective Al_2O_3 film. (a) DNA nanostructures are deposited on a silicon wafer. (b) The silicon wafer is coated with Al_2O_3 by atomic layer deposition. (c) A polymer film (*e.g.*, PLLA) is spin-coated onto the silicon wafer. (d) The four edges of the polymer film (*ca.* 1 mm wide) are scraped off with a blade. (e) A PDMS layer is adhered to the polymer film as a backing support. (f) Droplets of water are added to the exposed edges of the silicon wafer and the PDMS/PLLA film is peeled off. 76

Figure 26. Fabrication of a PLLA Stamp by replication over a DNA nanotube master template with a 2 nm Al_2O_3 film and long-term stability of nanoscale features on a polymer stamp. AFM height images with corresponding cross-sectional analysis of DNA nanotubes after (a) deposited on a silicon wafer and (b) 20 cycles of ALD of Al_2O_3, and negative replicas of the DNA nanotubes on a PLLA stamp imaged (c) 1, (d) 8, and (e) 15 days after pattern transfer of the same area. White lines on the AFM images indicate where the cross-sections were determined. (f) Height/depth and (g) FWHM of the DNA nanotubes and their replica trenches in four different locations of the images from a to e. Locations 1, 2, 3, and 4 correspond to 1, 2, 3, and 4 in the cross-sections of images a and c. Scale bars represent 500 nm. Note: The images from c to e are diagonally flipped to match the orientations of images a and b. 78

Figure 27. Stability of a DNA nanotube master template without a protective inorganic oxide film during multiple pattern replication processes using 1 × TAE/Mg^{2+} buffer. AFM height images of DNA nanotubes in the same location of a silicon wafer (a) before and after (b) 1st, (c) 2nd, and (d) 3rd pattern transfer to PLLA stamps using 1 × TAE/Mg^{2+} buffer. The bottom row

contains the zoomed-in views of the areas in the yellow dashed boxes in the top row. Scale bars represent (top row) 3 μm and (bottom row) 500 nm. 80

Figure 28. Stability of a DNA nanotube master template with a 2 nm Al_2O_3 film for multiple pattern replication processes to polymer stamps and removal of polymer residues with UV/O_3 treatment. AFM height images with corresponding cross-sectional analysis of DNA nanotubes in the same location after (a) deposited on a silicon wafer, (b) 20 cycles of ALD of Al_2O_3, (c) 1st, (d) 2nd, (e) 3rd, (f) 4th, and (g) 5th pattern transfer to PLLA stamps, and (h) UV/O_3 treatment for 1 h and washing with deionized water. White lines on the AFM images indicate where the cross-sections were determined. (i) Histograms of the AFM height images from a to h. (j) Height and (k) FWHM of the DNA nanotubes in three different locations of the images from a to h. Locations 1, 2, and 3 correspond to 1, 2, and 3 in the cross-section of image a. Scale bars represent 500 nm. Note: The DNA master template was contaminated before the 5th spin coating of PLLA in dichloromethane solution. Images a and b are also shown in Figure 26. 81

Figure 29. Stability of a DNA nanotube master template with a 2 nm Al_2O_3 film for multiple pattern replication process to polymer stamps over an area of 30×30 μm^2 and removal of polymer residues with UV/O_3 treatment. AFM height images of DNA nanotubes in the same location of a silicon wafer after (a) 20 cycles of ALD of Al_2O_3, (b) 1st, (c) 2nd, (d) 3rd, (e) 4th, and (f) 5th pattern transfer to PLLA stamps, and (g) UV/O_3 treatment for 1 h and washing with deionized water. Holes formed by the breakage of the Al_2O_3 film are indicated by the yellow arrows. AFM (h) height and (i) phase images with corresponding cross-sectional analysis of the area in the yellow dashed box in image g. White lines on the AFM images indicate where the cross-sections were determined. Scale bars represent (a–g) 4 μm and (h,i) 1 μm. Note: The DNA

master template was contaminated before the 5th spin coating of PLLA in dichloromethane solution.. 83

Figure 30. Long-term stability of a DNA nanotube master template with a 2 nm Al_2O_3 film. AFM height images with corresponding cross-sectional analysis of DNA nanotubes in the same location of a silicon wafer at the (a) beginning and the (b) end of 40 day period. White lines on the AFM images indicate where the cross-sections were determined. (c) Height and (d) FWHM of the DNA nanotubes in four different locations of images a and b. Locations 1, 2, 3, and 4 correspond to 1, 2, 3, and 4 in the cross-section of image a. Scale bars represent 500 nm.......... 86

Figure 31. Stability of a DNA nanotube master template with a 5 nm Al_2O_3 film for multiple pattern replication process to polymer stamps and removal of polymer residues with UV/O_3 treatment. AFM height images with corresponding cross-sectional analysis of DNA nanotubes in the same location after (a) deposited on a silicon wafer, (b) 50 cycles of ALD of Al_2O_3, (c) 1st and (d) 5th pattern transfer to PLLA stamps, and (e) UV/O_3 treatment for 1 h and washing with deionized water. White lines on the AFM images indicate where the cross-sections were determined. (f) Histograms of the AFM height images from a to e. (g) Height and (h) FWHM of the DNA nanotubes in four different locations of the images from a to e. Locations 1, 2, 3, and 4 correspond to 1, 2, 3, and 4 in the cross-section of image a. Scale bars represent 500 nm.......... 89

Figure 32. Stability of a DNA nanotube master template with a 5 nm Al_2O_3 film for multiple pattern replication process to polymer stamps over an area of 30×30 μm^2 and removal of polymer residues with UV/O_3 treatment. AFM height images of DNA nanotubes in the same location of a silicon wafer after (a) 50 cycles of ALD of Al_2O_3 and (b) 1st and (c) 5th pattern transfer to PLLA stamps. Scale bars represent 4 μm.. 90

Figure 33. Comparison of the height differences between the maximum peaks of the histograms in Figures 28i and 31f. 91

Figure 34. Fabrication of a PLLA Stamp by replication over a DNA origami triangle master templates with 2 nm and 5 nm Al_2O_3 films. AFM height images with corresponding cross-sectional analysis of DNA origami triangles after (a) deposited on silicon wafers, (b) 20 cycles (top) or 50 cycles (bottom) of ALD of Al_2O_3, and (d) pattern transfer to PLLA stamps, and (c) negative replicas of the DNA origami triangles on the PLLA stamps. White lines on the AFM images indicate where the cross-sections were determined. Scale bars represent 200 nm........... 93

Figure 35. Analysis of dangling loops and vertices of a DNA origami triangle master template with a 2 nm Al_2O_3 film and a PLLA stamp. AFM height images with corresponding cross-sectional analysis of (a) DNA origami triangles deposited on a silica wafer after 20 cycles of ALD of Al_2O_3 and (b,c) negative replicas of the DNA origami triangles on a PLLA stamp. White lines on the AFM images indicate where the cross-sections were determined. The dangling loops are indicated by the yellow arrows. Red cursors in the AFM images and corresponding cross-sections define the outer sides of the vertices that are measured. In image b, the bump appears in the zoomed-in curve valley of the cross-section (bottom), confirming the presence of the bump at the vertex. In image c, the bump does not appear at the curve valley, indicating that no bump exists in the vertex. Zoomed-in AFM images of (d) DNA origami triangles and (e) their negative replicas. The dangling loops and vertices with the holes/bumps are indicated by the yellow arrows and blue dots, respectively. Scale bars represent (a–c) 200 nm and (d,e) 100 nm. Note: Images b and c are identical. Image b is rotated 90° clockwise to match the orientation of its corresponding cross-section. The images from a to c are also shown in Figure 34. 94

Figure 36. Analysis of dangling loops and vertices of a DNA origami triangle master template with a 5 nm Al_2O_3 film and a PLLA stamp. AFM height images with corresponding cross-sectional analysis of (a) DNA origami triangles deposited on a silica wafer after 50 cycles of ALD of Al_2O_3 and (b,c) negative replicas of the DNA origami triangles on a PLLA stamp. White lines on the AFM images indicate where the cross-sections were determined. The dangling loops are indicated by the yellow arrows. Red cursors in the AFM images and corresponding cross-sections define the outer sides of the vertices that are measured. In image b, the bump appears in the zoomed-in curve valley of the cross-section (bottom), confirming the presence of the bump at the vertex. In image c, the bump does not appear at the curve valley, indicating that no bump exists in the vertex. Zoomed-in AFM images of (d) DNA origami triangles and (e) their negative replicas. The dangling loops and vertices with the holes/bumps are indicated by the yellow arrows and blue dots, respectively. Scale bars represent (a–c) 200 nm and (d,e) 100 nm. Note: Images b and c are identical. Image b is rotated 90° clockwise to match the orientation of its corresponding cross-section. Images b and c are also shown in Figure 34. 95

Figure 37. Yield of shape conservation process of a DNA origami triangle master template by ALD and pattern replication process to a PLLA stamp. Average (a) height, (b) FWHM, (c) inner length, and (d) outer length (n = 10) of features on DNA origami triangle master templates with 2 nm and 5 nm Al_2O_3 layers and PLLA stamps at each step of fabrication process, after (DNA) DNA origami triangles were deposited on silicon wafers, (ALD) ALD of Al_2O_3, and (After) pattern transfer to PLLA stamps, and (PLLA) their negative replicas on the PLLA stamps. 96

Figure 38. Investigation of surface morphology of a DNA nanostructure master template with a 20 nm Al_2O_3 Film. AFM height images with corresponding cross-sectional analysis of DNA (a,b) nanotubes and (c,d) origami triangles deposited on silica wafers (a,c) before and (b,d) after

200 cycles of ALD of Al_2O_3. White lines on the AFM images indicate where the cross-sections were determined. (e) Height and (f) FWHM of the DNA nanotubes in four different locations of the images from a to b. Locations 1, 2, 3, and 4 correspond to 1, 2, 3, and 4 in the cross-section of image a. Scale bars represent (a,b) 500 nm and (c,d) 200 nm. 99

Figure 39. General preparation process of a DNA nanotube substrate with an additional divalent cation. 109

Figure 40. Pattern transfer from DNA nanotubes to a silicon wafer with RIE. AFM height images in the same location of DNA nanotubes deposited on a silicon wafer before (top) and replicas of the DNA nanotubes on the silicon wafer after (bottom) RIE. To DNA nanotube solutions, (a) deionized water, and 125 mM (b) $CaCl_2$, (c) $CoCl_2$, and (d) $CdCl_2$ aqueous solutions were added. Scale bars represent (a,c,d) 500 nm and (b) 3 μm. 110

Figure 41. Intrinsic surface characteristic of a silicon wafer with RIE. AFM height images of a silicon wafer with a native oxide layer cleaned with piranha solution before (left) and after (right) RIE. Scale bars represent 500 nm. 111

Figure 42. Negative tone pattern transfer from DNA nanotubes with addition of $CaCl_2$ to a silicon wafer with RIE. AFM height images with corresponding cross-sectional analysis in the same location of (a) DNA nanotubes deposited on a silicon wafer with 125 mM $CaCl_2$ and (b) negative replicas of the DNA nanotubes on the silicon wafer after RIE, UV/O_3 treatment for 1 h, and washing with deionized water. Red lines on the AFM images indicate where the cross-sections were determined. Scale bars represent 3 μm. The left (top) image is also shown in Figure 40. 112

Figure 43. Removal of polymer residues on an etched DNA nanotube substrate with UV/O_3 treatment. (a) AFM height images with corresponding cross-sectional analysis in the same

location of negative replicas of DNA nanotubes before (left) and after (right) UV/O_3 treatment for 1 h and washing with deionized water. AFM height images with corresponding cross-sectional analysis in the same location of the areas in the (b) blue and (c) yellow dashed boxes in image a. Red lines on the AFM images indicate where the cross-sections were determined. Locations 1 and 2 correspond to 1 and 2 in the cross-sections of image b. Scale bars represent (a) 3 μm and (b,c) 500 nm. Image a (right, lower) is also shown in Figure 42............................... 114

Figure 44. Effect of calcium concentration on a DNA nanotube substrate. AFM height images with corresponding cross-sectional analysis in the same location of silicon wafers after DNA nanotubes were deposited (top), RIE (middle), and UV/O_3 treatment for 1 h and washing with deionized water (bottom). To the DNA nanotubes in 10 × TAE/Mg^{2+} buffer solutions, (a) 62.5 mM, (b) 125 mM, and (c) 250 mM $CaCl_2$ solutions were added. The bottom row contains the zoomed-in views of the areas in the blue dashed boxes in the middle row. Red lines on the AFM images indicate where the cross-sections were determined. Scale bars represent 3 μm (top, middle) and 500 nm (bottom). 117

Figure 45. Direct comparison of a DNA nanotube substrate with 125 mM $CaCl_2$ before and after RIE and UV/O_3 treatment at the same location. AFM height images with corresponding cross-sectional analysis of a silicon wafer with DNA nanotubes (a) before and (b) after RIE, UV/O_3 treatment for 1 h, and washing with deionized water. To the DNA nanotubes in 10 × TAE/Mg^{2+} buffer solutions, 125 mM $CaCl_2$ solution was added. Red lines on the AFM images indicate where the cross-sections were determined. Scale bars represent 3 μm. 118

Figure 46. Surface analysis of a DNA nanotube substrate after RIE and UV/O_3 treatment. Photo image of DNA nanotube substrates after RIE and UV/O_3 treatment. To the DNA nanotubes in 10 × TAE/Mg^{2+} buffer solutions, (a) 62.5 mM, (b) 125 mM, and (c) 250 mM $CaCl_2$ solutions were

added. Silicon wafers had an area of $1 \times 1\ cm^2$. "<'" marks on the substrates were drawn with a diamond pen for AFM imaging at the same location. 118

Figure 47. Representative images of degrees of etching. AFM height images with corresponding cross-sectional analysis of silicon wafers without DNA nanotubes after RIE, UV/O_3 treatment for 1 h, and washing with deionized water. The wafers were incubated with (a) 250 mM $CaCl_2$ and $10 \times$ TAE/Mg^{2+} buffer solutions to which (b) 62.5 mM, (c) 125 mM, and (d) 250 mM $CaCl_2$ solutions were added. The AFM images were classified as (a) completely etched (E), (b) islands with flat top (I), (c) moderately etched (M), and (d) completely flat, unetched (F). Red lines on the AFM images indicate where the cross-sections were determined. Scale bars represent 3 µm. 121

Figure 48. Analysis of a silicon substrate incubated with 250 mM $CaCl_2$ after RIE and UV/O_3 treatment. (a) Optical microscopic and (b) AFM height images with corresponding cross-sectional analysis of a silicon wafer incubated only with 250 mM $CaCl_2$ after RIE, UV/O_3 treatment for 1 h, and washing with deionized water. The optical image was taken while the AFM image was taken. The inset in image a is the photo image of the wafer. The silicon wafer had an area of $1 \times 1\ cm^2$. White dashed box approximates the location of the optical microscopic and AFM images. The yellow arrow points toward the center of mark of the evaporation while the blue arrow points toward the center of the wafer. Red lines on the AFM images indicate where the cross-sections were determined. Scale bars represent 3 µm. 122

Figure 49. XPS analysis of calcium coverage on a silicon substrate. Out of five XPS measurements for each sample, that which had the highest calcium coverage was chosen. 124

Figure 50. Relationship between height of DNA nanotubes to depth of trenches. AFM height images with corresponding cross-sectional analysis of (a) single/low and (b) multiple/high DNA

nanotubes on a silicon wafer before (left) and after (right) RIE, UV/O_3 treatment for 1 h, and washing with deionized water. To the DNA nanotubes in 10 × TAE/Mg^{2+} buffer solutions, 125 mM $CaCl_2$ solutions were added. Red lines on the AFM images indicate where the cross-sections were determined. Scale bars represent 500 nm. 125

Figure 51. Proposed mechanism of negative tone pattern transfer from DNA nanostructures to a silicon wafer with protected surrounding surface. (a) The calcium-containing precipitates cover the surface of a DNA nanotube substrate. (b) The area of the silicon wafer underneath the DNA nanotubes is etched away while the surrounding silicon wafer is minimally influenced from plasma. 126

LIST OF EQUATIONS

Equation 1. Critical dimension 1

Equation 2. Depth of focus 1

Equation 3. Numerical aperture 2

1.0 INTRODUCTION

1.1 STATE-OF-THE-ART LITHOGRAPHIC TECHNOLOGY

The desire for smaller and faster electronic devices has been a primary driving force for shrinking the pattern size of an integrated circuit. Since Moore, the cofounder of Intel Corporation, predicted in 1965 that the number of transistors in an integrated circuit would double approximately every 24 months,[1] the size of features in a chip has been reduced to nanometer scale during the past half century.[2] Currently, photolithography and its derivatives are state-of-the-art technologies employed in the semiconductor chip manufacturing industries.[3]

Photolithography transfers patterns from a photomask to a photo-reactive photoresist layer, then to a semiconductor substrate. The sharpness of a projected image onto the substrate is governed by two factors: the critical dimension (CD), also called the smallest feature size or the resolution, and the depth of focus (DOF) of the pattern on the substrate, both of which are determined by the following equations:

$$CD = k_1 \bullet \lambda/NA$$

Equation 1. Critical dimension

$$DOF = k_2 \bullet \lambda/(NA)^2$$

Equation 2. Depth of focus

where k_1 and k_2 are the process related coefficients, λ is the wavelength of the imaging light and NA is the numerical aperture of the projection lens.

Between decreasing the wavelength and increasing the numerical aperture for smaller feature size, it is more beneficial to reduce the wavelength of the light because it minimizes the depth of focus less according to Equations 1 and 2.[4] While the critical dimension is preferred to be a smaller value, the depth of focus is limited in that it should be greater than the roughness of the photo-reactive photoresist layer. During the early stages of the chip fabrication industry, a mercury arc lamp was the dominant source of light. The wavelength utilized in photolithography progressed from 436 nm ("G-line") to 365 nm ("I-line") of the spectral lines of the mercury arc lamp. Excimer laser lithography was first demonstrated by Jain *et al.* in 1982 and used a KrF laser to access the deep ultraviolet region. Consequently, the excimer laser came to replace the mercury lamp. The wavelength of the excimer laser shifted from 248 nm for a KrF laser to 193 nm for an ArF laser. The ArF laser has become a primary light source in deep ultraviolet lithography (DUV) and has been used in the current state-of-the-art integrated circuit manufacturing. Intel started the mass production of 45 nm chips in late 2007, using DUV with a double patterning method and a 193 nm ArF laser source.[5]

Immersion lithography (IL) can be used to further reduce the feature size below 45 nm by increasing the numerical aperture value. IL is a derivative of DUV where the space between the last lens and the photoresist layer on the substrate in DUV is filled with a liquid whose refractive index is greater than that of air. Compared to DUV, IL increases the numerical aperture according to the following equation:

$$NA = n \cdot \sin\theta$$

Equation 3. Numerical aperture

where n is the refractive index of the liquid and θ is the angle of incidence or refraction. Both the critical dimension and the depth of focus in IL are reduced.

In 2013, Intel successfully built a laptop equipped with a 14 nm codenamed Broadwell processor utilizing IL with an ArF laser source at 193 nm wavelength and a multiple patterning technique.[6] As technology progressed from a 22 nm Haswell chip to a 14 nm Broadwell chip, the power consumption was reduced to 70%.[7, 8] In addition, the size of the chip significantly decreased to be installed in a tablet PC and the performance of a graphic processing unit increased up to 60%. Intel is now in the large volume production of the 14 nm transistor, with semiconductor fabrication plants currently located in Oregon, Arizona, and Ireland.[9]

While IL with water immersion and multi-patterning techniques has been the current state-of-the-art 10 nm technology, it is not suitable for reducing the critical dimension below 10 nm due to the higher cost and lower throughput from process complexity of the multi-patterning procedure.[10-11] For the shrinkage of the feature size below 10 nm within the near future, electron-beam lithography (EBL) and extreme ultraviolet lithography (EUV) have become next-generation lithography techniques. While EUV uses a 13.5 nm ultraviolet wavelength from laser-pulsed Sn plasma, reflected from a mask into a resist layer (Figure 1), EBL directly draws a pattern onto a resist layer using an electron beam without passing through any masks.[12] Although EBL achieved arbitrary patterning at the 1 nm length scale,[13-14] it is yet to replace IL due to EBL's extensive writing times for large and complex patterns.[15] To reach the sub-10 nm regime, Samsung recently demonstrated the use of EUV with complementary metal–oxide–semiconductor fin field effect transistor technology to fabricate a 7 nm node.[16] Integrated circuit manufacturers have waited to utilize EUV for the mass production of integrated chips because it is expected to reduce the production cost by removing the complex multiple patterning steps of IL.[7,17-18] EUV, however, is difficult to commercialize for mass production, which would make it hard for this method to replace the IL method already in use. The commercialization of EUV is

limited by many factors, some of which include the source power, the maintenance of vacuum condition, the aggregation of polymer resist, and the proximity effect of secondary electrons.[19-20] These problems ultimately contribute to low throughput. Furthermore, the cost to build a new fabrication plant is extremely capital intensive. Intel is investing 7 billion dollars to construct a new plant in Arizona to process future 7 nm products.[21]

Moreover, a wide variety of methods have been developed to offer nanoscale even with sub-10-nm features. These methods include, but are not limited to: dip-pen nanolithography,[22] indentation lithography,[23] nanosphere lithography,[24] block copolymer lithography,[25-28] and chemical lift-off lithography.[29-31] Soft lithography techniques were further employed to offer features with sub-nanometer or molecular-scale resolution by utilizing other relief structures such as crystallographic steps and cracks[32-33] and single-walled carbon nanotubes.[34-36] However, the patterns were restricted to simple linear or basic geometric shapes sometimes with a height/depth of a monolayer of molecules. Overall, there has been a high demand for an alternative patterning method which satisfies high throughput and low cost with diverse nanoscale features and high spatial resolution.

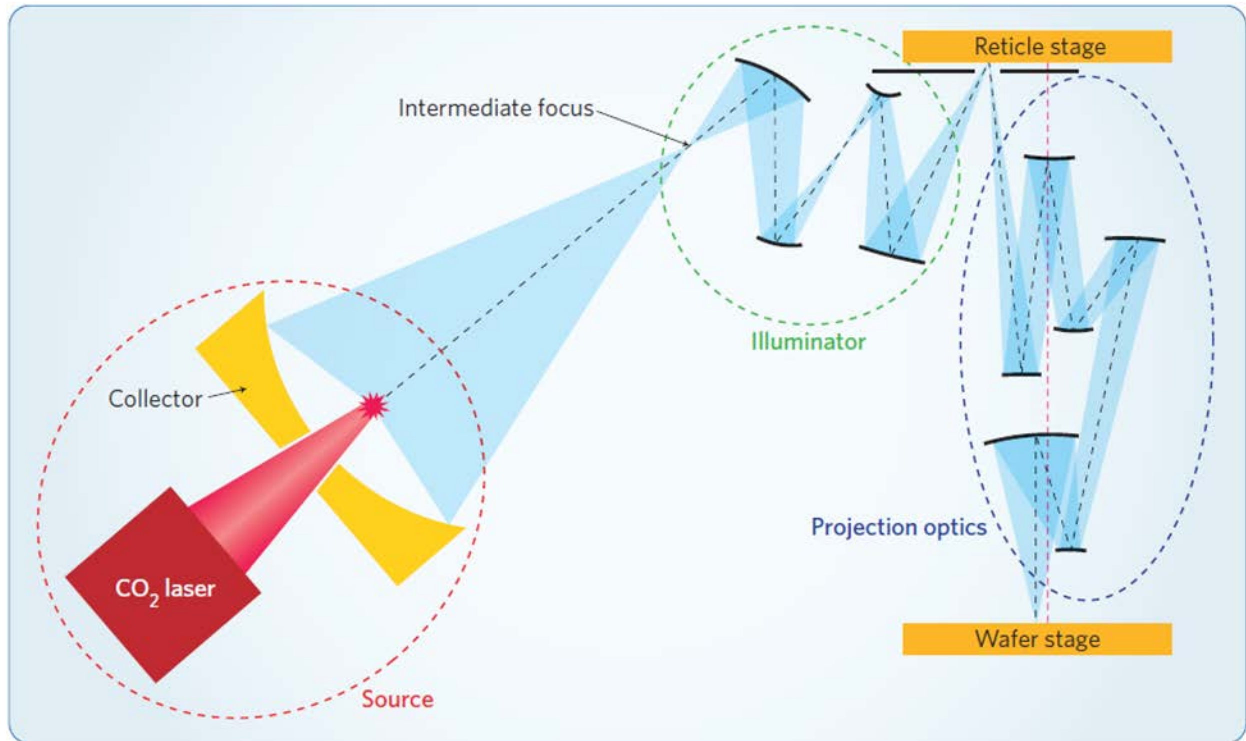

Figure 1. Schematic representation of extreme ultraviolet lithography. Reprinted with permission from: reference 20 Copyright © 2010, Springer Nature.

1.2 DNA NANOTECHNOLOGY

DNA, an abbreviation for deoxyribonucleic acid, is a molecule selected by nature to convey genetic information in all living organisms with RNA, an abbreviation for ribonucleic acid. DNA is a polymer and its monomer is a nucleotide which consists of a base, a sugar, and a negatively charged phosphate group.[37] The alternating sugar and phosphate groups form the backbone of DNA. The base is connected to the sugar and there are four types of bases; adenine (A), cytosine (C), guanine (G), and thymine (T). These bases are classified either purines (A and G) or pyrimidines (C and T) and what makes DNA special is Watson-Crick base pairing between them: One particular type of purines binds to one particular type of pyrimidines such that adenine always pairs with thymine and guanine always pairs with cytosine by hydrogen bonding. Watson-Crick base pairing allows the hybridization of DNA to be precise and predictable.

The programmable self-assembled nature of DNA strands makes DNA not only a hereditary material, but also an ideal molecule for designing nanometer-scale structures.[38] A DNA helix has a diameter of 2 nm, and turns a full circle every 10 base pairs with a linear length of 3.5 nm. Combined with its precise and predictable molecular recognition through Watson-Crick base pairing, DNA can provide enormous variability for fabricating arbitrarily-shaped multi-dimensional DNA nanostructures with a theoretical resolution of 2 – 3 nm.[39-44] Compared to other self-assembled structures, for example, made by peptide/protein assemblies[45-46] and block copolymers,[47-48] this degree of control over shape and size is unprecedented. Also, the fast growth of biomedical research lowers the current market price of custom synthetic oligonucleotides down to \$ 17.5 per base per 10 μmol.[49] With this commercial price, it costs less than \$ 6 to cover an area of 1 m^2 of a substrate with a monolayer of DNA. Given these advantages in precision and cost, DNA nanostructures have received attention as a patterning

template for ultra-high resolution to replace the expensive current state-of-the-art photolithography. Since Seeman pioneered the idea of utilizing a sequence of DNA to build mechanically robust nanostructures in 1982,[50] the field of structural DNA nanotechnology has evolved remarkably from immobile Holliday junctions to complex shapes fabricated from 'single-stranded tiles' in the past 30 years.[51-52] The fabrication of DNA nanostructures with their properties and applications has become an important research area, and are briefly reviewed in the following sections.

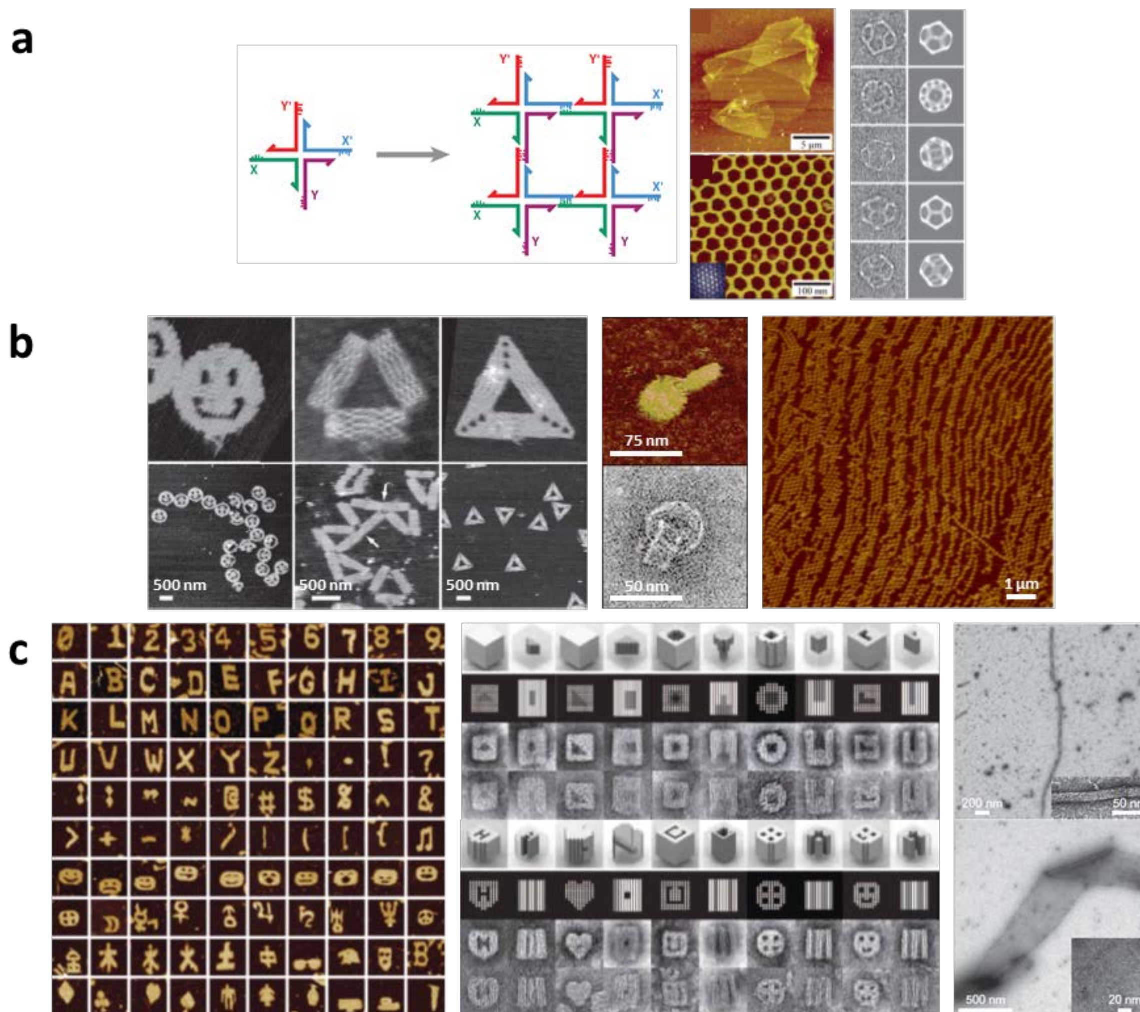

Figure 2. DNA nanostructures. (a) Schematic representation of a four-arm branched DNA molecule with sticky end tails to form larger arrangements (left). AFM images of crystalline hexagonal DNA 2D array self-assembled from three-point-star motifs with sticky ends (middle, top) and its zoomed-in view (middle, bottom). Individual raw cryo-electron microscopic images and corresponding projections of 3D DNA dodecahedron structure reconstructed from the cryo-electron microscopic images (right). (b) AFM images of DNA origami shapes (left). AFM (top) and TEM (bottom) images of a nanoflask (middle). AFM image of origami checkerboard lattices on a single mica surface (right) (c) Complex shapes designed using a molecular canvas made of DNA single stranded tiles (left). Computer-generated models and TEM images of shapes made from a 3D molecular canvas made of DNA bricks (middle). One- and two-dimensional DNA crystals made of DNA bricks (right). Reprinted with permission from: reference 51 Copyright © 2010 Annual Reviews, Inc (a, left), reference 59 Copyright © 2005, American Chemical Society (a, middle), reference 65 Copyright © 2008, Springer Nature (a, right), reference 39 Copyright © 2006, Springer Nature (b, left), reference 43 Copyright © 2011, American Association for the Advancement of Science (b, middle), reference 71 Copyright © 2014, Springer Nature (b, right), reference 44 Copyright © 2012, Springer Nature (c, left), reference 73 Copyright © 2012, American Association for the Advancement of Science (c, middle), reference 74 Copyright © 2014, Springer Nature (c, right).

1.2.1 DNA Nanostructures

1.2.1.1 DNA Tiles

In 1982, Seeman first introduced the concept of DNA nanostructures to the scientific community by presenting the idea of utilizing a sequence of DNA to build a mechanically robust four-arm junction structure.[50] The four-arm junction consists of four complementary DNA single strands with unpaired sticky end tails (Figure 2a, left). This structure is often called a Holliday junction due to its structural resemblance to the Holliday recombination intermediates,[53] and is classified as a tile structure due to its possibility to be assembled into a two-dimensional array as a repeating unit. Afterwards, several DNA tiles were synthesized, but the intrinsic flexibility of the core region of the junction only allowed the tiles to be oligomerized.[54-55] To overcome these problems, in 1993, Fu *et al.* and Zhang *et al.* developed more inflexible double-crossover tiles containing paired four-arm junctions in their structures.[56-57] Since then, a wide variety of tile structures have been fabricated and assembled into extended two- and three-dimensional nanostructures including, but not limited to, hexagonal arrays (Figure 2a, middle),[58-59] nanogrids and nanoribbons,[60] nanotubes,[61] cubes,[62] icosahedrons,[63] crystals,[64] tetrahedrons, dodecahedrons (Figure 2a, right), and buckyballs.[65]

1.2.1.2 DNA Origamis

The DNA origami method, first introduced by Rothemund *et al*. in 2006, is especially important to bottom-up approaches for nanofabrication.[39] The origami method makes it possible to create almost any arbitrarily shaped two-dimensional DNA nanostructures with high yield. In this method, a long scaffold strand is folded in place with over 200 short synthetic oligonucleotide staple strands in a self-assembled manner. To fabricate a DNA origami structure, single stranded

7,249-nucleotide M13mp18 genomic DNA was selected as the scaffold strand. The sequences of the staple strands were determined according to Watson-Crick complements of the scaffold DNA to fold the scaffold strand into the designated shape. Some short remainder strands were also designed to complement the unused sequence of the scaffold strand. The staple and remainder strands were artificially synthesized. The synthesis was a one-pot annealing process in which the scaffold strand was mixed with a 100-fold excess of the staple and remainder strands at room temperature, and the mixture was thermally annealed from 95 °C to 20 °C in less than 2 hours. The DNA origami method has been so successful that it has been widely accepted and applied to construct various two- and three-dimensional structures even with curvatures (Figure 2b, left and middle).[40-42, 66-67]

The DNA origami method with M13mp18 scaffold yields individual origami structures with diameters of *ca.* 100 nm.[39] For practical use in integrated circuits, the microscale organization of DNA nanostructures with more features is needed. Several groups have focused on this problem. Endo *et al.*[68] and Rajendran *et al.*[69] designed “2D DNA jigsaw pieces” which are rectangular nanostructures folded using the DNA origami method. The jigsaw piece is furnished with a tenon, a mortise, and single stranded overhangs to promote selective connections via π-stacking interaction, and sequence- and shape-complementarity. Furthermore, Woo *et al.* demonstrated two methods to assemble DNA origami structures into a more extended structure in microscale. In the first method, the geometric arrangement of blunt-end stacking interaction was suggested using both binary code and shape complementarity to connect individual DNA structures.[70] In the second method, the two-dimensional lattices of DNA origami rectangles were formed based on the stepwise manipulation of surface diffusion by changing the

concentrations of Mg^{2+} and Na^{+} between the DNA origami and the mica substrate (Figure 2b, right).[71]

1.2.1.3 DNA Single-stranded tiles and Bricks

In 2012, Wei *et al.* developed a method of creating one- or two-dimensional complex shapes from the simplest DNA tile form, a so-called "single-stranded tile".[44] The single-stranded tile is different from the tile suggested by Seeman such that it is a single-stranded 42-nucleotide DNA without a junction, as its name indicates. Furthermore, while the central design feature is a long scaffold in the DNA origami method, the single-stranded tile method exploits artificially sequenced and synthesized DNA oligonucleotides allowing greater possibility for choices of both sequence and material. In this method, all uniquely sequenced tiles are identically shaped in a desired structure. Each tile has four consecutive domains and binds to four local neighboring tiles through Watson-Crick base pairing interaction between the domains. As a result, a tile is two 21-nucleotide antiparallel helices joined by a single phosphate linkage, and arranges into a rectangular lattice in a "brick-wall" pattern. The lattice can be regarded as a "molecular canvas", where each tile becomes a "molecular pixel". A nanostructure is then fabricated by excluding the subsets of strands corresponding to the pixels not included in the desired shape in a one-pot annealing process. Although DNA nanotubes with various circumferences were previously synthesized using the same approach,[72] this was the first time when more than 100 sophisticated two-dimensional shapes were fabricated (Figure 2c, left).

The single-stranded tile method was extended to construct complex three-dimensional nanostructures which in turn were further assembled into a microscopic organization as reported by Ke *et al.*[73,74] To move from two- to three-dimensional structures, a tile is now modified to

contain 32-nucleotides. The tile again has four consecutive domains which are 8 nucleotides long. In this case, the tile binds to four local neighboring tiles in a 90° dihedral angle. Each tile becomes a modular component, and the concept of “tile” was generalized to “brick” due to its resemblance of that of LEGO©. Each 8-base pairing between the domains of the neighboring bricks was defined as a voxel, and a collection of bricks with dimensions of 10 by 10 by 10 voxels can be regarded as a molecular canvas. The undesired subsets of bricks were omitted from the molecular canvas in a one-pot annealing process, and more than 100 complex three-dimensional nanostructures were fabricated with sophisticated both surface and interior features including cavities and tunnels (Figure 2c, middle). The resulting nanostructures can be further gathered into a one- or two-dimensional macroscopic DNA crystals (Figure 2c, right).

1.2.2 Current Limitations on DNA Nanostructures

Although DNA nanostructures are considered to be an ideal template for the fabrication of a nanoelectronic device, the application of DNA nanostructures in patterning still has a long way to go. To be implemented at an industrial scale, the following issues must be overcome: limited stability and deterministic assembly of DNA nanostructures.[75]

1.2.2.1 Limited stability of DNA nanostructures

The limited stability of DNA nanostructures is a major disadvantage in the transfer of their nanoscale patterns. DNA is a soft material and the stability of DNA nanostructures is still limited.[76] For example, typical methods to etch and deposit inorganic layers involve harsh chemical environments such as plasma enhanced etching, which might remove DNA nanostructures before their patterns are transferred to the inorganic substrates. Herein we briefly summarize the stability of DNA nanostructures deposited onto a substrate because the deposited ones are more relevant to the bottom-up nanofabrication than the dissolved ones and allow the multistep processing of the DNA nanostructures, such as the patterning of the substrate. This summary also only focuses on the overall preservation of shape of DNA nanostructures because the geometry, rather than the chemical integrity, of DNA nanostructures often plays the most important role for most DNA-based nanofabrications.

Choosing DNA origami triangles as a model, the stability of DNA nanostructures deposited onto a SiO_2 substrate were examined under a wide range of chemical and physical environments (Figure 3).[76] The shape of the DNA origami triangles can be maintained at up to 200 °C under both argon and air atmospheres. On the heating beyond 200 °C, the DNA nanostructures decomposed. Pillers *et al.* also reported the thermal stability of DNA origami

rectangles deposited on mica.[77] Their work showed that the DNA origami structures were still intact after 10 minute heating at 150 °C while they degraded after heating at 250 °C. The DNA origami triangles were stable in common organic solvents such as hexane, ethanol, and toluene for at least 24 hours. In deionized water and 0.01 M – 0.2 M NaCl solutions, however, the DNA nanostructures randomly disintegrated and lifted off from the SiO_2 surface even in a short 10 second immersion. The DNA nanostructures were stable in pH range 7−11, and resulted in the deformation of the overall structure in a specific pattern in both the pHs above and below this range. Upon immersion into solutions below a pH of 7, the DNA origami triangles disintegrated into six distinct pieces, indicating that the disintegration initiated at the tips and midpoints of the trapezoidal sides of the DNA origami triangles due to the intensive folding and/or the lack of support of the scaffold strand. At a pH above 11, the overall triangular shape was maintained; however, the details of the DNA nanostructure were blurred, likely due to both dehybridization and hydrolysis. Finally, upon exposure to UV/O_3, the DNA nanostructures survived 5 minutes and degraded uniformly in less than 15 minutes.

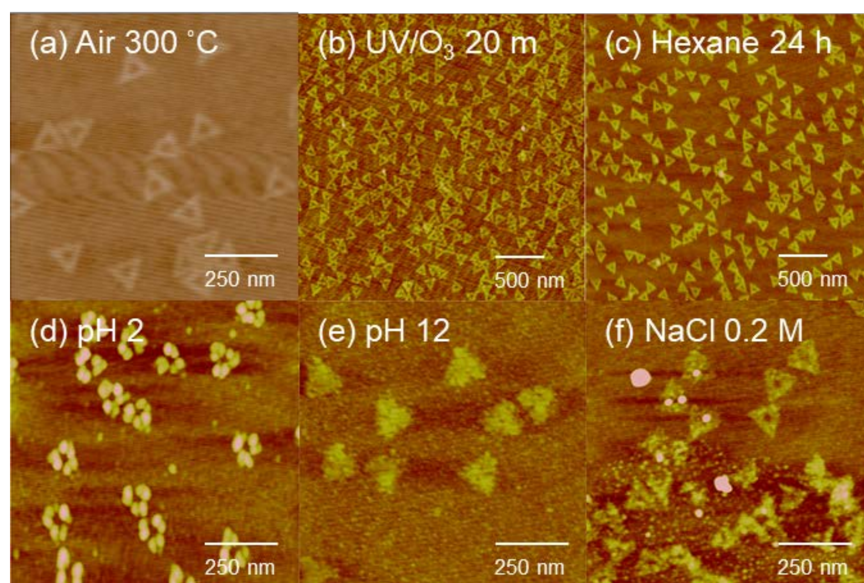

Figure 3. Limited stability of DNA origami nanostructures under diverse environments. AFM height images of DNA origami triangles deposited on silicon wafers after (a) heated at 300 °C for 10 minutes, (b) 20 minutes of UV/O_3 treatment, and immersed in (c) hexane for 24 hours, (d) pH 1.88, (e) pH 12.00, and (f) 0.2 M NaCl solution for 10 seconds. Scale bars represent (a,d–f) 250 nm and (b,c) 50 nm. Reprinted with permission from: reference 76 Copyright © 2014, American Chemical Society.

1.2.2.2 Deterministic assembly of DNA nanostructures

To be able to fabricate a complex nano-electronic or photonic device, it is necessary to deposit DNA nanostructures in predefined locations. Currently developed methods use either electron-beam lithography or deep ultraviolet lithography to create a pattern where a DNA nanostructure is preferentially deposited. In 2009, Kershner *et al.* created binding sites for DNA origami triangles with electron-beam lithography on SiO_2 and diamond-like carbon (Figure 4a).[78] In 2012, Yun *et al*. created binding sites with deep ultraviolet lithography on graphene oxide and nitrogen-doped reduced graphene oxide (Figure 4b).[79] In both cases, the concentration of Mg^{2+} was critical for the deterministic assembly of the DNA origami nanostructures. In 2014, Gopinath *et al.* presented two techniques for replacing the electrostatic bonds through Mg^{2+} between DNA and substrate with covalent bonds, allowing Mg^{2+}-free solution conditions.[80]

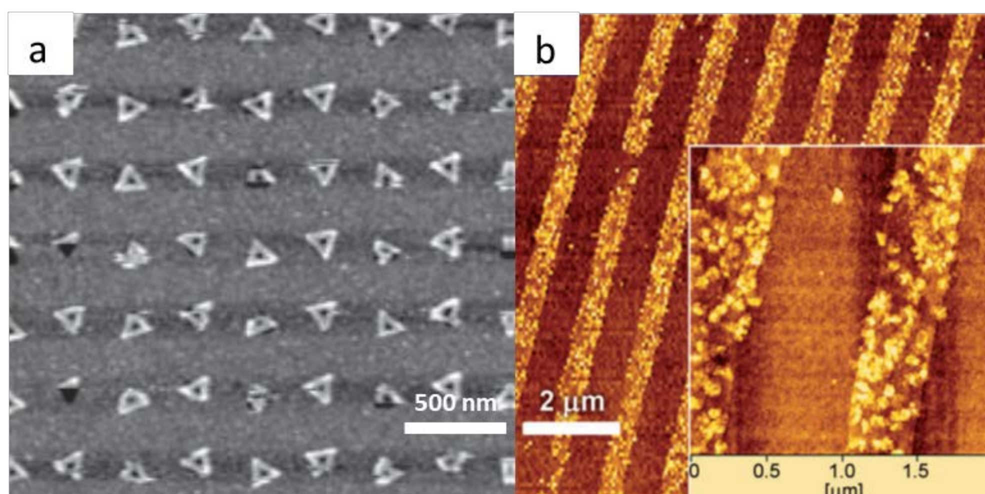

Figure 4. Deterministic assembly of DNA nanostructures. AFM images of DNA origami nanostructures assembled (a) on *ca.* 110 nm patterned triangles on a diamond-like carbon/diamond-like carbon on silicon surface and (b) on patterned nitrogen-doped reduced graphene oxide film. Scale bars represent (a) 500 nm and (b) 2 µm. Reprinted with permission from: reference 78 Copyright © 2009, Springer Nature (a), reference 79 Copyright © 2012 WILEY-VCH Verlag GmbH & Co. KGaA, Weinheim (b).

1.2.3 DNA Nanostructure based Nanofabrication

Since DNA nanostructures were introduced, there has been an explosive growth in DNA-based nanofabrication over the past decades. Regardless of the limitations, DNA nanostructures have precision and cost benefits that make them an attractive alternative to the expensive current state-of-the-art photolithography techniques. While numerous nanomaterials have been assembled onto DNA nanostructures as templates, such as proteins[60, 81-83] and carbon nanotubes,[84-87] one major branch of the nanofabrication is the metallization of DNA. Starting with the metallization of λ-DNA with Ag by Braun *et al.* in 1998,[88] linear and double-stranded DNA[89-91] and DNA origami[92-96] were metallized continuously or site-specifically with the different kinds of metals via solution phase chemistry (Figure 5a,b). Furthermore, Jin *et al*. reported a successful pattern transformation from DNA nanostructures to a chemical vapor deposited graphene sheet by the metallization of the DNA nanostructures (Figure 5c).[97] However, the metallization technique generally results in a loss of resolution up to 50 nm due to the formation of globular metallic coating on DNA.[91-92, 96] The major problem of this strategy is that a large number of small nucleation centers introduced on the DNA template grow in an inhomogeneous manner. Consequently, discontinuous or inhomogeneous grains with different diameters are deposited. As an alternative method, both Sun *et al.* and Helmi *et al.* introduced a method in which a three-dimensional inorganic nanostructure of a few tens of nm grew from a single nucleation seed in a DNA origami mold.[98-99]

Besides their metallization, DNA nanostructures have also been widely used as masks to pattern both hard and soft materials. Deng *et al.* patterned metal films with metal evaporation onto one- and two-dimensional DNA nanostructures on mica substrates followed by the lift-off of the films.[100] Becerril *et al.* used aligned DNA bundles as shadow masks for angled metal

vapor deposition and subsequent etching, demonstrating a spatial resolution in the sub-10 nm range.[101] Surwade *et al.* demonstrated the success of DNA-mediated HF vapor-phase etching and chemical vapor deposited growth of SiO_2 in both positive and negative tones by differentiating the adsorption of water between DNA nanostructures and a SiO_2 substrate at room temperature (Figure 5d).[102-103] In both cases, loss of resolution occurred. The positive tone replicas of DNA nanostructures on a SiO_2 substrate were also formed in anhydrous HF vapor etching with sub-10 nm resolution.[104] Furthermore, DNA nanostructures were converted into carbon nanostructures while their shape was conserved by atomic layer deposition of Al_2O_3 and thermal annealing (Figure 5e).[105] Finally, polymer film such as polyacrylamide gel was faithfully patterned using linear DNA bundles (Figure 5f).[106] The resulting polymer films can serve as molds to further transfer the patterns to other polymer.

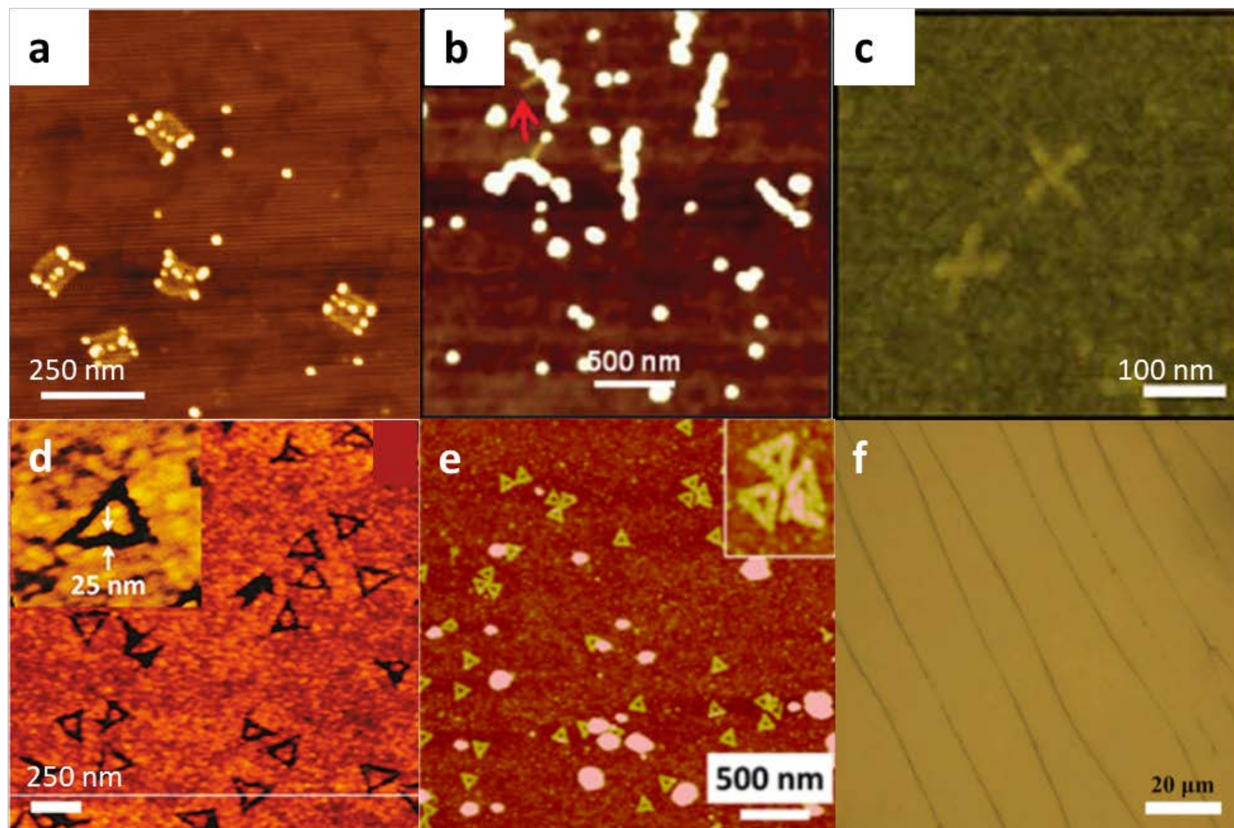

Figure 5. DNA Nanostructure based Nanofabrication. AFM images of (a) H-shaped Au nanoparticle assemblies on DNA origami rectangles on a mica, (b) continuous Au nanoparticle assemblies on T-shaped DNA origami on a SiO_2 wafer, (c) final etched graphene shapes after Au metallized DNA masks were removed, (d) triangular trenches produced upon the exposure of DNA origami triangles on a SiO_2 wafer to HF vapor under high-moisture condition, (e) carbonized DNA origami triangles, and (f) triangular trenches on a PMMA stamp. Reprinted with permission from: reference 94 Copyright © 2011, American Chemical Society (a), reference 96 Copyright © 2012, American Chemical Society (b), reference 97 Copyright © 2013, Springer Nature (c), reference 102 Copyright © 2011, American Chemical Society (d), reference 105 Copyright © 2016, American Chemical Society (e), reference 106 Copyright © 2015, Springer Nature (f).

1.2.4 Nanoscale Patterning of Soft and Hard Materials with DNA Nanostructures

This dissertation focuses on the nanoscale patterning of soft and hard materials with DNA nanostructures. In chapter two, an advanced nanoimprint lithography method is presented to fabricate polymer stamps to transfer patterns from multi-dimensional DNA nanostructures in negative tone patterns with high fidelity. In chapter three, an approach to increase the stability of DNA nanostructure master templates fabricated in chapter two is developed through conformal coating with a nanometer-thin protective inorganic oxide layer created using atomic layer deposition. In chapter four, the first method of high contrast pattern transfer directly from DNA nanostructures to a silicon substrate is reported by reactive ion etching with the help of calcium ion. Each step of the above fabrication processes was imaged with atomic force microscopy, which is briefly reviewed in the following section.

1.2.4.1 Atomic force microscopy

Atomic force microscope (AFM) is a branch of scanning probe microscopy which probes the surface features of a sample with a sharp tip.[107,108] AFM offers a substantial amount of information about surface properties from the nano- to micro-scale with unprecedented clarity. A flexible cantilever with a sharp tip at its end is deflected due to interatomic forces, most commonly van der Waals forces, as the tip probes over a sample. A laser beam reflects from the back of the deflected cantilever, amplifying the deflection as the beam is displaced from the center of a position-sensitive photodetector. The tip-sample relative position is controlled by a scanner which is a three-dimensional positioning system made of a piezoelectric material. The piezoelectric material changes dimensions in response to an applied voltage, or vice versa. The

piezoelectric scanner is designed to mechanically elongate and contract proportionally to an applied voltage.

In contact mode AFM, the tip physically contacts the sample. As the tip probes the sample, the cantilever is deflected due to the contact force to accommodate changes in topography by operating in one of two modes: constant-height or constant-force mode. In constant-height mode, the height of the scanner is fixed during the scanning and the spatial variation of deflection of the cantilever is directly used to produce the topographic image. In constant-force mode, the deflection of the cantilever, which in turn corresponds to the total force applied to the tip, is constant. The scanner moves up and down in the z axis to maintain the deflection constant and its motion generates the topographic image. In non-contact mode AFM or tapping mode AFM, the cantilever oscillates above the surface of a sample with a magnitude of several tens to hundreds of angstroms. While the cantilever is vibrating, it taps the surface of the sample in intermittent-contact, which changes the oscillation frequency and amplitude of the tip. These changes are used to drive the piezo scanner to control the tip-sample distance and ultimately to extract the topography of the sample surface.

2.0 DNA NANOSTRUCTURE-MEDIATED MOLECULAR IMPRINTING LITHOGRAPHY

2.1 CHAPTER PREFACE

Materials contained in this chapter were published as a research article in *ACS Nano*; figures used in this chapter have been reprinted with permission from: *ACS Nano*, 2017, *11* (1), pp 227–238. Copyright © 2017, American Chemical Society.

List of Authors: Cheng Tian,† Hyojeong Kim,† Wei Sun, Yunah Kim, Peng Yin, and Haitao Liu

(†): equal contribution

Author Contributions: C.T., H.K., and H.L. designed and directed the experiments. C.T., H.K., and Y.K. conducted the experiments. All authors discussed the results. C.T., H.K., and H.L. wrote the manuscript with input from all authors.

2.2 INTRODUCTION

Soft lithography uses stamps to transfer micro and nanoscale patterns.[109-113] The stamps are usually fabricated by casting liquid precursors onto master templates with patterned structures. Soft lithography has been well developed and widely used for nanofabrication due to its simplicity, low cost, and compatibility with a wide range of substrates, especially with soft and/or nonplanar surfaces.[110, 113-114] The application of soft lithography, however, is fundamentally limited by the spatial resolution and diversity of structures on the stamps.

Significant efforts have been put into the preparation of master templates, from which the stamps are derived.[113, 115] Conventional lithography methods, such as deep ultraviolet lithography (DUV) and extreme ultraviolet lithography (EUV), are the most general approach for fabrication of the master templates. DUV and EUV use 193 nm ArF excimer laser and 13.5 nm radiation from laser pulsed Sn plasma, respectively. DUV with water immersion and multi-patterning techniques provides the current state-of-the-art 10 nm technology; however, it is not suitable for the shrinkage of feature size below 10 nm due to the higher cost and lower throughput from the process complexity of the multi-patterning procedure.[10-11] To reach the sub-10 nm regime, Samsung recently demonstrated the use of EUV with complementary metal–oxide–semiconductor fin field effect transistor technology to fabricate a 7 nm node.[16] In addition to the conventional lithographic methods, dip-pen nanolithography,[22] indentation lithography,[23] nanosphere lithography,[24] and block copolymer lithography[25-28] have been applied to offer nanoscale with even sub-10-nm features. Other relief structures such as crystallographic steps and cracks,[32-33] and single-walled carbon nanotubes[34-36] have also been used to provide features with sub-nanometer or molecular-scale resolution. However, it still remains a challenge to

develop a general method of constructing master templates and stamps with diverse nanoscale features and high spatial resolution.

In recent years, programmable DNA self-assembly[116-118] has produced a wide range of one-dimensional (1D),[61, 72, 119-120] two-dimensional (2D),[39, 44, 58-59, 121-122] and three-dimensional (3D)[43, 73, 123-126] nanostructures with diverse and complex features. DNA nanostructures can be rationally designed and reliably synthesized. The assembly process is fast and easily implemented.[75] Thus, self-assembled DNA nanostructures can be used as nanofabrication templates due to the ease of controlling their shapes with nanometer-scale spatial resolution. Along this direction, many approaches have been developed to transfer the patterns of DNA nanostructures to a wide range of materials. We briefly review these efforts below.

DNA nanostructures have been employed as masks to transfer the patterns to evaporated noble metal films.[100] Metallization with various metals has also been achieved through wet chemistry,[81, 94, 96, 127-130] and the resulting metal nanostructures have been used to pattern graphene.[131] By exploiting the difference in adsorption of water between DNA nanostructures and a SiO_2 substrate, the DNA nanostructures have been used to modulate the rate of HF vapor phase etching to achieve pattern transfer to the SiO_2 substrate.[102] Based on the same principle, the adsorption of water could also control the rate of chemical vapor deposition of SiO_2 and TiO_2 on the DNA nanostructures and substrate to convert the patterns of the DNA nanostructures into those of the inorganic oxides.[103] Moreover, Al_2O_3 protected DNA nanostructures can be converted to carbon nanostructures by thermal annealing.[105] In addition to the 2D pattern transfer, 3D DNA nanostructures have served as molds to synthesize inorganic nanostructures with prescribed 3D shapes.[98-99]

DNA nanostructures are promising templates for materials science due to their structural complexity and diversity at the nanoscale. However, nanofabrication based on DNA nanostructures still faces several formidable challenges. First of all, the high cost of synthetic DNA strands hinders their application as master templates for large-scale patterning.[132] Second, there lacks a reliable and faithful pattern transfer method that is compatible with existing fabrication processes due to the low mechanical and chemical stability of DNA nanostructures. Third, the deterministic deposition of DNA nanostructures, which is critical to large-area fabrication, is still in its infancy. Existing approaches to controlling the deposition of DNA nanostructures suffer from low fidelity and high error rate.[78, 80, 133-134]

A strategy to partially overcome these problems is to establish a method to transfer complex DNA patterns to polymer substrates. The resulting polymer stamps can be used as templates for the following patterning process, which reduce the cost, simplify the fabrication process, and potentially overcome the difficulties of scalable patterning. Recently, linear DNA bundles with average height and width of *ca.* 90 nm and 879 nm, respectively, were employed as a master template for the fabrication of negative replicas on an unsaturated polyester resin, which was further used to pattern a polyacrylamide gel.[106] However, the lateral dimensions of the DNA bundles are relatively large (*ca.* 1 μm). To the best of our knowledge, none of the nanoscale DNA structures have been used as templates to fabricate polymer stamps with high diversity, complexity and fidelity.

Herein we demonstrate an approach to using DNA nanostructures as master templates in a direct pattern transfer from DNA nanostructures to polymers with high fidelity. The nanoscale features of the polymers can be rationally controlled by the design of the DNA nanostructures. A variety of DNA nanostructures were used to pattern poly(methyl methacrylate) (PMMA), poly(L-

lactide) (PLLA), and acryloxy perfluoropolyether (a-PFPE), including DNA nanotubes, 1D λ-DNAs, 2D DNA brick crystals with 3D features, hexagonal DNA 2D arrays, and DNA origami triangles. The resulting polymer stamp could serve as a mold to further transfer the pattern to an a-PFPE polymer substrate.

2.3 EXPERIMENTAL SECTION

2.3.1 Materials

Silicon wafer [Si (110), with native oxide] was purchased from University Wafers (Boston, MA). Scaffold strand M13mp18 for DNA origami triangle and λ-DNA were purchased from Bayou Biolabs (Metairie, LA) and New England Biolabs (Ipswich, MA), respectively. Short staple strands for DNA origami triangles and DNA strands for DNA nanotubes, two-dimensional (2D) arrays, and 2D brick crystals were synthesized by Integrated DNA Technologies (Coralville, IA). 2-Amino-2-(hydroxymethyl)-1,3-propanediol (Trizma base), ethylenediaminetetraacetic acid (EDTA), magnesium acetate tetrahydrate, sulfuric acid, hydrogen peroxide solution (30% H_2O_2), poly(methyl methacrylate) (PMMA), and poly(L-lactide) (PLLA) were purchased from Sigma-Aldrich (St. Louis, MO). Acetic acid (Glacial) and nickel chloride hexahydrate (ACS Certified) were purchased from Fisher Scientific (Fair Lawn, NJ). Dichloromethane was purchased from Acros Organics (Fair Lawn, NJ). Ethanol was purchased from Sigma-Aldrich and Decon Labs, Inc. (King of Prussia, PA). Polydimethylsiloxane (PDMS) backing stamp was prepared with Sylgard 184 silicone elastomer kit (Dow Corning, Midland, MI). Fluorinated acrylate oligomer CN4002 (1400 g/mol) was purchased from Sartomer Americas (Exton, PA) and photoinitiator Irgacure 4265 was purchased from BASF (Florham Park, NJ). All materials were used as received. An UV lamp (100 watts, 365 nm) was purchased from Cole-Parmer (Vernon Hills, IL). High purity water (18.3 MΩ) was produced by a Barnstead MicroPure Standard water purification system (Thermo Scientific, Waltham, MA) and used throughout the entire experiment.

2.3.2 Preparation of a Silicon Wafer

A silicon wafer with a native oxide layer was cleaned by immersion in hot piranha solution [7:3 (v:v) concentrated H_2SO_4: 30% H_2O_2] for at least 20 minutes. The wafer was thoroughly washed with deionized water and dried with N_2 gas. *Warning: Piranha solution presents an explosion hazard and should be handled with extreme care; it is a strong oxidant and reacts violently with organic materials. All work should be performed in a fume hood. Wear proper protective equipment.*

2.3.3 Preparation of a PDMS Backing Film

PDMS precursor and curing agent were thoroughly mixed at a 9:1 (v:v) ratio by hand at least for 5 minutes and degassed in a vacuum desiccator. The PDMS prepolymer was poured over a piranha cleaned silicon wafer and further degassed in the vacuum desiccator. The mixture on the silicon wafer was cured for 1 hour at 60 °C. The thickness of the resulting PDMS layer was *ca.* 1–2 mm.

2.3.4 DNA Nanostructures

2.3.4.1 Preparation and deposition of DNA nanotubes on a silicon wafer

The design and synthesis of DNA nanotubes were previously reported.[119] DNA single strands were diluted in 10 × TAE/Mg^{2+} buffer (125 mM Mg^{2+}) with a final concentration of 1 μM. The DNA solution was slowly cooled from 95 °C to 23 °C over 48 hours and stored at 4 °C overnight. Nickel chloride solution (70 μL of 2 mM) was placed on a clean silicon wafer and immediately blown away with N_2 gas. The annealed DNA nanotube solution was deposited on the pretreated silicon wafer with nickel chloride and incubated in a humid chamber for 15 minutes. The sample was dried using N_2 gas, immersed in an ethanol:water [9:1 (v:v)] solution for 10 seconds to remove ionic salts, and then dried again using N_2 gas.

2.3.4.2 Preparation and deposition of 2D DNA brick crystals on a silicon wafer

The design and synthesis of 2D DNA brick crystals followed the previously published method.[74] Unpurified DNA strands were mixed in an equimolar stoichiometric ratio in 0.5 × TE buffer [Trizma base (5 mM, pH 8.0) and EDTA (1 mM)] supplemented with 40 mM $MgCl_2$. The final concentration of each strand was 200 nM. The DNA solution was annealed in a PCR thermo-cycler using a fast-linear cooling step from 80 °C to 60 °C over 1 hour and then from 60 °C to 25 °C over 72 hours. The annealed DNA solution was diluted by 10 times in 0.5 × TE buffer with 40 mM $MgCl_2$. The diluted DNA solution (10 μL) was deposited on a clean silicon wafer and incubated in a humid chamber for 15 minutes. The sample was dried using N_2 gas, immersed in an ethanol:water [9:1 (v:v)] solution for 5 seconds, and then dried again using N_2 gas.

2.3.4.3 Preparation and deposition of hexagonal DNA 2D arrays on a silicon wafer

The design and synthesis of hexagonal DNA 2D arrays were previously reported.[59] To increase the surface coverage, DNA 2D arrays were directly assembled on a silicon wafer.[135-136] A desired set of three DNA single strands were mixed in 1 × TAE/Mg^{2+} buffer at a concentration of 25 nM in terms of 3-point-star motifs. A clean silicon wafer was immersed in 10 × TAE/Mg^{2+} buffer [Trizma base (400 mM, pH 8.0), acetic acid (200 mM), EDTA (10 mM), and $Mg(CH_3COO)_2$ (125 mM)] for 3 hours to increase the surface concentration of magnesium ions which were used to bind DNA on the silicon wafer.[136] After the 3 hours of incubation, the silicon wafer was directly immersed into the prepared DNA solution. The DNA solution together with the silicon wafer was slowly cooled from 95 °C to 23 °C in one day. After the annealing, the silicon wafer was taken out of the DNA solution, immediately immersed in an ethanol:water [7:3 (v:v)] solution for 5 seconds, and then dried using N_2 gas.

2.3.4.4 Preparation and deposition of λ-DNAs on a silicon wafer

λ-DNA (500 μg/mL) was diluted in 1 × TAE/Mg^{2+} buffer by three times. Since λ-DNA was difficult to attach to a silicon wafer, nickel ions were used to provide an extra binding force between DNA and the silicon wafer. Nickel chloride solution (100 μL of 1 mM) was deposited on a clean silicon wafer for 10 seconds and immediately dried using N_2 gas. Then 10 μL of the diluted λ-DNA solution was deposited on the silicon wafer and incubated in a humid chamber for 15 minutes. The sample was dried using N_2 gas, immersed in an ethanol:water [9:1 (v:v)] solution for 5 seconds, and then dried again using N_2 gas.

2.3.4.5 Preparation and deposition of DNA origami triangles on a silicon wafer

The design and assembly of DNA origami triangles were previously reported.[39] Scaffold strand M13mp18 (8.6 µL, 1.6 nM) was mixed with 232 short synthetic staple strands (15 µL, 16 nM), deionized water (77 µL), and TAE/Mg^{2+} buffer (181 µL). The TAE/Mg^{2+} buffer was prepared by dissolving Trizma base (40 mM, pH 8.0), acetic acid (2 mM), EDTA (2 mM), and magnesium acetate tetrahydrate (150 mM) and further diluting the solution to make the concentration of magnesium ions 12.5 mM. The solution was cooled from 95 °C to 20 °C at a rate of 1 °C/min. After the annealing, 140 µL of the DNA origami solution was purified by rinsing away excess staple strands using 500–600 µL of the TAE/Mg^{2+} buffer in a Microcon YM-100 100 kDa MW centrifuge filter (Millipore, Billerica, MA) on a single speed bench top Galaxy Ministar microcentrifuge (VWR, Radnor, PA). This rinsing process was repeated twice. The final volume of the DNA origami solution was 140 µL, same as before the purification. The purified triangular DNA origami solution (10 µL) was deposited on a clean silicon wafer and incubated in a humid chamber for 15 minutes. The sample was dried using N_2 gas, immersed in an ethanol:water [9:1 (v:v)] solution for 5 seconds to remove salts, and then dried again using N_2 gas.

2.3.5 Fabrication of a PMMA or PLLA Stamp by Replication over DNA Nanostructures

Fabrication of PMMA and PLLA stamps consisted of several steps.[137] First, a PMMA or PLLA film was spin-coated onto a silicon wafer with DNA nanostructures at 3000–4000 rpm for 30 seconds using polymer in dichloromethane solution (3 wt. %). This spin coating was repeated three times to increase the film thickness. Second, the surface perimeter with a width of *ca.* 1 mm around the edges of the polymer film was scraped off to expose the underlying template.

Third, a PDMS backing stamp adhered to the polymer film. Fourth, several drops of deionized water were added to one edge of the exposed silicon substrate and were allowed to penetrate the interface between the hydrophobic polymer and hydrophilic silicon wafer. After a minute, when the interface was fully filled with water, the PDMS/polymer film was immediately peeled off and gently dried using N_2 gas.

2.3.6 Fabrication of an a-PFPE Stamp by Replication over DNA Nanostructures

a-PFPE prepolymer resin consisted of fluorinated acrylate oligomer CN 4002, and photoinitiator Irgacure 4265 (0.5 wt. %). The prepolymer resin was mixed for at least 2 hours using a Teflon magnetic stirrer on a stirring plate. This photocurable liquid resin was filtered through a 0.2 μm pore size syringe filter and spin-coated onto a silicon wafer with DNA nanostructures at 4000 rpm for 30 seconds. On top of the spin-coated a-PFPE prepolymer film, the filtered a-PFPE liquid resin was pooled to make the a-PFPE stamp thick enough to be peeled off with a tweezer after curing. The a-PFPE prepolymer film was cured with UV light (365 nm) for 2 hours under N_2 gas. The a-PFPE stamp was peeled off from the wafer with a tweezer.

2.3.7 Replica Molding of Pattern on a PMMA or PLLA Stamp into an a-PFPE Stamp

This process is the same as the one outlined in **2.3.6**, except a PMMA or PLLA stamp was used instead of a silicon wafer with DNA nanostructures.

2.3.8 Characterization

2.3.8.1 Transmission electron microscopy (TEM)

An annealed sample of 2D DNA brick crystals (2.5 μL) was adsorbed on a glow-discharge-treated carbon coated TEM grid for 2 minutes. The grid was then stained by a 2% aqueous uranyl formate solution containing 25 mM NaOH for 10 seconds. Imaging was performed using a JEM-1400 TEM operating at 80 kV (JEOL USA, Inc., Peabody, MA).

2.3.8.2 Atomic force microscopy (AFM)

Imaging was performed by tapping-mode on an MFP-3D atomic force microscope (Oxford Instruments Asylum Research, Inc., Santa Barbara, CA) with NSC15/Al BS, RTESPA-300 or SSS-FMR-SPL AFM probe in air. The tip-surface interaction was minimized by optimizing scan set-point. NSC15/AL BS AFM probe (325 kHz, 40 N/m) was purchased from MikroMasch (Lady's Island, SC). RTESPA-300 AFM probe (300 kHz, 40 N/m) was purchased from Bruker (Camarillo, CA). SSS-FMR-SPL AFM probe (75 kHz, 2.8 N/m) was purchased from NanoAndMore USA (Watsonville, CA) and especially used for the high-resolution imaging of DNA origami triangles on silicon wafers and corresponding triangular trenches on PMMA and PLLA stamps. Fourier transform was carried out by ImageJ, imaging processing software.[138]

2.4 RESULTS AND DISCUSSION

2.4.1 General Fabrication Process of a Polymer Stamp using a DNA Nanostructure Master Template

The fabrication of a polymer stamp consisted of five steps as shown in Figure 6.[137] A silicon wafer with native oxide was cleaned by piranha solution and served as a substrate for DNA deposition (Figure 6a,b). After DNA nanostructures were deposited, polymer solution in dichloromethane (*e.g.*, PMMA) was spin-coated on the substrate to cover the DNA (Figure 6b,c). Around the edges of the polymer film, the surface perimeter was scraped off with a blade to expose the underlying silicon substrate (Figure 6c,d). A PDMS backing stamp was then adhered to the polymer film as a flexible support to assist in the removal of the polymer film from the silicon substrate in the next step (Figure 6d,e). In the last step, drops of deionized water were added to one edge of the exposed silicon substrate and were allowed to penetrate the interface between the hydrophobic polymer and the hydrophilic silicon wafer. The PDMS/polymer film was peeled off and gently dried under nitrogen gas. Negative replicas of the DNA nanostructures formed on the sub-surface of the polymer film that was in conformal contact with the DNA (Figure 6e,f). This whole process can be completed in several minutes.

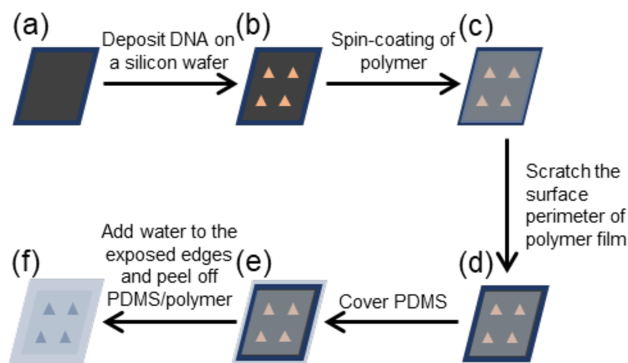

Figure 6. General fabrication process of a polymer stamp using a DNA nanostructure master template. (a) A silicon wafer. (b) DNA nanostructures are deposited on the silicon wafer. (c) A polymer film (*e.g.*, PMMA) is spin-coated onto the silicon wafer. (d) The surface perimeter of the polymer film (*ca.* 1 mm wide) is removed from the four edges of the film. (e) A PDMS backing stamp is adhered to the polymer film as a flexible support. (f) Droplets of water are added to one edge of the exposed silicon wafer and the PDMS/polymer film is peeled off.

2.4.2 Fabrication of a PMMA Stamp by Replication over DNA Nanostructures

2.4.2.1 Fabrication of a PMMA stamp by replication over DNA nanotubes

We first demonstrate the fabrication of PMMA stamps using self-assembled DNA nanotubes which have a length of up to 60 μm and a width in the range of 30–70 nm.[119] The topography of DNA nanotube master templates and PMMA stamps was characterized by atomic force microscopy (AFM). In the AFM images, the height of the DNA nanotubes was measured to be 4.0 ± 0.5 nm. This small height is expected due to the collapse of the DNA nanotubes during the drying process (Figure 7a,c). The bundling of DNA nanotubes, however, was evident in some areas. After the polymer film was peeled off, the trenches corresponding to the DNA nanotubes were observed on the PMMA stamp. The depth of the 1D trenches was 3.2 ± 0.7 nm, in good agreement with the height of the DNA nanotubes (Figure 7b,d). The measured width of the nanotubes on the master templates (67.1 ± 5.3 nm) was larger than the expected value, and that

of the 1D trenches on the PMMA stamps (39.7 ± 5.1 nm) was smaller than the expected value. We attribute this observation to the AFM probe convolution effect and the removal of salt residues during the fabrication of the PMMA stamp. The bundling of DNA nanotubes produced wider and deeper 1D trenches. These results confirm a successful replication process from the DNA nanotubes to the PMMA stamps.

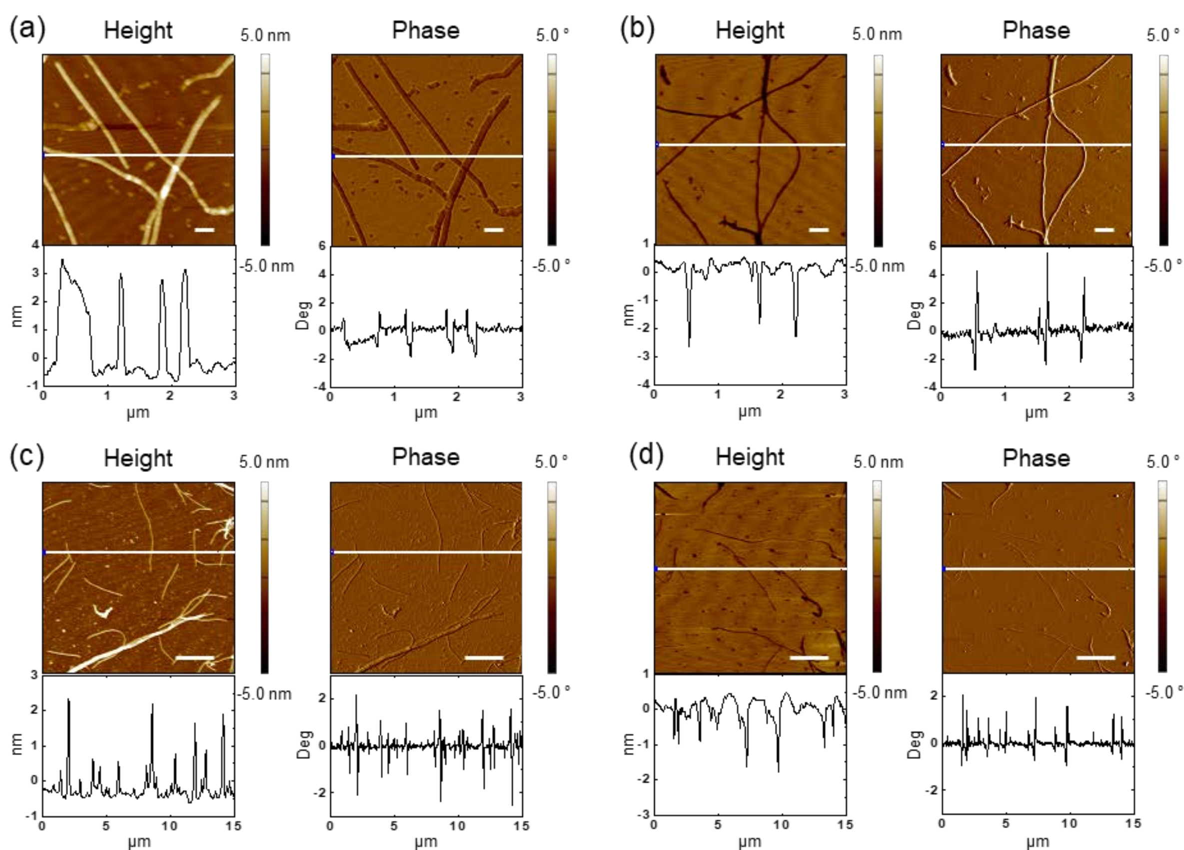

Figure 7. Fabrication of a PMMA stamp by replication over DNA nanotubes. AFM height (left) and phase (right) images with corresponding cross-sectional analysis of (a,c) DNA nanotubes deposited on silicon wafers and (b,d) negative replicas of the DNA nanotubes on PMMA stamps. White lines on the AFM images indicate where the cross-sections were determined. Scale bars represent (a,b) 300 nm and (c,d) 3 µm.

2.4.2.2 Fabrication of a PMMA stamp by replication over 2D DNA brick crystals

Besides 1D nanostructures, 2D DNA brick crystals with defined 3D features could also serve as master templates to transfer 3D patterns to PMMA stamps. Such 2D DNA brick crystals were prepared through the recently developed "DNA brick" approach.[74] After an one-pot annealing process, 2D DNA brick crystals with parallel channels were assembled (Figure 8a). The channels are designed to be 10 nm high and 15 nm wide, and are separated by ridges with a height of 10 nm and a width of 15 nm (Figure 8b), assuming 2.5 nm diameter per hydrated DNA helix.[74] The assembled brick crystals were imaged by transmission electron microscopy (TEM) (Figure 8c). The parallel channels were clearly visible in the TEM image, and the measured pitch of the brick crystals was 24.9 ± 0.5 nm, smaller than the theoretical value of 30 nm. The decreased pitch is attributed to the staining and dehydration of the DNA brick crystals during TEM sample preparation and imaging in a vacuum. The AFM images show a consistent shape of the 2D brick crystals (Figure 8d,f). The average height of the 2D brick crystals in the AFM image was 7.3 ± 0.3 nm, which is much smaller than the theoretical value of 20 nm, and the average pitch was 29.9 ± 1.8 nm and consistent with the expected value of 30 nm. The channels within the DNA brick crystals were clearly visible in the AFM phase images; however, their full depth was not resolved in the height images, likely due to the tip convolution effect. In addition, a high concentration of magnesium ions (40 mM) had to be used to stabilize the DNA brick crystals, resulting in their aggregation (Figure 8d–g).

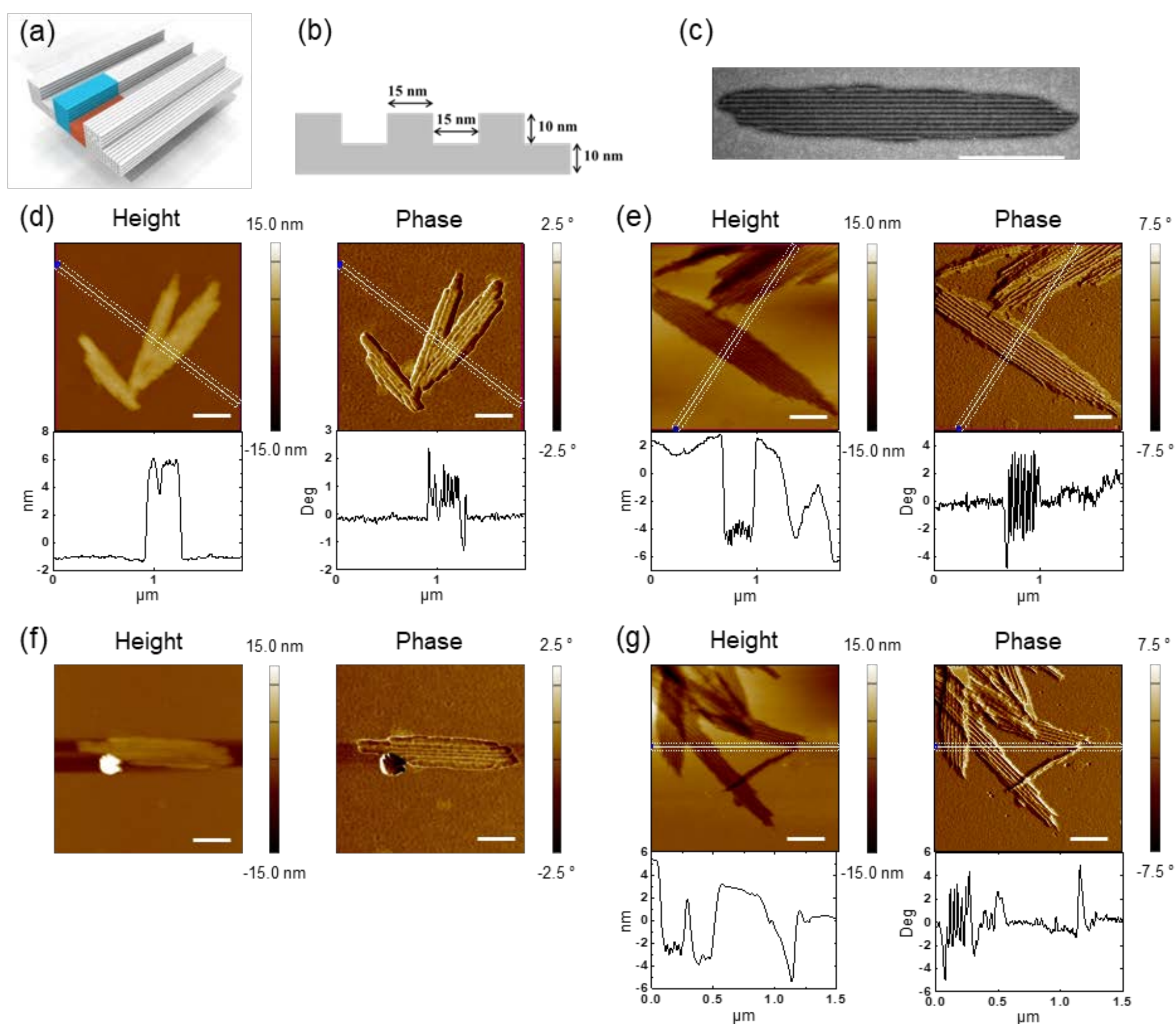

Figure 8. Fabrication of a PMMA stamp by replication over 2D DNA brick crystals. (a) Scheme of 2D DNA brick crystal. The repeating units are represented as the blue and orange blocks. (b) Cross-sectional view of the scheme of 2D DNA brick crystal. (c) TEM image of 2D DNA brick crystal. AFM height (left) and phase (right) images with corresponding cross-sectional analysis of (d,f) 2D DNA brick crystals deposited on silicon wafers and (e,g) negative replicas of the 2D DNA brick crystals on PMMA stamps. White lines on the AFM images indicate where the cross-sections were determined. Scale bars represent (c) 500 nm and (d–g) 300 nm.

After the replication process, the negative replicas of the DNA brick crystals could clearly be seen on the PMMA stamps (Figure 8e,g). The average depth of the negative patterns was 7.7 ± 0.3 nm, in good agreement with that of the original 2D brick crystals (7.3 ± 0.3 nm) on the silicon wafers. The trenches within the negative replicas were clearly visible in the phase images and the average pitch was 30.3 ± 0.6 nm, which is close to that of the DNA brick crystal master templates. Although the trenches were clearly visible in the height images, their depth was not fully resolved and was much smaller than the expected value of 10 nm. This observation is similar to that of the DNA brick crystals on the substrates. The consistency of the shape, height, and pitch between the 2D DNA brick crystals and their replicas on the PMMA stamps indicates a faithful replication process.

2.4.2.3 Fabrication of a PMMA stamp by replication over hexagonal DNA 2D arrays

In addition to DNA nanotubes and 2D DNA brick crystals, DNA nanostructures with smaller feature sizes could also be used as master templates in our method. Hexagonal DNA 2D arrays were tested as master templates for the pattern transfer. The hexagonal DNA 2D arrays were self-assembled from DNA 3-point-star motifs (Figure 9a).[59] Each edge of the motif consists of two DNA double strands with a length of 4.5 turns. To increase the surface coverage of the DNA 2D arrays, silicon substrate mediated annealing was used to directly grow the hexagonal arrays on a silicon wafer.[135-136] A freshly cleaned silicon wafer was immersed in the DNA solution and annealed with DNA strands from 95 °C to 23 °C over one day. During this process, the DNA motifs were adsorbed and confined to the SiO_2 surface to facilitate the self-assembly.[120] Figure 9b shows that after the annealing, most areas of the silicon wafer were covered by a monolayer of the DNA 2D arrays with a hexagonal shape. Big white spots were also observed, which we attribute to DNA aggregates and salt residues attached to the monolayer of DNA. The cross-sectional analysis shows that the repeating distance of the DNA 2D array was 29.7 $\pm$ 0.7 nm, in good agreement with the theoretical value of 30.3 nm.[59] The Fourier transform of the AFM phase image further shows the expected six-fold symmetry of the DNA array (Figure 9c). On the surface of PMMA, the negative replicas of the DNA 2D arrays appeared as arrays of pillars and were highlighted by the white arrows in Figure 9d. The Fourier transform of the pillars shows six-fold symmetry which is consistent with the pattern of the DNA master template (Figure 9e). The periodicity of the pillars was measured by the average distance between the adjacent pillars and found to be 29.7 ± 0.9 nm, almost identical to that of the DNA master template. The pillar-like PMMA pattern of the same symmetry and periodicity confirms the pattern replication from the hexagonal DNA 2D arrays to the PMMA stamps.

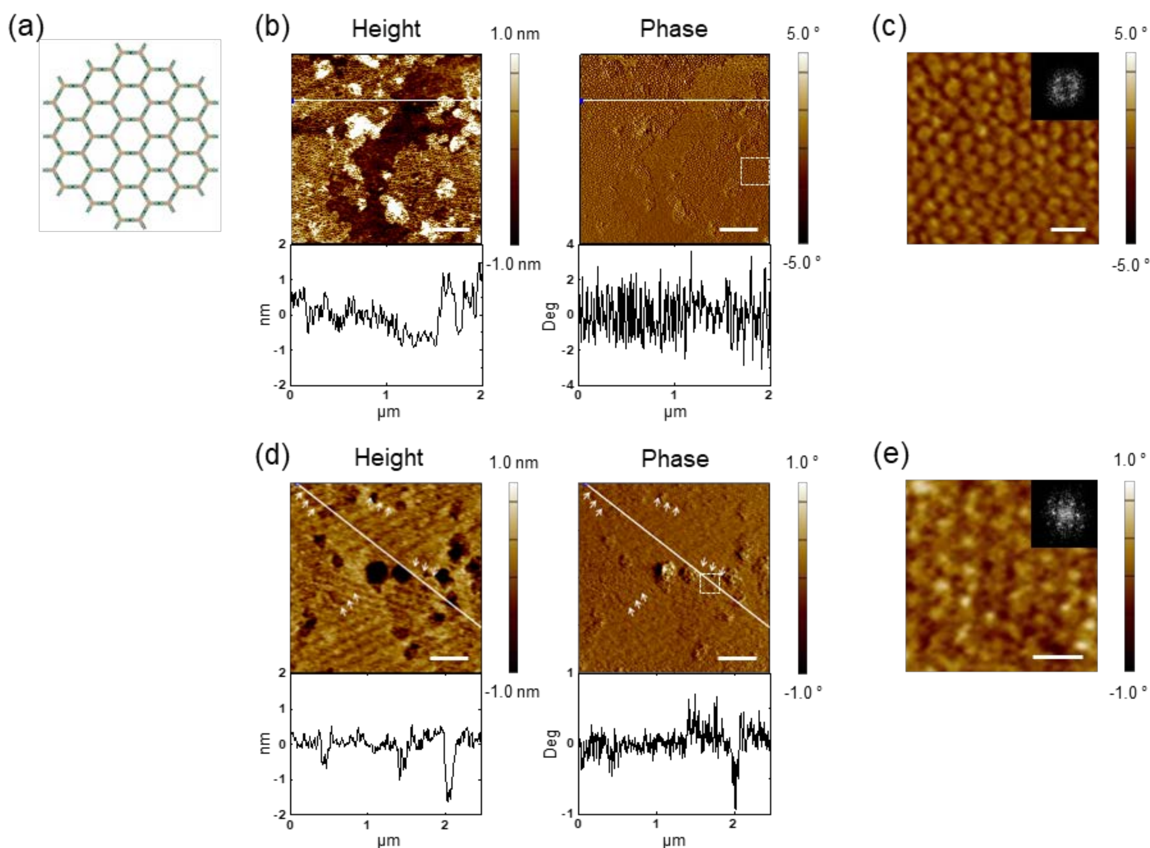

Figure 9. Fabrication of a PMMA stamp by replication over hexagonal DNA 2D arrays. (a) Scheme of hexagonal DNA 2D array assembled from 3-point-star motifs. (b) AFM height (left) and phase (right) images with corresponding cross-sectional analysis of DNA 2D arrays assembled on a silicon wafer. (c) Zoomed-in view of the area in the white dashed box in image b. The inset is the Fourier transform of image c. (d) AFM height (left) and phase (right) images with corresponding cross-sectional analysis of negative replicas of the arrays on a PMMA stamp. (e) Zoomed-in view of the area in the white dashed box in image d. The inset is the Fourier transform of image e. White arrows indicate the replicated patterns on the PMMA stamp. White lines on the AFM images indicate where the cross-sections were determined. Scale bars represent (b,d) 400 nm and (c,e) 50 nm.

2.4.2.4 Fabrication of a PMMA stamp by replication over λ-DNAs

To probe the resolution limit of this method, the feature size of DNA nanostructures is further decreased to an individual DNA double helix. λ-DNA, a double-stranded phage DNA with a length of *ca.* 16 μm, was employed as a master template. The height and full width at half maximum (FWHM) of the individual λ-DNA were measured to be 0.3 ± 0.1 nm and 14.7 ± 3.2 nm, respectively (Figure 10a,c), although the bundling of λ-DNA was observed as well. After replication, narrow 1D trenches with a depth of 0.4 ± 0.1 nm and a FWHM of 11.1 ± 1.7 nm were observed on PMMA stamps (Figure 10b,d), which represent the negative replicas of the individual λ-DNA. This result shows that even a single DNA double strand of a diameter of 2 nm can serve as a master template for the pattern transfer, suggesting the possibility of applying this method to pattern molecular-scale features.

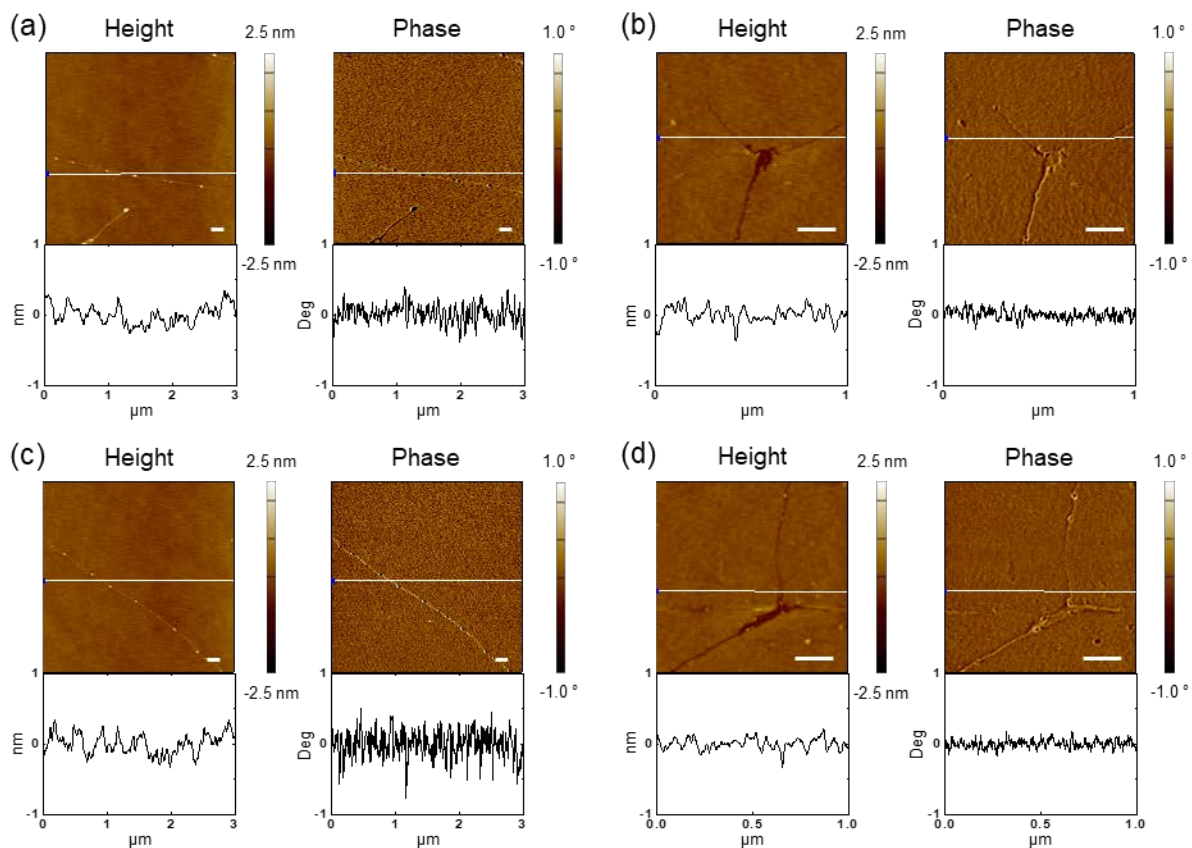

Figure 10. Fabrication of a PMMA stamp by replication over λ-DNAs. AFM height (left) and phase (right) images with corresponding cross-sectional analysis of (a,c) λ-DNAs deposited on silicon wafers and (b,d) negative replicas of the λ-DNAs on PMMA stamps. White lines on the AFM images indicate where the cross-sections were determined. Scale bars represent 200 nm.

2.4.2.5 Fabrication of a PMMA stamp by replication over DNA origami triangles

All of the nanostructures tested above are either 1D or 2D nanostructures with linear or periodic patterns, respectively. To increase the complexity of the patterns on the stamps, DNA origami triangles[39] were employed as master templates for the pattern transfer. The DNA origami triangle is composed of a single layer of DNA double strands with a theoretical height of 2 nm and contains three trapezoidal domains (Figure 11a). The edges of the adjacent trapezoidal domains are connected by bridging staple strands, forming three small triangular holes at each vertex and one large triangular hole in the center. According to the design, the inner length (the length of the sides of the central triangular hole), outer length, and FWHM of the trapezoidal domains of the DNA triangles are 55.0 nm, 129.6 nm and 27.0 nm, respectively. The AFM images show that the DNA triangles were randomly distributed on silicon wafers and the central, large triangular holes were clearly visible (Figures 11b and 12a). Because of the resolution limitation of the AFM images, the bridging staple strands between the trapezoidal domains were not visible. As a result, the three small triangular holes at the vertex were shown as a linear gap. A dangling loop was visible in some DNA triangles; in other structures, the dangling loop might have attached on top of the DNA triangle or beneath the structure so that it was not visible (Figure 12a). According to the cross-sectional analysis, the average height, inner length, outer length, and FWHM of the trapezoidal domains of the DNA triangles were 1.6 ± 0.1 nm, 45.6 ± 2.0 nm, 131.2 ± 5.4 nm, and 38.0 ± 3.1 nm, respectively. The measured height of DNA nanostructures in AFM images might vary due to the differences in the probe-substrate and probe-sample interactions.[139] Due to the AFM probe convolution effect, the measured outer length and FWHM of the DNA triangles increased and the measured inner length of the DNA triangles decreased compared with the theoretical values.

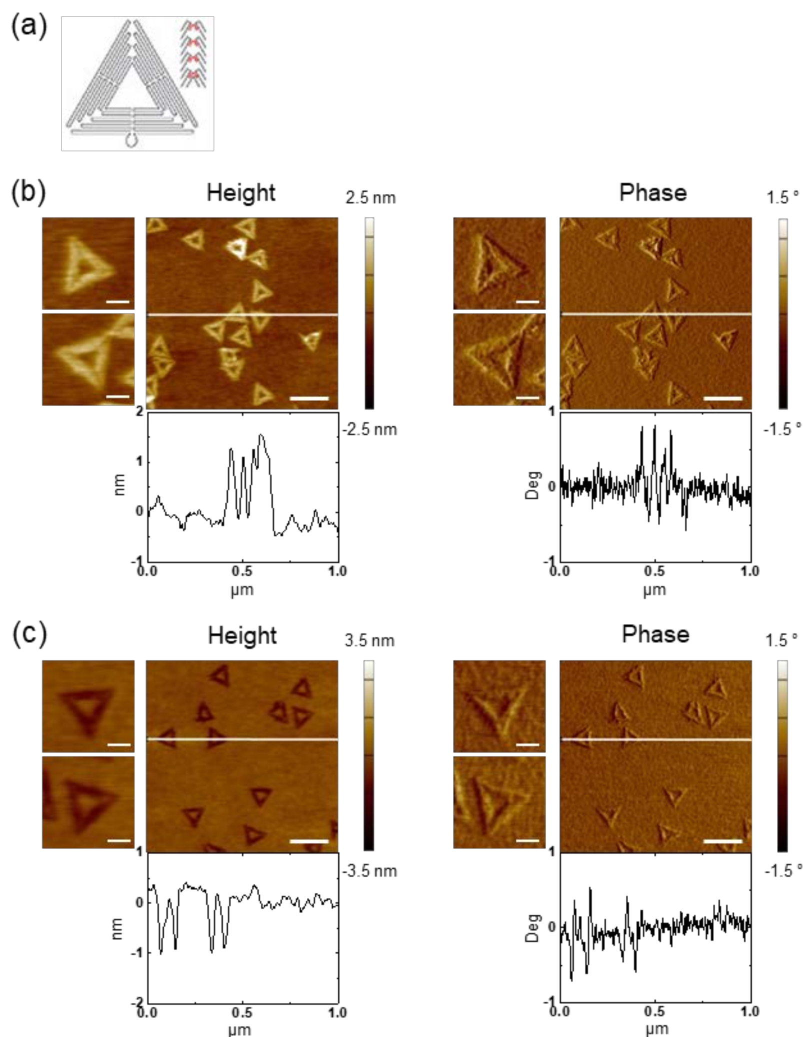

Figure 11. Fabrication of a PMMA stamp by replication over DNA origami triangles. (a) Folding path of DNA scaffold strand in DNA origami triangle. Red lines represent staple strands bridging trapezoidal sides. Reprinted with permission from: reference 39 Copyright © 2006, Springer Nature. AFM height (left) and phase (right) images with corresponding cross-sectional analysis of (b) DNA origami triangles deposited on a silicon wafer and (c) negative replicas of the DNA origami triangles on a PMMA stamp. Zoomed-in images are to the left of the corresponding images. White lines on the AFM images indicate where the cross-sections were determined. Scale bars represent (zoomed-in images) 50 nm and (zoomed-out images) 200 nm.

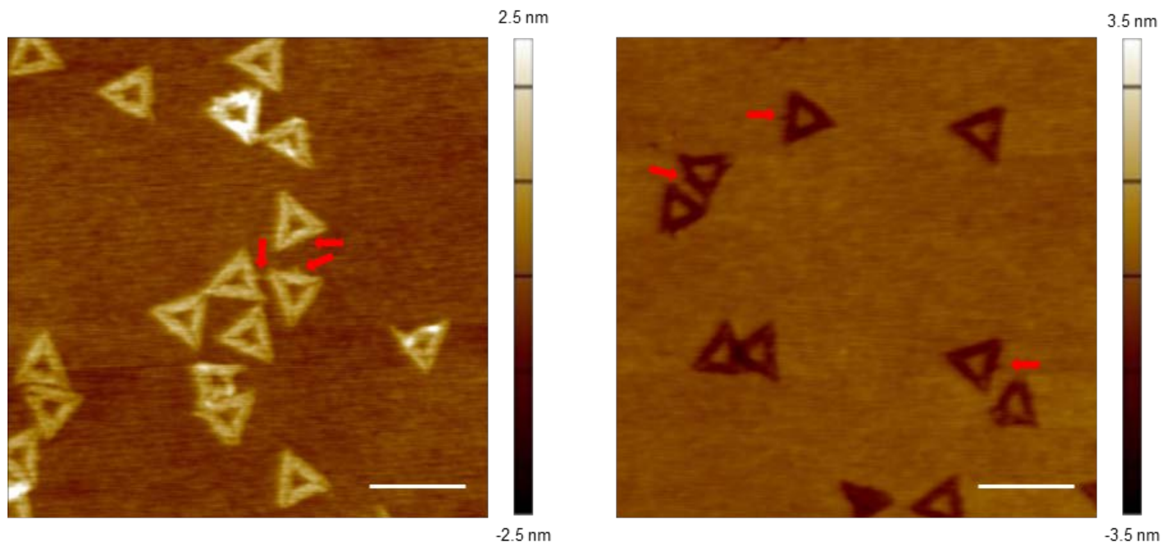

Figure 12. Analysis of dangling loops of a DNA origami triangle master template and a PMMA stamp. AFM height images of (a) DNA origami triangles deposited on a silicon wafer and (b) negative replicas of the DNA origami triangles on a PMMA stamp. The dangling loops of the DNA triangles and the corresponding patterns of the triangular trenches are indicated by the red arrows. Scale bars represent 200 nm.

After pattern transfer, triangular trenches appeared on PMMA films, resembling the shape of the DNA origami triangles (Figures 11c and 12b). Even the pattern of the dangling loop had been transferred to the PMMA stamps (Figure 12b). The averaged depth, inner length, outer length, and FWHM of the triangular trenches were 1.0 ± 0.2 nm, 54.3 ± 2.6 nm, 126.8 ± 3.8 nm, and 26.5 ± 3.1 nm, respectively. The decreased depth of the trenches is attributed to the removal of salts during the pattern transfer. The inner length, outer length, and FWHM of the triangular trenches are all consistent with the design. Similar to the DNA master templates, the small triangular holes did not show up on the PMMA stamps. Instead, we observed a small bump at the vertex of the triangular trench, which is the replica of the linear gap between the trapezoidal domains. This bump can be seen in the cross-sectional analysis of the vertex of the triangular trenches (Figure 13a,b). However, the height of the bump is much smaller than 1 nm, and in some trenches, the bump was not observed at all (Figure 13c). Both observations could be due to the mechanical instability of the bumps during the AFM imaging and/or the inherent limitation of the pattern transfer. As the feature size of the DNA master template decreases, especially when nanometer-sized holes exist in the DNA nanostructure, PMMA molecule might not be able to fully fill the holes during the pattern transfer, resulting in the decreased height and missing features in the PMMA replica. These results demonstrate that the overall features of the triangular DNA origami can be successfully transferred to the PMMA stamps with high fidelity, and the local features (*ca.* sub-5 nm) can be replicated to some extent.

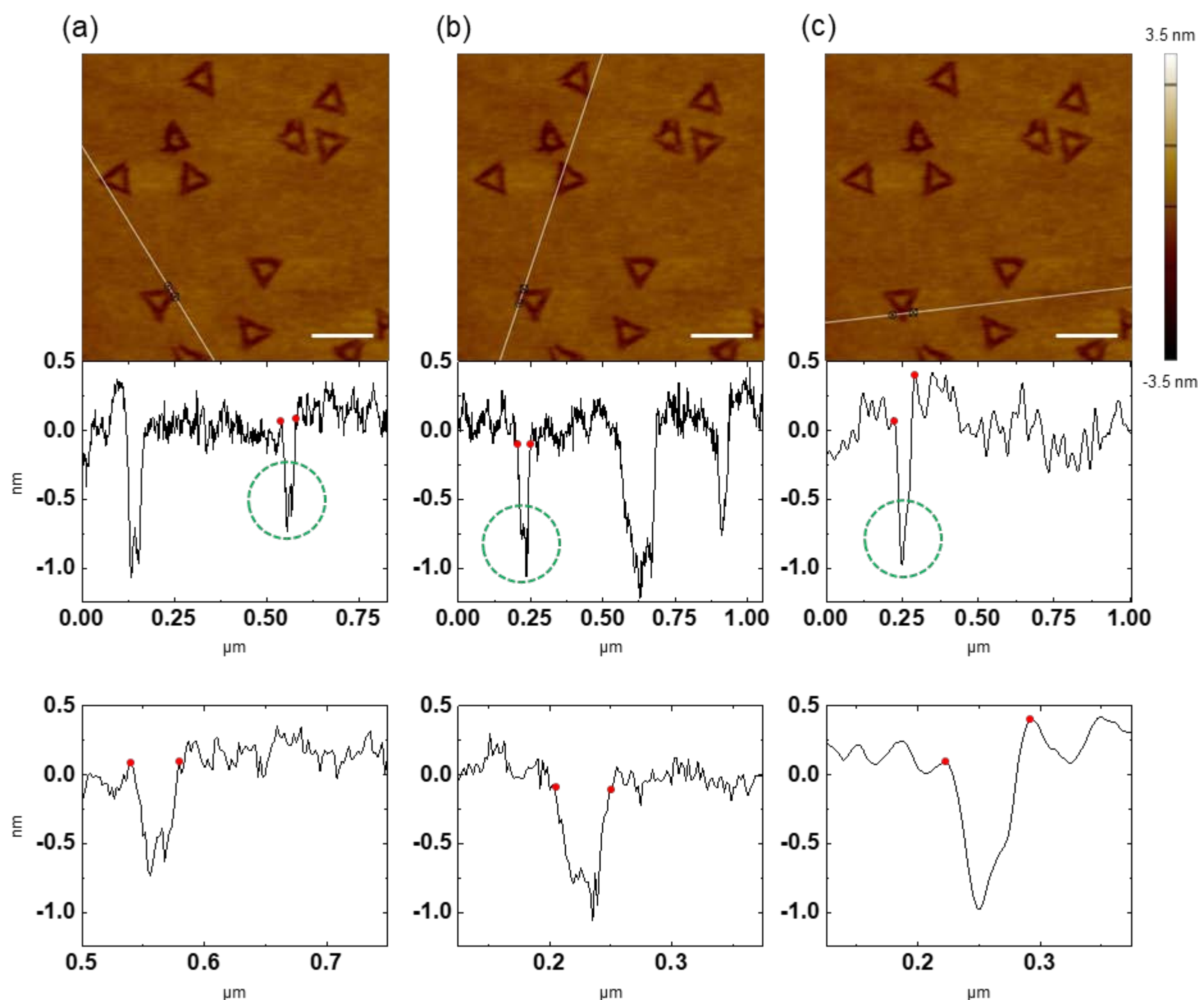

Figure 13. Analysis of vertices of triangular trenches on a PMMA stamp. (a–c) AFM height images with corresponding cross-sectional analysis of negative replicas of DNA origami triangles on a PMMA stamp. White lines on the AFM images indicate where the cross-sections were determined. Red cursors in the AFM images and corresponding cross-sections define the outer sides of the vertices that are measured. Dashed green circles (middle) highlight the curve valleys that correspond to the trenches at the vertices. In images a and b, the bump appears in the zoomed-in curve valley of the cross-section (bottom), confirming the presence of the bump at the vertex. In image c, the bump does not appear at the curve valley, indicating that no bump exists in the vertex. Scale bars represent 200 nm. Note: Images a–c are identical.

2.4.3 Fabrication of a PLLA Stamp by Replication over DNA Nanostructures

Other polymers such as PLLA could also be used as the stamp material in our method (Figures 14–16). Both DNA nanotubes and DNA origami triangles could be precisely replicated to PLLA stamps. Similar to the pattern transfer from the DNA triangles to the PMMA stamps, the dangling loops and the linear gaps between the trapezoidal domains could also be transferred to the PLLA stamps (Figure 16). The cross-sectional analysis of the AFM images indicates that the averaged depth and FWHM of triangular trenches on the PLLA stamps were 1.1 ± 0.2 nm and 27.1 ± 6.0 nm, respectively. The replication to the PLLA stamps offers a comparable resolution as observed for the PMMA stamps, demonstrating the potential for replicating DNA nanostructure patterns into a wider range of polymers.

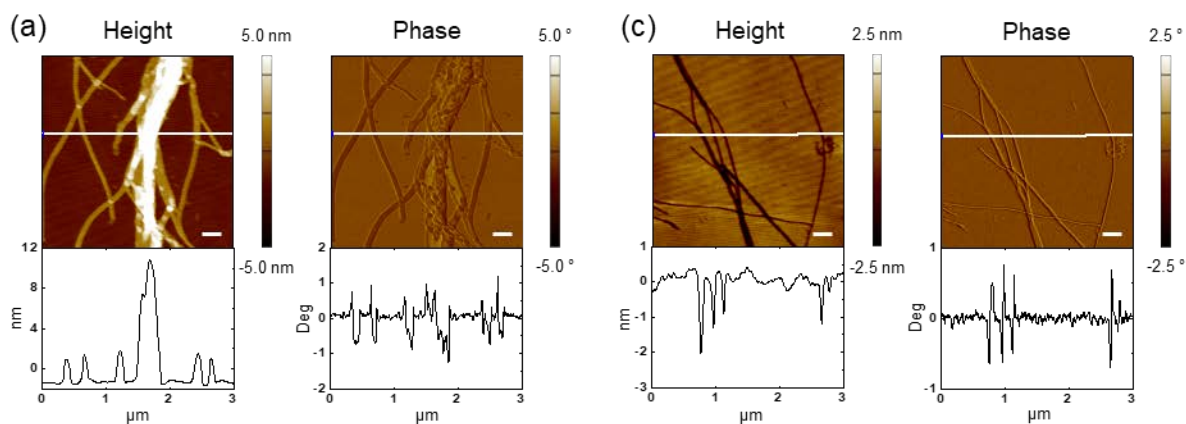

Figure 14. Fabrication of a PLLA stamp by replication over DNA nanotubes. AFM height (left) and phase (right) images with corresponding cross-sectional analysis of (a) DNA nanotubes deposited on a silicon wafer and (b) negative replicas of the DNA nanotubes on a PLLA stamp. White lines on the AFM images indicate where the cross-sections were determined. Scale bars represent 300 nm.

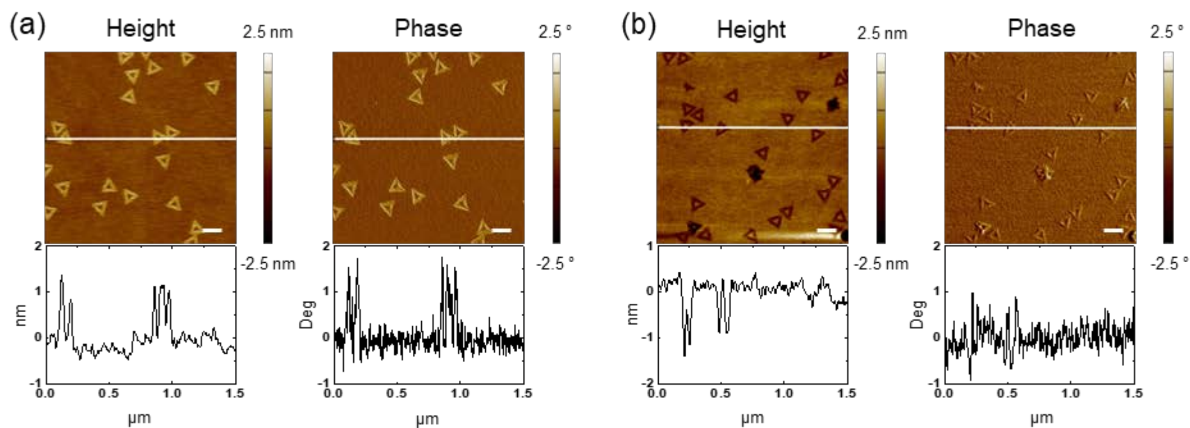

Figure 15. Fabrication of a PLLA stamp by replication over DNA origami triangles. AFM height (left) and phase (right) images with corresponding cross-sectional analysis of (a) DNA origami triangles deposited on a silicon wafer and (b) negative replicas of the DNA origami triangles on a PLLA stamp. White lines on the AFM images indicate where the cross-sections were determined. Scale bars represent 150 nm.

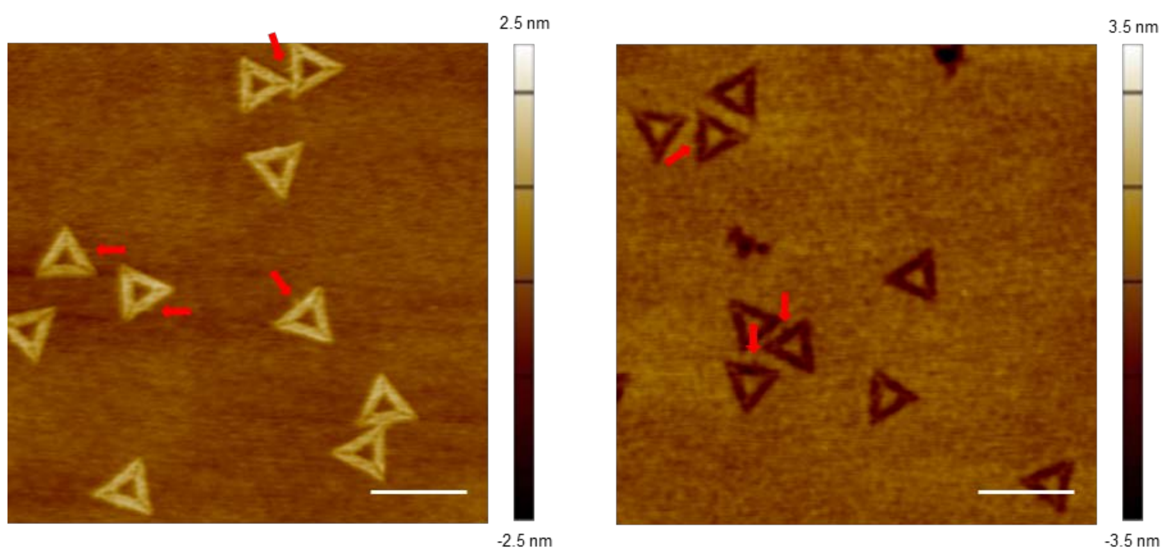

Figure 16. Analysis of dangling loops of a DNA origami triangle master template and a PLLA stamp. AFM height images of (a) DNA origami triangles deposited on a silicon wafer and (b) negative replicas of the DNA origami triangles on a PLLA stamp. The dangling loops of the DNA triangles and the corresponding patterns of the triangular trenches are indicated by the red arrows. Scale bars represent 200 nm.

2.4.4 Yield of Replication Process and Stability of a DNA Nanostructure Master Template for Pattern Replication Process to a PMMA or PLLA Stamp

To evaluate the yield of the replication process and its impact on DNA master templates, we imaged DNA master templates and polymer stamps in the same location. Figure 17 shows the height and phase images of DNA nanotube master templates and their corresponding PMMA stamps before and after the process. The negative replicas on the PMMA stamps (Figure 17c,i) matched well with the DNA nanotubes on the master templates (Figure 17a,g), demonstrating a faithful pattern transfer. However, the nanotubes were partially damaged after the replication process (Figure 17b,h), which we attribute to the water used to separate the master template and the stamp. To confirm the negative effect of water, we first used less water and decreased the incubation time (*i.e.*, the time between adding water to the master template and peeling off the polymer stamp). As a result, less DNA damage was observed (Figure 18). The DNA master templates cannot be repeatedly used to transfer the patterns to the PMMA or PLLA stamps at this stage because water, which is used to release the stamp, may damage the features of the DNA nanostructures.

The AFM phase images further support that the DNA nanostructures were not pulled off from the silicon wafer by the polymer stamp. In our method, DNA nanostructures and a silicon wafer are bound through Mg^{2+}, via an electrostatic interaction. Since the phase image is sensitive to chemical composition, if the DNA nanostructures were trapped in the trenches, they would be visible only in the phase image but not in the height image. Therefore, the yield of the pattern transfer can be also assessed by examining the consistency between the AFM height and phase images. In all the figures mentioned above, the position and shape of the features in the height

and phase images matched with each other, suggesting the absence of trapped DNA nanostructures in the polymer stamps.

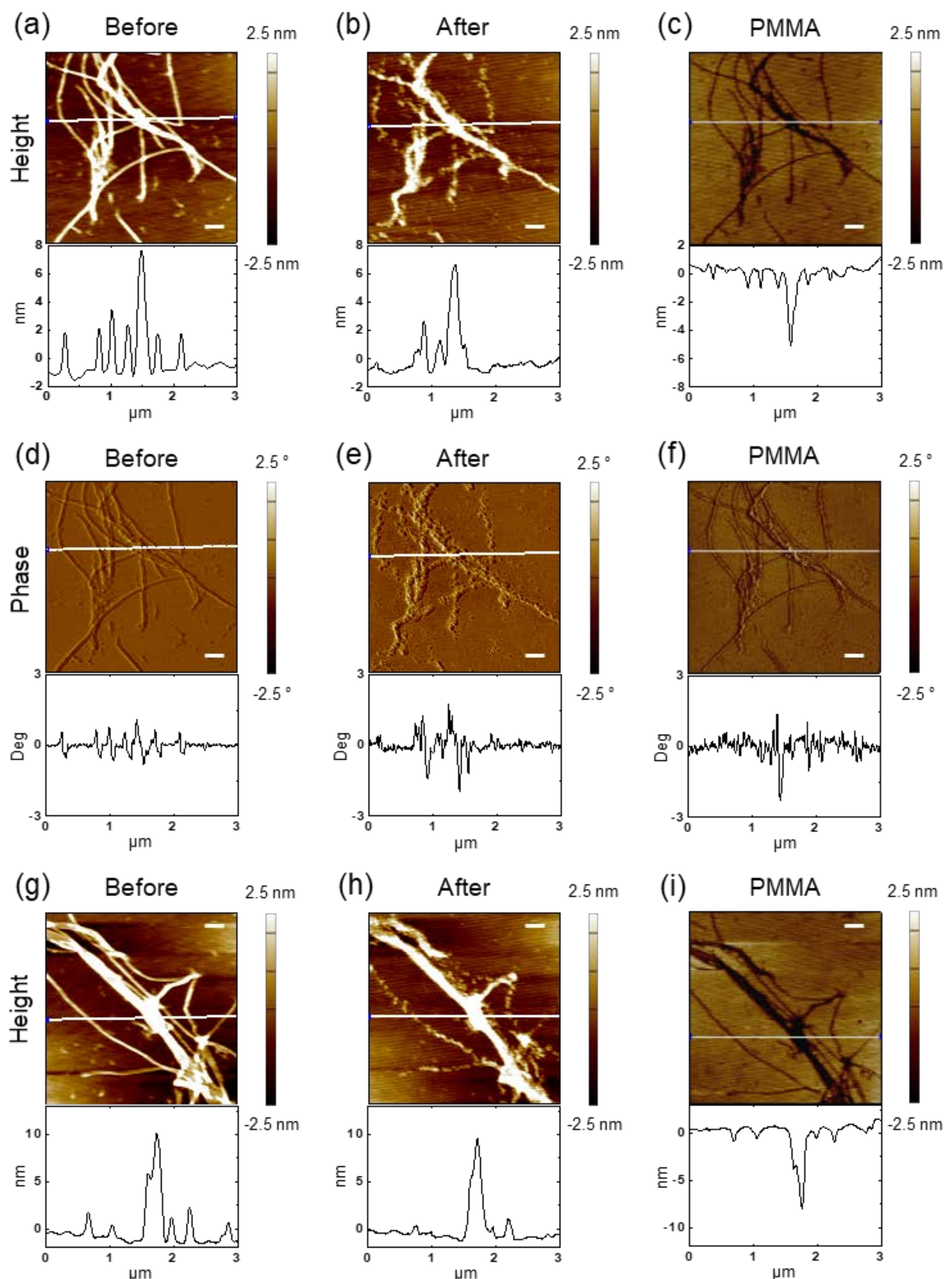

Figure 17. Yield of replication process and stability of a DNA nanotube master template after pattern replication process to a PMMA stamp. AFM height (top and bottom) and phase images (middle) with corresponding cross-sectional analysis of DNA nanotubes deposited on silicon wafers before (left) and after (middle) replication to PMMA stamps, and PMMA replicas (right) of the same area. White lines on the AFM images indicate where the cross-sections were determined. Scale bars represent 300 nm. Note: The images of the PMMA stamps were flipped horizontally to match the orientation of those of the DNA master templates.

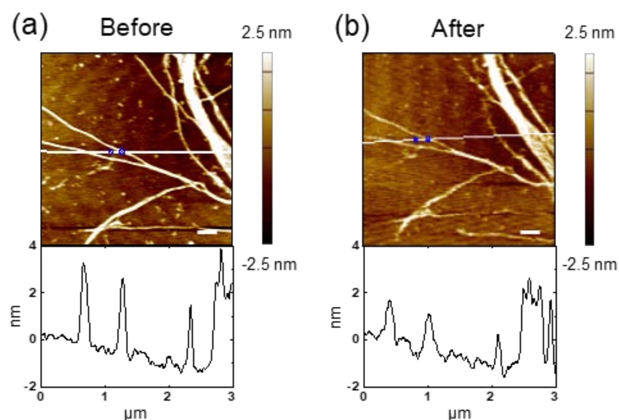

Figure 18. Stability of a DNA nanotube master template after pattern replication process to a PMMA stamp. AFM height images with corresponding cross-sectional analysis of DNA nanotubes on a silicon wafer in the same location (a) before and (b) after replication to a PMMA stamp. White lines on the AFM images indicate where the cross-sections were determined. Scale bars represent 300 nm. Compared to the results shown in Figure 12, this experiment used less water and decreased the incubation time (*i.e.*, the time between adding water to the master template and peeling off the polymer stamp).

2.4.5 Fabrication of an a-PFPE Stamp by Replication over DNA Nanostructures

DNA nanotubes were also replicated to a-PFPE polymer stamps, during which process water was not used. The AFM height images in Figure 19 illustrate that the topography of the DNA nanotubes was preserved after replication to the a-PFPE polymer, confirming that none of the DNA materials were transferred to the stamp and that water in fact causes the damage to the DNA nanostructure templates in the pattern transfer process to the PMMA films as mentioned in the previous section.

In addition to the high yield of replication, the DNA master templates can also be used in a repeated manner to transfer the patterns to the a-PFPE stamps because water is not required to release the stamps. Figure 20 shows the AFM images of the DNA nanotubes before and after 5th and 10th replication. The features of the DNA nanostructures were not damaged during the 10

times of replication. The repeated use of the DNA master templates would greatly reduce the cost and facilitate its applications. To achieve the repeated use of the DNA master templates, polymers with low surface energy (*e.g.*, a-PFPE) should be employed to facilitate the separation of the stamp from the master template without the help of water.

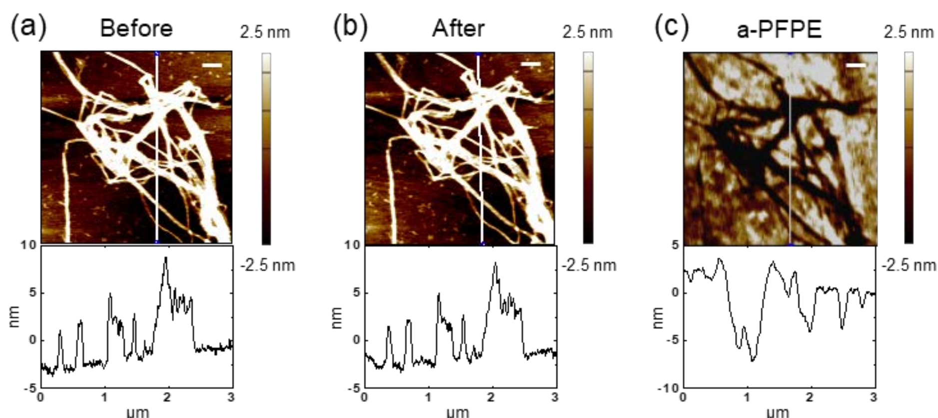

Figure 19. Fabrication of an a-PFPE stamp by replication over DNA nanotubes. AFM height images with corresponding cross-sectional analysis of DNA nanotubes deposited on a silicon wafer (a) before and (b) after replication to an a-PFPE stamp, and (c) negative replicas of the DNA nanotubes on the a-PFPE stamp of the same area. White lines on the AFM images indicate where the cross-sections were determined. Scale bars represent 300 nm. Note: Image c is flipped horizontally to match the orientation of those of the DNA master template.

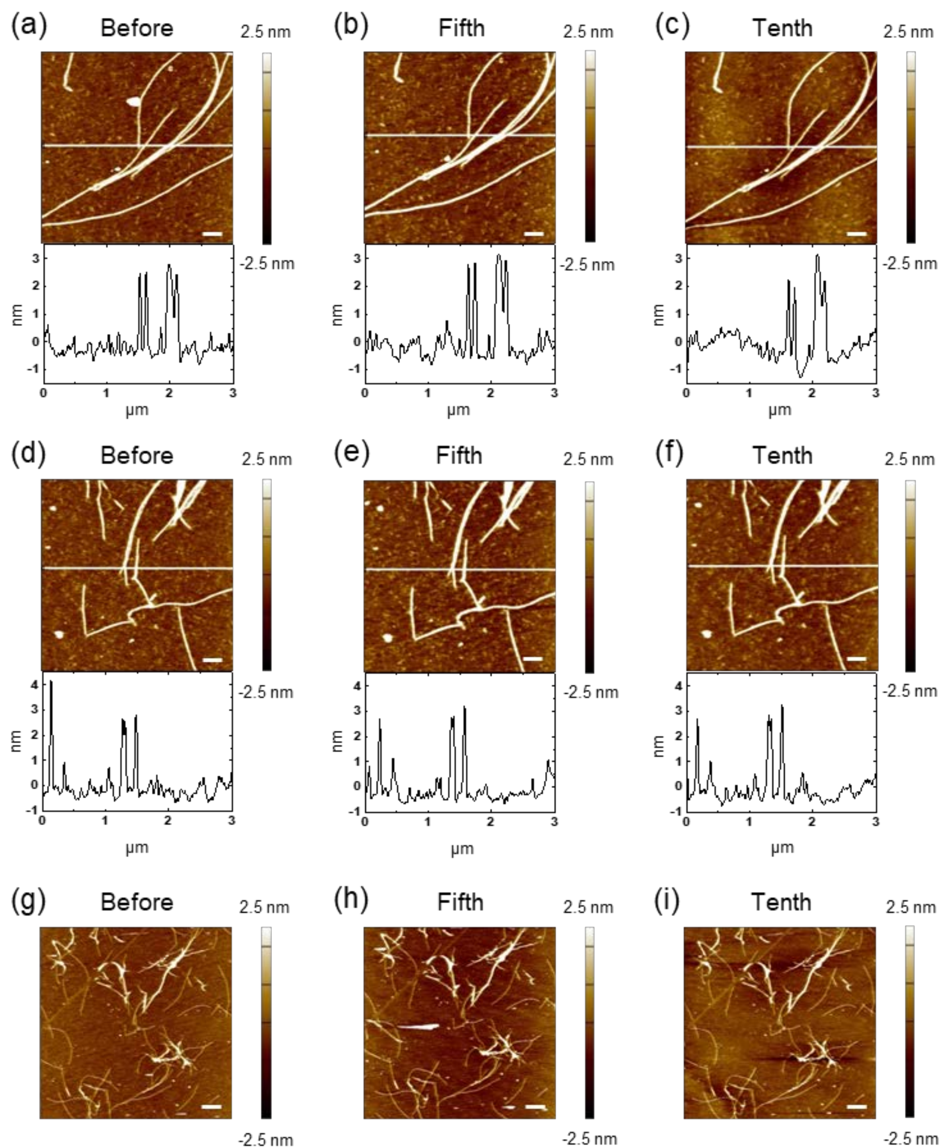

Figure 20. Stability of a DNA nanotube master template for multiple pattern replication process to a-PFPE stamps. AFM height images with corresponding cross-sectional analysis of DNA nanotubes in three different locations before (left) and after 5th (middle) and 10th (right) pattern transfer to a-PFPE stamps of the same area. White lines on the AFM images indicate where the cross-sections were determined. Scale bars represent (a–f) 300 nm and (g–i) 1.5 µm.

2.4.6 Long-term Stability of Nanoscale Features on a Polymer Stamp

The stability of the stamp is also crucial for its application of soft lithography. To assess the stability of the features on PMMA, a DNA origami triangle-patterned PMMA stamp was imaged immediately after being peeled off and again after 10 days of aging in the air (Figure 21). As mentioned above, the depth and FWHM of the triangular trenches in the fresh PMMA film were 1.0 ± 0.2 nm and 26.5 ± 3.1 nm, respectively. After 10 days of aging in the air, the triangular trenches were 0.9 ± 0.1 nm in depth and 27.8 ± 2.8 nm in width. The 10 days of aging in the air did not change the features on the PMMA film significantly. The PMMA stamps possess enough stability for long-term storage.

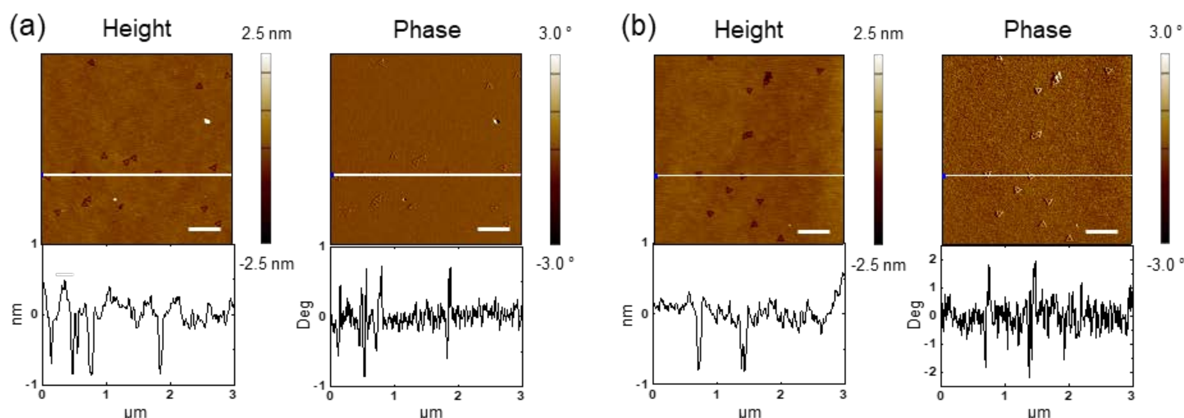

Figure 21. Long-term stability of nanoscale features on a polymer stamp. AFM height (left) and phase (right) images with corresponding cross-sectional analysis of a PMMA stamp (a) immediately after being peeled off and (b) after 10 days of aging in the air. White lines on the AFM images indicate where the cross-sections were determined. Scale bars represent 500 nm.

2.4.7 Application of a Polymer Stamp to Replica Molding

The resulting polymer stamp could serve as a mold to transfer the pattern to other materials. Figure 22 shows the replica molding of nanotube patterns on a PMMA stamp into a photo-curable a-PFPE.[36] In this experiment, the a-PFPE prepolymer solution was spin cast as a thin film on the PMMA stamp with DNA nanotube relief and then cured under UV illumination. Due to the low surface energy of a-PFPE, the PMMA and a-PFPE films could be separated. The DNA nanotube patterns were observed on the a-PFPE film with a height of 2.5 ± 0.5 nm and a width of 41.6 ± 6.9 nm, demonstrating a faithful pattern transfer from the PMMA stamp to the a-PFPE polymer film (Figure 22). Compared with the DNA nanotube master template, both the depth/height and width of the patterns on the PMMA and a-PFPE were smaller. The average height/depth and width of the DNA nanotubes, PMMA trenches, and nanotube patterns on the a-PFPE were 4.0 nm and 67.1 nm, 3.2 nm and 39.7 nm, and 2.5 nm and 41.6 nm, respectively. The exact reason for this decrease in the dimensions is not clear at this stage. One possibility is that the removal of the salt residues during the fabrication of the PMMA stamp leads to the smaller size. We also note that a similar decrease in the feature size was previously reported on replicating carbon nanotube patterns to a-PFPE and then to polyurethane.[36] In addition, the surface of the a-PFPE film has PMMA residues transferred from the PMMA stamp. The surface roughness of the a-PFPE film was measured to be 322.7 pm, which is much larger than that of the PMMA stamp (158.2 pm) before the pattern transfer although similar to that of the a-PFPE stamp (412.8 pm) that was produced directly from the DNA master template and shown in Figure 19. We attribute the high surface roughness of the a-PFPE film fabricated from the PMMA stamp to the solubility of PMMA in the a-PFPE prepolymer solution during the molding process and the intrinsic property of a-PFPE as the high surface roughness of this material was

also reported before.[36] Besides the PMMA stamp, the PLLA stamp could also serve as a mold to transfer the pattern to the a-PFPE with comparable fidelity (Figure 23).

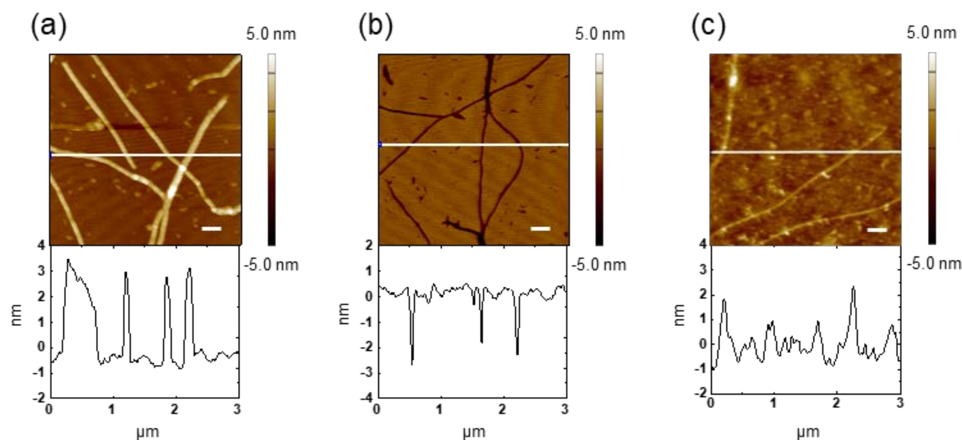

Figure 22. Application of a PMMA stamp to replica molding. AFM height images with corresponding cross-sectional analysis of (a) DNA nanotubes on a silicon wafer, (b) negative replicas of the DNA nanotubes on a PMMA stamp, and (c) positive replicas of the DNA nanotubes on an a-PFPE substrate transferred from the PMMA stamp by replica molding. White lines on the AFM images indicate where the cross-sections were determined. Scale bars represent 300 nm. Note: Images a and b are also shown in Figure 7.

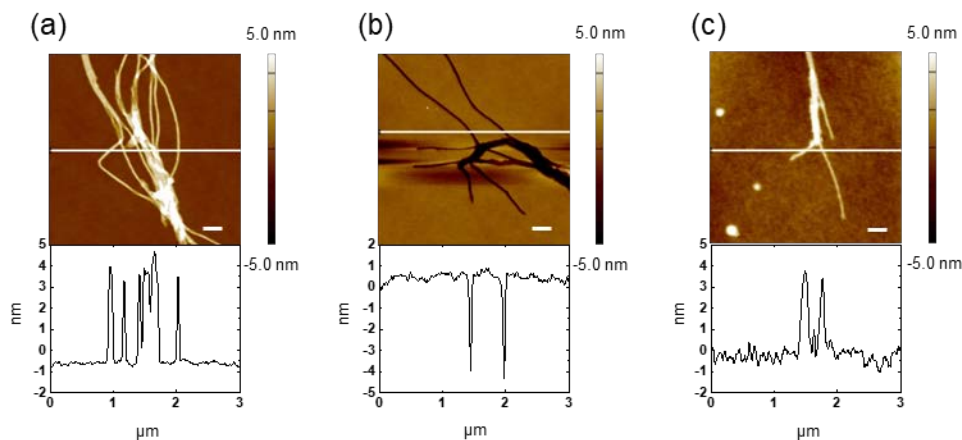

Figure 23. Application of a PLLA stamp to replica molding. AFM height images with corresponding cross-sectional analysis of (a) DNA nanotubes on a silicon wafer, (b) negative replicas of the DNA nanotubes on a PLLA stamp, and (c) positive replicas of the DNA nanotubes on an a-PFPE substrate transferred from the PLLA stamp by replica molding. White lines on the AFM images indicate where the cross-sections were determined. Scale bars represent 300 nm.

Finally, we investigated the repeated use of the polymer stamp for the application of replica molding. We found that the polymer stamp often delaminated from the PDMS backing layer and/or broke during the separation of the stamp from the a-PFPE film. We attribute this observation to the micrometer-scale thinness of the stamp and its low affinity to PDMS. We were still able to verify that the nanoscale features on both the PMMA and PLLA stamps were not damaged after molding the a-PFPE films (Figure 24) although the surface of the PMMA stamp became rougher as the PMMA residues moved along with the a-PFPE film during the separation process (Figure 24a). Therefore, the polymer stamp should be reusable if an alternative molding process could be developed to protect the physical integrity of the polymer stamp. We note that others have reported the repeated use of polymer stamps, including PMMA, for replica molding and other nanoscale patterning applications.[140-147] Work is underway to fully explore the applications of the polymer stamps that we produced in this study.

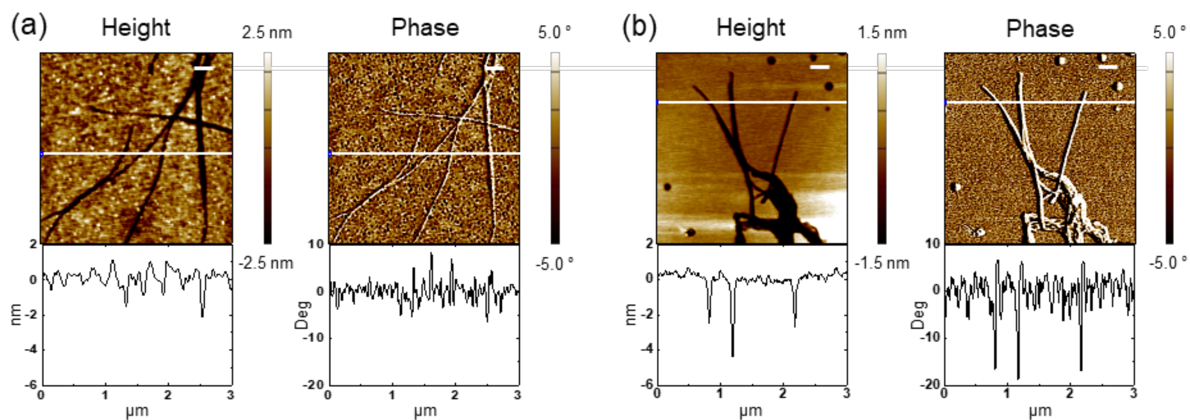

Figure 24. Stability of nanoscale features on PMMA and PLLA stamps during replica molding. AFM height (left) and phase (right) images with corresponding cross-sectional analysis of (a) PMMA and (b) PLLA stamps after transfer of pattern to a-PFPE. White lines on the AFM images indicate where the cross-sections were determined. Scale bars represent 300 nm.

2.5 CONCLUSIONS

We have demonstrated a general method of fabricating polymer stamps using DNA nanostructure master templates with high fidelity. DNA nanotubes, 1D λ-DNAs, 2D DNA brick crystals with 3D features, hexagonal DNA 2D arrays, and DNA origami triangles have been tested as master templates to replicate their features to PMMA, PLLA and photo-crosslinked a-PFPE. The resulting PMMA and PLLA stamps have been further applied as molds to transfer the patterns to a-PFPE. In addition to replica molding, the polymer stamp can be potentially used in many other applications, such as in particular contact printing of small molecules and proteins.[112-113, 147-148] Since DNA master templates with diverse features can be rationally designed and constructed, our method could enable the fabrication of polymer stamps with the varieties of nanoscale features, some of which (*e.g.*, alphabets) are inaccessible by other self-assembly methods. The integration of DNA nanotechnology with soft lithography offers alternative master templates and enriches the nanoscale features of polymer stamps to facilitate their applications.

In our method, the separation of the polymer stamp from the DNA nanostructure master template relies on using water to lower the adhesion between the film and the template. The additional key advantages of our method are that any polymer with hydrophobicity and/or low surface energy can be patterned with and easily peeled off of the DNA nanostructure master template. Furthermore, the glass transition temperature (T_g) of the polymer does not have to be above the temperature at which the polymer is spin-coated onto the master template, but just above the temperature at which the patterned polymer is processed with further application.

To apply DNA nanostructures in the scalable nanofabrication, the limitation of the large-area patterning in our method must be overcome. High-throughput nano-patterning is important for the nanofabrication and has been realized by electron-beam lithography[149-150] and the directed self-assembly of block copolymer.[26-28] However, the difficulties of controlling deposition of DNA nanostructures and defects in the self-assembled DNA nanostructures limit their applications in the large-area patterning. Further studies are still needed to address these challenges. In addition, the technical issues associated with the repeated use of the polymer stamp in our method need to be solved. At the current stage, this challenge could be compensated by generating multiple copies of a polymer stamp based on a DNA master template. Ways to increase the chemical and mechanical stability of the DNA nanostructure master template (*e.g.*, by a conformal coating of an inorganic oxide film[103, 105]) are being explored to further facilitate the scalable nanofabrication using this template.

3.0 INCREASING THE STABILITY OF DNA NANOSTRUCTURE TEMPLATE BY ATOMIC LAYER DEPOSITION OF ALUMINIUM OXIDE AND ITS APPLICATION IN IMPRINTING LITHOGRAPHY

3.1 CHAPTER PREFACE

Materials contained in this chapter were published as a research article in *Beilstein Journal of Nanotechnology Thematic Series "Nanoscale patterning and characterization"*; figures used in this chapter have been reprinted from: *Beilstein Journal of Nanotechnology*, 2017, *8*, pp 2363–2375.

List of Authors: Hyojeong Kim, Kristin Arbutina, Anqin Xu, and Haitao Liu

Author Contributions: H.K., and H.L. designed and directed the experiments. H.K., K.A., and A.X. conducted the experiments. All authors discussed the results. H.K., and H.L. wrote the manuscript with input from all authors.

3.2 INTRODUCTION

In 1982, Seeman first introduced the idea of utilizing DNA to build a mechanically robust nanostructure.[50] Since then, the field of structural DNA nanotechnology has evolved remarkably from immobile Holliday junctions to complex shapes fabricated from single-stranded tiles.[52, 116] Through rational design, the self-assembly of DNA can be brought into almost any shape with nanometer-scale precision and accuracy. Examples of such structures are one-dimensional (1D),[61, 72, 119-120] two-dimensional (2D),[39, 44, 59, 121] and three-dimensional (3D)[41, 43, 73, 151] nanostructures with diverse and complex features. Therefore, self-assembled DNA nanostructures are considered to be ideal templates for nanofabrication because it is easy to control their structural complexity and diversity at the nanoscale.

Many approaches have been developed to use DNA nanostructures as templates to pattern a wide range of materials, such as proteins,[60, 81-83] carbon nanotubes,[84-87] and metal nanoparticles[60, 81, 94, 96, 127-130] through the direct assembly of these materials onto the DNA nanostructures. Metallized DNA nanostructures have been used to pattern graphene.[131] DNA nanostructures have also been used as masks. The patterns of 1D DNA nanotubes and 2D DNA arrays were replicated to metal films by metal evaporation onto the DNA nanostructures and subsequent lift-off of the metal films.[100] Aligned DNA molecular bundles were used as shadow masks for angled metal vapor deposition and the exposed substrate within the shadow gaps was etched to generate trenches with linewidths of sub-10 nm resolution.[101] By differentiating the adsorption of water between DNA nanostructures and a SiO_2 substrate, the rates of HF vapor-phase etching of the SiO_2 substrate[102] and of chemical vapor deposition of SiO_2 and TiO_2 on the DNA nanostructures and the substrate[103] were modulated to replicate the patterns of the DNA nanostructures into those of the inorganic oxides. In both cases, the patterns of the nanostructures

were transferred in both positive and negative tone at room temperature. Similarly, DNA nanostructures were likewise used in the anhydrous HF vapor etching of a SiO_2 substrate, producing the positive imprints of the DNA nanostructures with sub-10 nm resolution.[104] DNA nanostructures were also converted into carbon nanostructures with shape conservation by atomic layer deposition of Al_2O_3 onto the nanostructures followed by thermal annealing.[105] In addition to the 2D pattern transfer processes, gold nanoparticles with specified 3D shapes were synthesized by growing seed particles in the internal cavities of 3D DNA nanostructures.[98-99]

Compared to the above developments, there are only a limited number of studies of using DNA nanostructures as master templates for soft lithography. Soft lithography relies on elastomeric stamps or molds bearing fine features of relief on their surfaces to transfer patterns.[113] The spatial resolution and diverse features of the relief structures on the stamps intrinsically limit the application of soft lithography. Thus, the preparation of master templates, where the stamps are derived, has become an important research area. State-of-the-art technologies for the fabrication of the master templates are deep ultraviolet lithography (DUV) and electron-beam lithography (EBL). However, both lithography techniques are not suitable to provide sub-10 nm resolution. DUV with ArF lasers (λ = 193 nm) and water immersion lenses is not able to provide a structure with spacing less than 40 nm because of its diffraction-limited resolution.[152] Although EBL is capable of reaching resolutions below 10 nm,[13] it is difficult to produce the master templates in larger numbers because of its high cost.[149-150, 153] In 2015, the aligned patterns of natural salmon milt DNA bundles were first transferred to negative replicas on an unsaturated polyester resin, which were further used to pattern positive replicas on a water-swollen polyacrylamide gel.[106] However, the shape of the DNA bundles is limited to 1D patterns, and their dimensions are relatively large compared to the resolution of the state-of-the-art

lithographic techniques. The average height and width of the DNA bundles were 90.5 ± 3.1 nm and 879 ± 23 nm, respectively.

Taking one step further in this direction, we have recently used DNA nanostructures as master templates for a direct pattern transfer to polymers with high diversity, complexity, and fidelity.[154] A wide range of DNA nanostructures, including DNA nanotubes, 1D λ-DNAs, 2D DNA brick crystals with 3D features, hexagonal DNA 2D arrays, and DNA origami triangles, were tested for the pattern replication process to poly(methyl methacrylate) (PMMA), poly(L-lactide) (PLLA), and photo-cross-linked acryloxy perfluoropolyether (a-PFPE). The resulting negative imprints of the DNA nanostructures on the PMMA and PLLA polymer stamps further served as molds to transfer the patterns to positive imprints on a-PFPE films. In our method, the separation of the polymer film from the DNA nanostructure master template relies on using water to lower the adhesion between the film and the template. The key advantage of our method is that any polymer with hydrophobicity and/or low surface energy can be patterned with the DNA nanostructure master template. Furthermore, because the method uses spin-coating instead of hot-pressing, it is compatible with polymers having a wide range of glass transition temperatures (T_g).

With our method, polymer stamps can be made with nanoscale features of dimensions ranging from several tens of nanometers to micrometers by logically designing and synthesizing DNA nanostructures. Our approach has one substantial technical problem, however, which is that the DNA nanostructure master templates cannot be used in a repetitive manner. The DNA nanostructures were partially damaged during the release of the PMMA and PLLA hydrophobic stamps from the hydrophilic master template. It still remains a challenge to develop an approach to increase the stability of the DNA nanostructure master templates.

In this paper, we establish a method to increase the chemical and/or mechanical stability of DNA nanostructure master templates by a nanometer-thin conformal coating of a protective inorganic oxide film grown by atomic layer deposition (ALD). We test the stability of DNA nanotube master templates with an Al_2O_3 layer against repeated pattern transfer, long-term storage and exposure to UV/O_3. The effect of thickness of the Al_2O_3 layer on the qualities of pattern transfer and shape conservation is also explored.

3.3 EXPERIMENTAL SECTION

3.3.1 Materials

Silicon wafer [Si (110), with native oxide] and M13mp18 scaffold strand for DNA origami triangles were purchased from University Wafers (South Boston, MA) and Bayou Biolabs (Metairie, LA), respectively. Staple strands for the DNA origami triangles and single strand for DNA nanotubes were synthesized by Integrated DNA Technologies (Coralville, IA). 2-Amino-2-(hydroxymethyl)-1,3-propanediol (Trizma base), ethylenediaminetetraacetic acid (EDTA), magnesium acetate tetrahydrate, sulfuric acid, hydrogen peroxide solution (30% H_2O_2), and poly(L-lactide) were purchased from Sigma-Aldrich (St. Louis, MO). Acetic acid (glacial), dichloromethane, and ethanol were purchased from Fisher Scientific (Fair Lawn, NJ), Acros Organics (Fair Lawn, NJ), and Decon Laboratories, Inc. (King of Prussia, PA), respectively. Polydimethylsiloxane (PDMS) backing stamp was fabricated with Sylgard 184 silicone elastomer kit (Dow Corning, Midland, MI). All materials were used as received. High-purity water (18.3 MΩ) was used throughout the entire experiment by using a Barnstead MicroPure Standard water purification system (Thermo Scientific, Waltham, MA).

3.3.2 Preparation of a Silicon Wafer

A silicon wafer with a native oxide layer was cleaned by hot piranha solution [7:3 (v/v) concentrated H_2SO_4/30% H_2O_2]. After H_2O_2 was slowly added to concentrated H_2SO_4 in a glass petri dish containing the silicon wafer, a glass cover was placed and a heating plate was set to 40 °C. After 20 minutes, the heating plate was turned off and the piranha solution was allowed to cool down for an additional 10 minutes. The wafer was thoroughly washed with deionized water and dried with N_2 gas. *Warning: Piranha solution is a strong oxidizing reagent and reacts violently with organic materials. All work should be handled in a fume hood with extra caution. Proper protective equipment is required.*

3.3.3 Preparation of a PDMS Backing Film

PDMS precursor was mixed with curing agent at a 9:1 (v/v) ratio. The prepolymer mixture was vigorously stirred by hand at least for 5 minutes and degassed in a vacuum desiccator. The mixture was poured over a piranha cleaned silicon wafer. The wafer with the mixture was placed in the vacuum desiccator for further degassing. The PDMS prepolymer on the silicon wafer was cured for 1 hour at 60 °C. The thickness of the resulting PDMS layer was *ca.* 1–2 mm.

3.3.4 Preparation and Deposition of DNA Nanostructures on a Silicon Wafer

3.3.4.1 Preparation and deposition of DNA nanotubes on a silicon wafer

The design and assembly of DNA nanotubes followed a previously published procedure.[119] Single strands of DNA nanotubes were diluted to a final concentration of 1 μM in 10 × TAE/Mg^{2+} buffer (125 mM Mg^{2+}). The DNA single strand solution was slowly cooled from 95 to 23 °C over 2 days and stored at 4 °C overnight. The annealed DNA nanotubes were assembled on a clean silicon wafer by incubating the DNA nanotube solution on the wafer for a minimum of 15 minutes in a humid chamber to minimize the evaporation of the buffer solution. The sample was dried with N_2 gas, immersed in an ethanol/water [9:1 (v/v)] solution for 10 seconds to remove ionic salt residues from the buffer solution, and re-dried with N_2 gas. After the deposition, the DNA nanotube master template was processed with ALD of Al_2O_3 within 24 hours.

3.3.4.2 Preparation and deposition of DNA origami triangles on a silicon wafer

DNA origami triangles were designed and assembled following a formerly reported method.[39] M13mp18 scaffold strand (8.6 μL, 1.6 nM) was thoroughly mixed with a desired set of synthetic 232 short staple strands (15 μL, 16 nM), deionized water (77 μL), and TAE/Mg^{2+} buffer solution (181 μL). The buffer solution was prepared by dissolving Trizma base (40 mM), EDTA (2 mM), acetic acid (2mM), and magnesium acetate tetrahydrate (150 mM) in deionized water and further diluting the solution to make the final concentration of magnesium ions 12.5 mM. The DNA solution was cooled from 95 to 20 °C at a rate of 1 °C/min. After the annealing, excess staple strands were removed by purifying 140 μL of the DNA origami triangle solution using 500–600 μL of the TAE/Mg^{2+} buffer in a Microcon YM-100 100 kDa MW centrifuge filter (Millipore,

Billerica, MA) on a single-speed benchtop Galaxy Ministar microcentrifuge (VWR, Radnor, PA) until the final volume of the DNA origami triangle solution was the same as before the purification. This rinsing process was repeated two more times.

DNA origami triangles were assembled on a clean silicon wafer by incubating the purified DNA solution on the wafer for a minimum of 15 minutes in a humid chamber to minimize the evaporation of the buffer solution. The sample was dried with N_2 gas, immersed in an ethanol/water [9:1 (v/v)] solution for 3 seconds to remove ionic salt residues from the buffer solution, and re-dried with N_2 gas. After the deposition, the DNA origami triangle master template was processed with ALD of Al_2O_3 within 24 hours.

3.3.5 Atomic Layer Deposition (ALD) of Al_2O_3 as a Protective Inorganic Film on a DNA Master Template

ALD of Al_2O_3 on a DNA/SiO_2 substrate followed a previously published method.[105] ALD was conducted using a Fiji ALD system by Norman Gottron in Nanofabrication Facility at Carnegie Mellon University (Ultratech/CNT, Waltham, MA). The chamber and substrate heaters were set to 200 °C. Total Ar gas flow was at 260 sccm and 200 mTorr. Trimethylaluminum (TMA) and H_2O were used as precursors and one ALD cycle consisted of a 0.06 s long TMA pulse, a 10 s long interval, a 0.06 s long H_2O pulse and a 10 s long interval. The deposition was looped 20 times, 50 times, and 200 times for the 2 nm, 5 nm, and 20 nm preset deposition thickness of the oxide films, respectively.

3.3.6 Fabrication of a PLLA Stamp by Replication over DNA Nanostructures with a Protective Al_2O_3 Film

PLLA stamps were fabricated following our previously demonstrated procedure.[154] PLLA in dichloromethane solution (3 wt. %) was spin-coated four times onto a DNA nanostructure master template with an Al_2O_3 film at 4000 rpm for 30 seconds. Around the edges of the PLLA film, the surface perimeter of the PLLA film with a width of *ca.* 1 mm were scraped off to expose the underlying template. A PDMS layer with a thickness of *ca.* 1–2 mm was placed on top of the PLLA film as a backing support. Droplets of water were added to the exposed edges of the template. If the water droplets filled out the interface between the PLLA film and the PDMS backing stamp, they were removed using a paper wiper to increase the adhesion between the polymer film and the backing stamp. After a minute, the PDMS/PLLA film was peeled off and the surface of the PLLA film was gently dried with N_2 gas.

3.3.7 UV/Ozone Treatment

A DNA nanotube master template with an Al_2O_3 film was placed in a PSD Pro 4 Digital UV Ozone Cleaner (Novascan Technologies, Inc., Ames, IA). Before UV irradiation, the chamber was flushed with O_2 for 3 minutes, and the sample was subjected to UV/O_3 treatment for 1 hour at room temperature.

3.3.8 Characterization

3.3.8.1 Ellipsometry

The experimental thickness of an Al_2O_3 film was measured by an Alpha-Spectroscopic Ellipsometer with Complete Ease Software using Cauchy model (JA Woollam Co., Lincoln, NE). The duration time was "Standard" and the measurement angle was 70°. For each sample, the average thickness of the Al_2O_3 layer was obtained by measuring the thickness with mean square error values below 5 at five different locations.

3.3.8.2 Atomic force microscopy (AFM)

The surface morphologies of a DNA nanostructure master template and a PLLA stamp at each step of fabrication process were imaged using tapping-mode on an MFP-3D atomic force microscope with RTESPA-300, NSC15/Al BS, or SSS-FMR-SPL AFM probe in air at room temperature (Oxford Instruments Asylum Research, Inc., Santa Barbara, CA). The RTESPA-300 (300 kHz, 40 N/m) and NSC15/AL BS (325 kHz, 40 N/m) AFM probes were purchased from Bruker (Camarillo, CA) and MikroMasch (Lady's Island, SC), respectively, and used to scan the DNA nanotube master templates and the corresponding PLLA stamps. The SSS-FMR-SPL AFM probe (75 kHz, 2.8 N/m) was purchased from NanoAndMore USA (Watsonville, CA) and was used to scan the DNA origami triangle master templates and the corresponding PLLA stamps.

3.4 RESULTS AND DISCUSSION

3.4.1 General Fabrication Process of a Polymer Stamp using a DNA Nanostructure Master Template with a Protective Al_2O_3 Film

A DNA nanostructure master template with a protective Al_2O_3 film and a corresponding PLLA stamp were adapted from our previously published method[154] and the fabrication process is shown in Figure 25. DNA nanostructures were deposited onto a silicon wafer with native oxide that was cleaned by piranha solution (Figure 25a). The entire surface of the DNA nanostructure master template was coated with a layer of Al_2O_3 by atomic layer deposition (ALD) (Figure 25b). After the ALD process, PLLA solution in dichloromethane (3 wt. %) was spin-coated onto the template to prepare a PLLA film (Figure 25c). Around the edges of the silicon wafer, the PLLA film was scraped off with a blade and the silicon wafer underneath the PLLA film was revealed (Figure 25d). A PDMS layer was placed on top of the PLLA film serving as a flexible backing support to assist in the separation of the polymer film from the template (Figure 25e). Drops of water were added to the exposed edges of the template, separating the hydrophobic PLLA film from the hydrophilic master template by penetration of the interface between them. After one minute, the PDMS/PLLA film was peeled off and the negative replica of positive pattern of the DNA nanostructure master template formed on the sub-surface of the PLLA film that was in conformal contact with the DNA (Figure 25f).

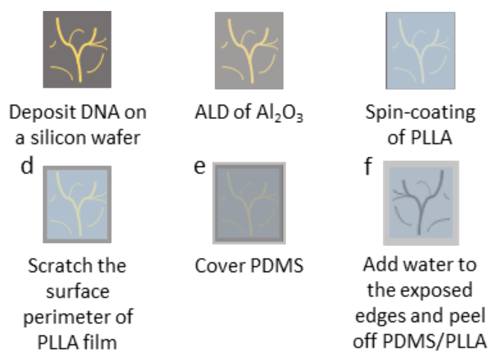

Figure 25. General fabrication process of a polymer stamp using a DNA nanostructure master template with a protective Al_2O_3 film. (a) DNA nanostructures are deposited on a silicon wafer. (b) The silicon wafer is coated with Al_2O_3 by atomic layer deposition. (c) A polymer film (*e.g.*, PLLA) is spin-coated onto the silicon wafer. (d) The four edges of the polymer film (*ca.* 1 mm wide) are scraped off with a blade. (e) A PDMS layer is adhered to the polymer film as a backing support. (f) Droplets of water are added to the exposed edges of the silicon wafer and the PDMS/PLLA film is peeled off.

3.4.2 Fabrication of a PLLA Stamp by Replication over a DNA Nanotube Master Template with a 2 nm or 5 nm Al_2O_3 Film

3.4.2.1 Fabrication of a PLLA stamp by replication over a DNA nanotube master template with a 2 nm Al_2O_3 film and long-term stability of nanoscale features on a polymer stamp

We first evaluate the fabrication process using a self-assembled DNA nanotube template. These DNA nanotubes are 30–70 nm in width and up to 60 µm in length.[119] The nanotubes are collapsed after deposition onto a silicon wafer, showing an average height (n = 10) of 3.4 ± 0.1 nm by atomic force microscopy (AFM). The surface topography of the DNA nanotube master template before (Figure 26a) and after (Figure 26b) deposition of a *ca.* 2 nm thick Al_2O_3 layer and the corresponding PLLA film (Figure 26c) were characterized by AFM. On the DNA nanotube master template, single DNA nanotubes are observed along with some bundles. After the PLLA stamp was peeled off, the negative replicas of the DNA nanotubes were observed on

the polymer stamp, demonstrating a faithful replication process. To quantify the degree of conservation of the surface topography, height/depth and full width at half maximum (FWHM) were measured in four different locations in the AFM images and compared at the same locations throughout the fabrication process (Figure 26f,g). Taking location 1 as an example, the height of the DNA nanotube before (3.73 nm) and after (3.39 nm) the ALD of Al_2O_3 film was in good agreement with the average depth of the trench (3.32 nm, measured three times at location 1 over a 15 day period) on the PLLA stamp. The FWHM of the nanotube (46.99 nm) slightly decreased after the ALD (41.14 nm) but was significantly larger than the average FWHM of the trench (23.50 nm) on the polymer stamp. The decrease of the FWHM after the ALD is suspected to be due to the dehydration of the nanotube during the ALD process and/or the differences in the probe-substrate and probe-sample interactions of individual AFM tips, which can give the different measurements of the same sample. We attribute the decrease in the FWHM from the DNA nanotube master template to the PLLA stamp to the AFM probe convolution effect. These results confirm a faithful pattern transfer from the DNA nanotube master template to the PLLA stamp through the ALD of Al_2O_3 layer on the template with high fidelity. Moreover, the patterned PLLA stamp was found to be stable at room temperature. We stored the stamp in a plastic petri dish and imaged it again after 1 week (Figure 26d) and 2 weeks (Figure 26e) at the same location. Both the depth and FWHM of the trenches along with cross-sectional analysis on the PLLA stamp at the four locations remained consistent, demonstrating the long-term stability of the PLLA stamp.

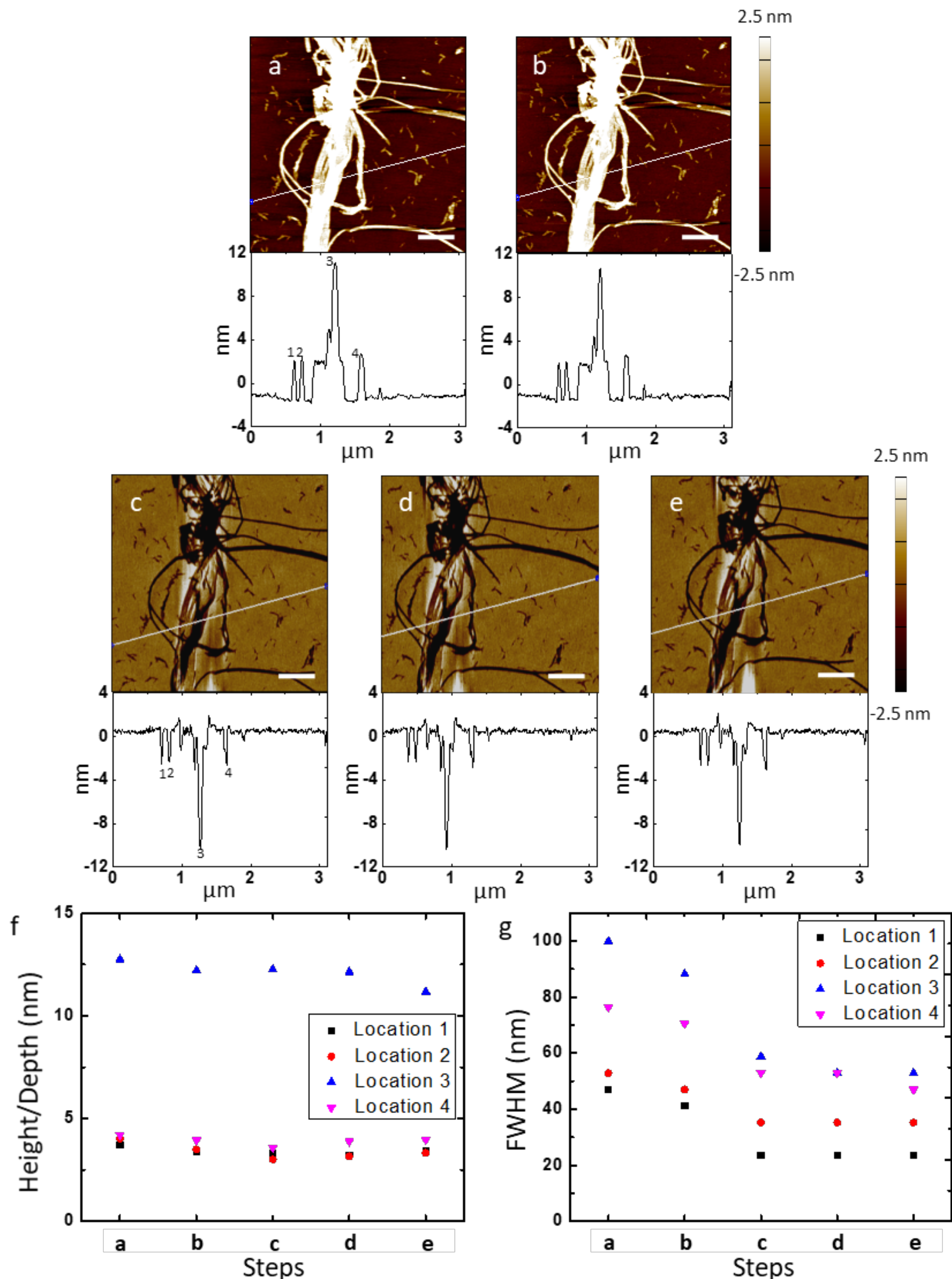

Figure 26. Fabrication of a PLLA Stamp by replication over a DNA nanotube master template with a 2 nm Al_2O_3 film and long-term stability of nanoscale features on a polymer stamp. AFM height images with corresponding cross-sectional analysis of DNA nanotubes after (a) deposited on a silicon wafer and (b) 20 cycles of ALD of Al_2O_3, and negative replicas of the DNA nanotubes on a PLLA stamp imaged (c) 1, (d) 8, and (e) 15 days after pattern transfer of the same area. White lines on the AFM images indicate where the cross-sections were determined. (f) Height/depth and (g) FWHM of the DNA nanotubes and their replica trenches in four different locations of the images from a to e. Locations 1, 2, 3, and 4 correspond to 1, 2, 3, and 4 in the cross-sections of images a and c. Scale bars represent 500 nm. Note: The images from c to e are diagonally flipped to match the orientations of images a and b.

3.4.2.2 Stability of a DNA nanotube master template with a 2 nm Al_2O_3 film for multiple pattern replication process to polymer stamps

As mentioned earlier, the most critical challenge of using a DNA master template without a protective film is the potential damage to the DNA during the separation of the polymer film from the template.[154] We attribute such damage to the water used to assist in the separation. The DNA nanostructures were still damaged even if we replaced the water with the buffer solution that was used to synthesize and store the DNA nanostructures (Figure 27). To evaluate the effectiveness of the protective Al_2O_3 film on the DNA master template, we imaged the DNA nanostructures in the same location after deposited on a silicon wafer, after 20 cycles of ALD of Al_2O_3, and after 1st, 2nd, 3rd, 4th and 5th replication to PLLA stamps (Figures 28a–g and 29a–f). As the AFM images indicate, the surface morphology of the DNA template was still well maintained after the 1st pattern transfer (Figures 28c and 29b), showing that the stability of the nanostructures was increased by the *ca.* 2 nm thick Al_2O_3 film. However, as the replication process was repeated another four more times, the overall height of the DNA nanostructures decreased although their shape was unchanged. To highlight the change in the height of the DNA nanostructures, we plot the height distribution of the AFM images in Figure 28i. The height difference between the absolute maximum peak (which represents the background silicon wafer) and the next relative maximum peak (which represents the height of the DNA nanotubes) significantly decreased during the 3rd replication process. The height and FWHM with cross-sectional analysis of the DNA template at the three same locations further support the change in the height of the template (Figure 28j,k). The FWHM at all three locations was comparable during the 3rd replication process. The height of the DNA nanotube bundle decreased from 10.90 nm to 7.12 nm, while the height of the single DNA nanotubes decreased from 3.97 nm and 3.70

nm to 3.32 nm and 2.85 nm, respectively. These results indicate that the higher feature (decrease of *ca.* 35% of its initial height) on the template is less mechanically stable than the lower one (decrease of *ca.* 15% of its initial height). Along this direction, holes were also formed after the 2nd and 5th pattern transfer to the PLLA stamps, highlighted by the yellow arrows (Figure 29c,f). The AFM height and phase images with cross-sectional analysis of the hole after the 5th pattern transfer show that the depth of the hole matched well to the thickness of the Al_2O_3 layer and the bundle of the DNA nanotubes originally presented in the hole was removed, possibly by the water used during the separation of the stamp (Figure 29h,i). Overall, the protective 2 nm Al_2O_3 layer marginally increases the stability of the DNA nanostructures.

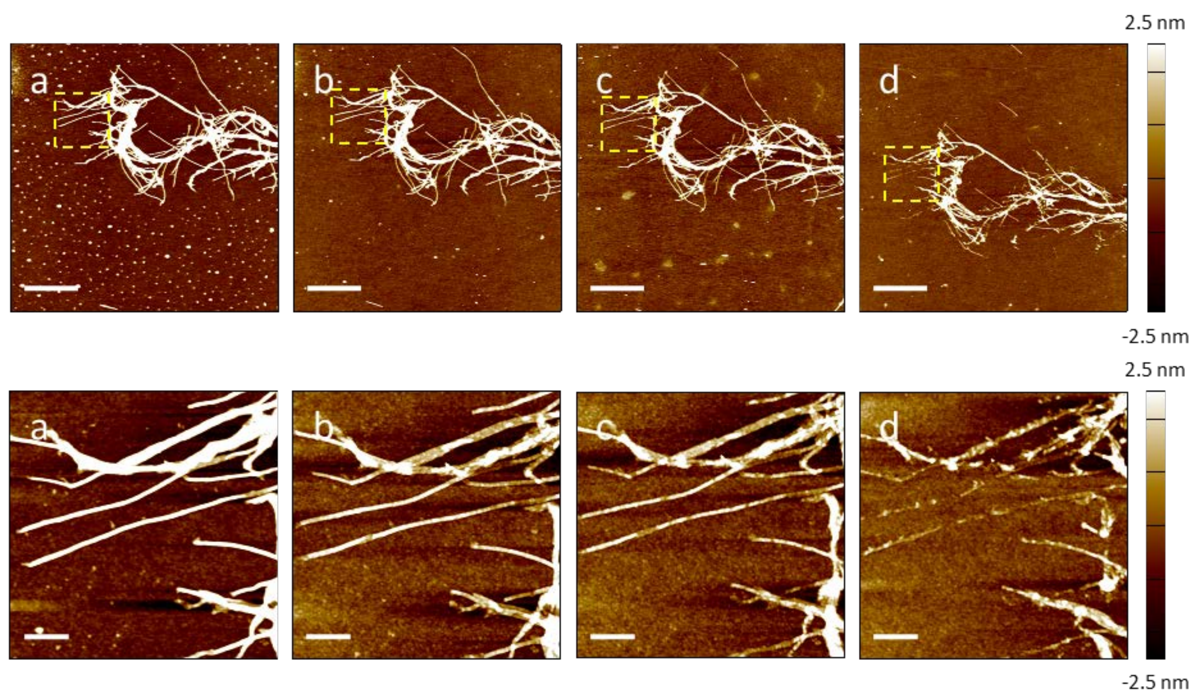

Figure 27. Stability of a DNA nanotube master template without a protective inorganic oxide film during multiple pattern replication processes using 1 × TAE/Mg^{2+} buffer. AFM height images of DNA nanotubes in the same location of a silicon wafer (a) before and after (b) 1st, (c) 2nd, and (d) 3rd pattern transfer to PLLA stamps using 1 × TAE/Mg^{2+} buffer. The bottom row contains the zoomed-in views of the areas in the yellow dashed boxes in the top row. Scale bars represent (top row) 3 μm and (bottom row) 500 nm.

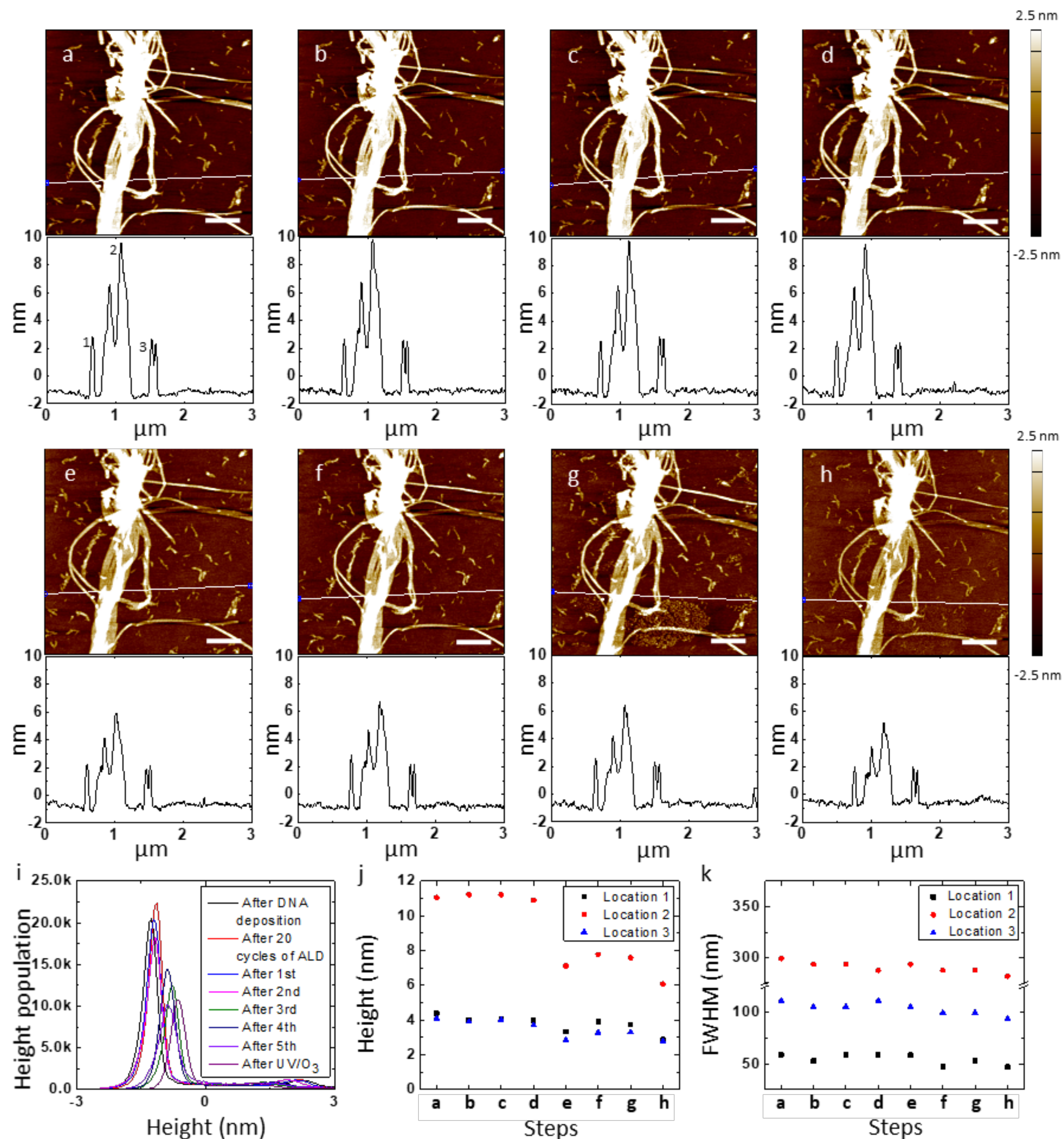

Figure 28. Stability of a DNA nanotube master template with a 2 nm Al_2O_3 film for multiple pattern replication processes to polymer stamps and removal of polymer residues with UV/O_3 treatment. AFM height images with corresponding cross-sectional analysis of DNA nanotubes in the same location after (a) deposited on a silicon wafer, (b) 20 cycles of ALD of Al_2O_3, (c) 1st, (d) 2nd, (e) 3rd, (f) 4th, and (g) 5th pattern transfer to PLLA stamps, and (h) UV/O_3 treatment for 1 h and washing with deionized water. White lines on the AFM images indicate where the cross-sections were determined. (i) Histograms of the AFM height images from a to h. (j) Height and (k) FWHM of the DNA nanotubes in three different locations of the images from a to h. Locations 1, 2, and 3 correspond to 1, 2, and 3 in the cross-section of image a. Scale bars represent 500 nm. Note: The DNA master template was contaminated before the 5th spin coating of PLLA in dichloromethane solution. Images a and b are also shown in Figure 26.

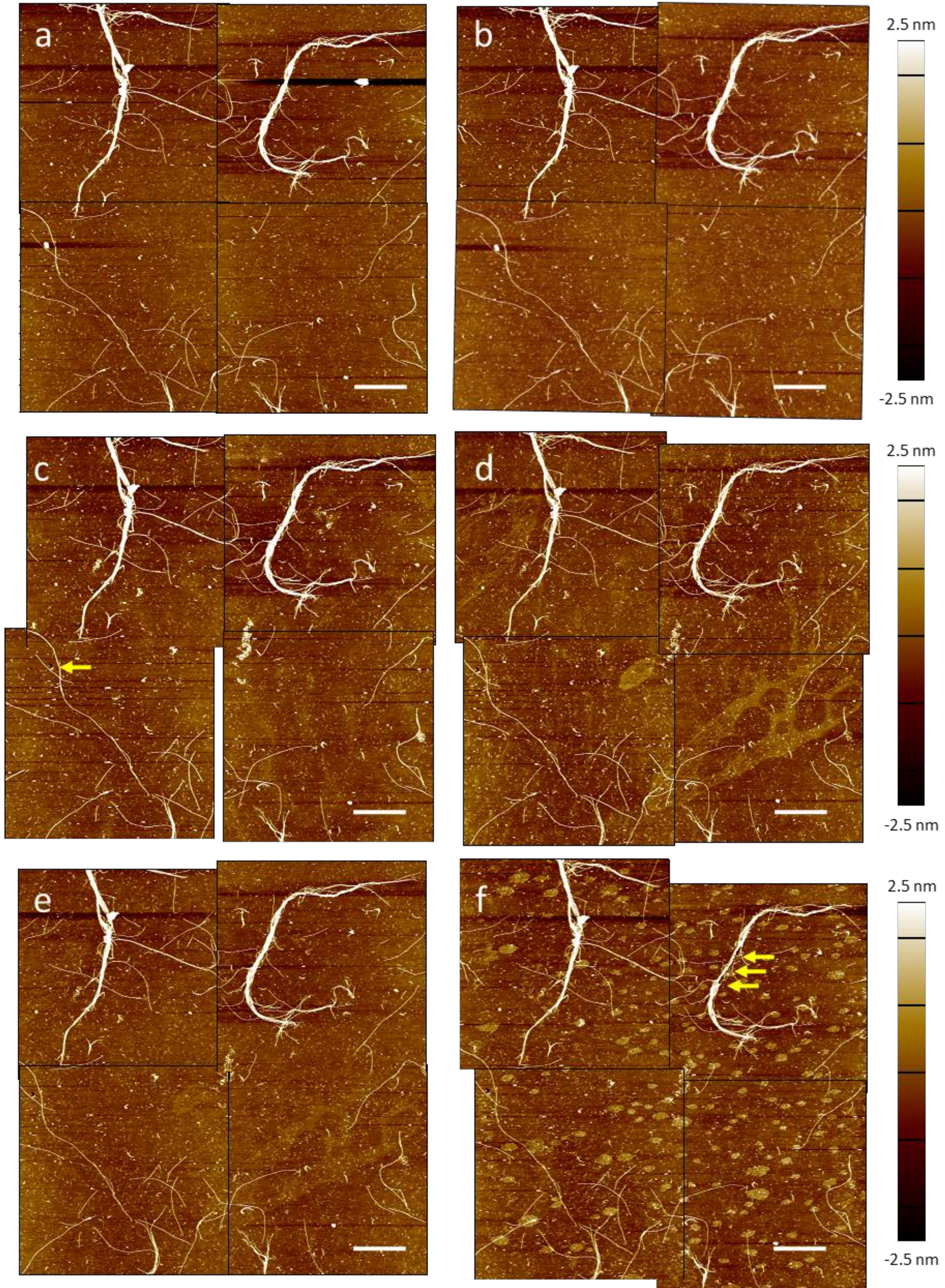
a
b
c
d
e
f
2.5 nm
-2.5 nm
2.5 nm
-2.5 nm
2.5 nm
-2.5 nm

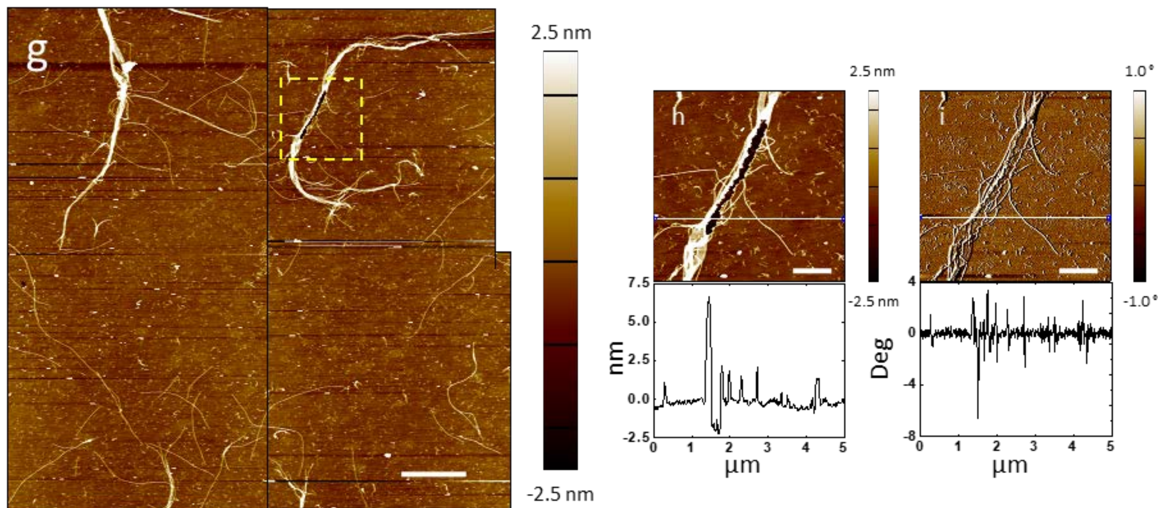

Figure 29. Stability of a DNA nanotube master template with a 2 nm Al_2O_3 film for multiple pattern replication process to polymer stamps over an area of 30 × 30 μm^2 and removal of polymer residues with UV/O_3 treatment. AFM height images of DNA nanotubes in the same location of a silicon wafer after (a) 20 cycles of ALD of Al_2O_3, (b) 1st, (c) 2nd, (d) 3rd, (e) 4th, and (f) 5th pattern transfer to PLLA stamps, and (g) UV/O_3 treatment for 1 h and washing with deionized water. Holes formed by the breakage of the Al_2O_3 film are indicated by the yellow arrows. AFM (h) height and (i) phase images with corresponding cross-sectional analysis of the area in the yellow dashed box in image g. White lines on the AFM images indicate where the cross-sections were determined. Scale bars represent (a–g) 4 μm and (h,i) 1 μm. Note: The DNA master template was contaminated before the 5th spin coating of PLLA in dichloromethane solution.

3.4.2.3 Removal of polymer residues on a DNA nanotube master template with a 2 nm Al_2O_3 film with UV/O_3 treatment

Being able to clean the master template is also important for its repeated use. During the five pattern transfers to the PLLA stamps, the surface of the DNA master template was contaminated with polymer residues (Figure 28g, lower middle area). To verify whether the polymer residues on the DNA master template can be removed with UV/O_3 treatment, after the 5th replication process, the template was subjected to UV/O_3 cleaning for an hour, washed with deionized water, and dried with N_2 gas (Figures 28h and 29g). The AFM images before and after the treatment show that the morphology of the DNA template was not altered while the polymer residues were removed. The height difference between the absolute maximum peak and the next relative maximum peak in the histogram of the AFM image, however, significantly decreased from 2.28 nm to 1.69 nm (Figure 28i). The height of the DNA nanotubes at the three same locations decreased from 3.72 nm, 7.58 nm, and 3.29 nm to 2.87 nm, 6.07 nm, and 2.78 nm, respectively (Figure 28j). The FWHM at these locations also decreased from 52.88 nm, 287.94 nm, and 99.89 nm to 46.98 nm, 281.87 nm, and 93.96 nm, respectively (Figure 28k). These results suggest that although the UV/O_3 treatment is able to eliminate the organic residues on the surface of the master template, the DNA nanostructures beneath the 2 nm of Al_2O_3 coating are likely damaged by the oxidation by O_3.

3.4.2.4 Long-term stability of a DNA nanotube master template with a 2 nm Al_2O_3 film

The long-term stability of the ALD-coated template was also studied. We kept the template in a plastic petri dish that was stored in a common lab bench drawer for 40 days. The AFM images with corresponding cross-sectional analysis were scanned in the same location of the template at the beginning and the end of this period (Figure 30a,b). Not surprisingly, the 40 days of aging in air did not alter the surface topography of the DNA nanostructure master template. While the height of the DNA nanotubes at four different locations remained consistent (Figure 30c), the FWHM at these locations slightly decreased (Figure 30d). We speculate that the decrease in the FWHM results from the differences between the AFM probe convolution effects of individual tips because the decreases are similar to the resolution limit of the AFM image (i.e., one or two pixels in the AFM images). At room temperature, solid-state DNA undergoes degradation and/or aggregation within 30 days when it is exposed to atmospheric water and oxygen.[155-156] Compared to DNA, which is a soft material, Al_2O_3 is much more stable and robust. Through the conformational coating of Al_2O_3, the shelf life of the DNA nanotubes is assumed to be increased while maintaining their morphology longer than the nanotubes without a protective film. Overall, the 20 cycles of ALD of Al_2O_3 allow the DNA nanostructure master template to possess enough chemical stability for long-term storage.

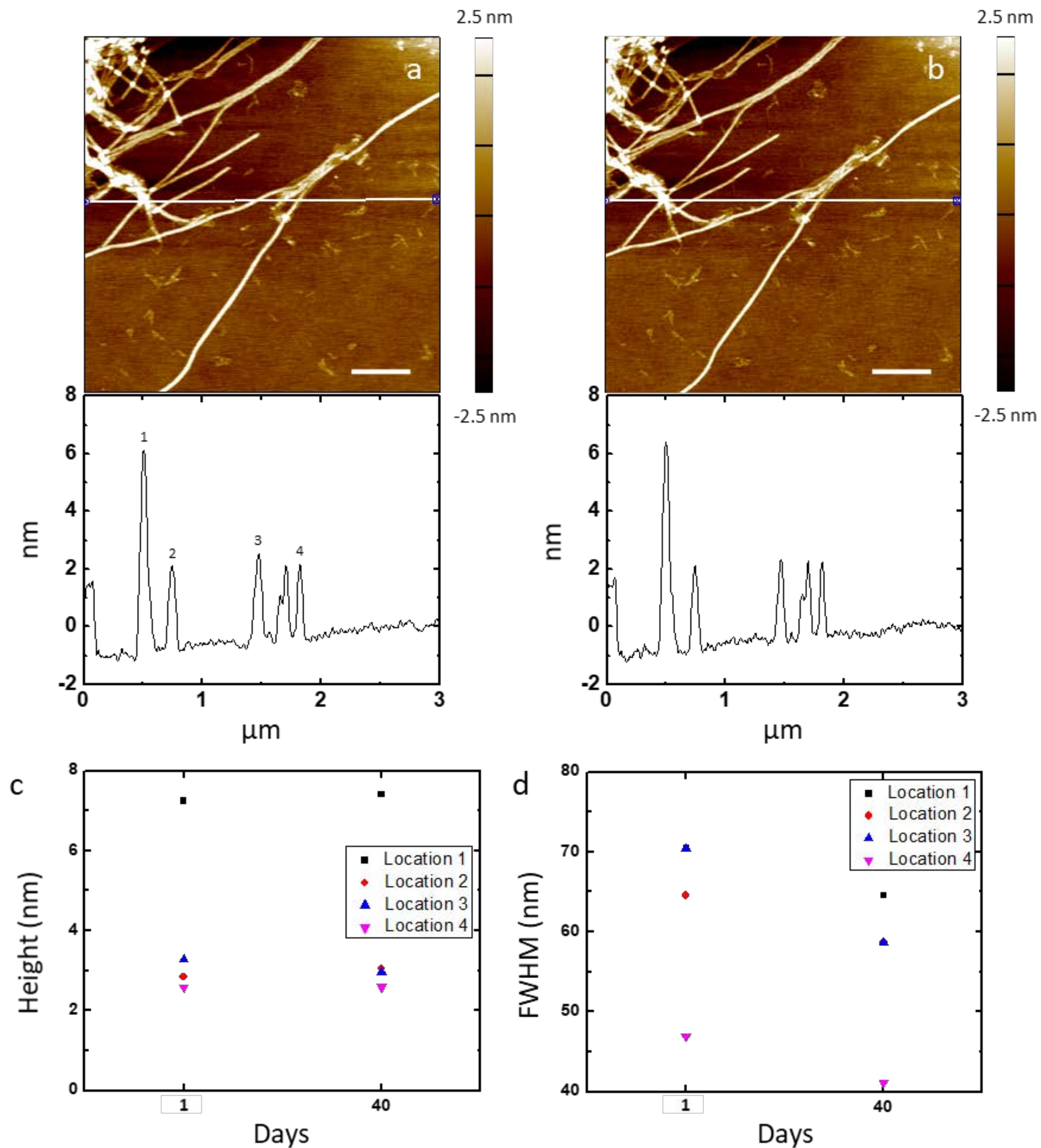

Figure 30. Long-term stability of a DNA nanotube master template with a 2 nm Al_2O_3 film. AFM height images with corresponding cross-sectional analysis of DNA nanotubes in the same location of a silicon wafer at the (a) beginning and the (b) end of 40 day period. White lines on the AFM images indicate where the cross-sections were determined. (c) Height and (d) FWHM of the DNA nanotubes in four different locations of images a and b. Locations 1, 2, 3, and 4 correspond to 1, 2, 3, and 4 in the cross-section of image a. Scale bars represent 500 nm.

3.4.2.5 Stability of a DNA nanotube master template with a 5 nm Al_2O_3 film for multiple pattern replication process to polymer stamps and removal of polymer residues with UV/O_3 treatment

The *ca.* 2 nm thick Al_2O_3 layer increased the mechanical stability of the DNA nanotube master template to only a limited extent. To verify whether the mechanical stability of the template can be strengthened with the increased thickness of the Al_2O_3 layer while preserving its nanoscale morphology, a *ca.* 5 nm thick Al_2O_3 layer was deposited onto the template, and the reusability and morphology conservation were evaluated. The DNA nanostructures in the same location were scanned with AFM after deposition on a silicon wafer, 50 cycles of ALD of Al_2O_3, and 1st and 5th replication to PLLA stamps, then exposed to UV/O_3 treatment, washed with deionized water, and dried with N_2 gas (Figures 31a–e and 32a–c). Throughout each stage of the fabrication process, we analyzed the height difference between the absolute maximum peak and the next relative maximum peak in the histogram and height and FWHM at four different locations; all these data showed little change throughout the fabrication process (Figure 31f–h). The *ca.* 5 nm thick Al_2O_3 film is impermeable to O_3 and protects the underlying DNA nanostructures against the UV/O_3 oxidation. Also, no holes due to the breakage of the protective Al_2O_3 film were found, demonstrating that the both chemical and mechanical stabilities of the DNA nanostructure master template improve with a thicker Al_2O_3 layer. The direct comparison of the height differences between the maximum peaks of the histograms of the 20 and 50 cycles of ALD of Al_2O_3 through the multiple pattern transfer clearly shows the increased stability of the *ca.* 5 nm thick Al_2O_3 film compared to the *ca.* 2 nm thick film (Figure 33). We note that the polymer residues were not observed on the surface of the DNA nanotube master template with the *ca.* 5 nm thick Al_2O_3 film even after the 5th replication. The surface roughness of Al_2O_3 film

grown using ALD slowly increases as the number of cycles goes up.[157] Therefore, it does not cause the reduced polymer adsorption on the 5 nm thick Al_2O_3 film. Further study is needed to elucidate the difference between the 2 nm and 5 nm of Al_2O_3 films.

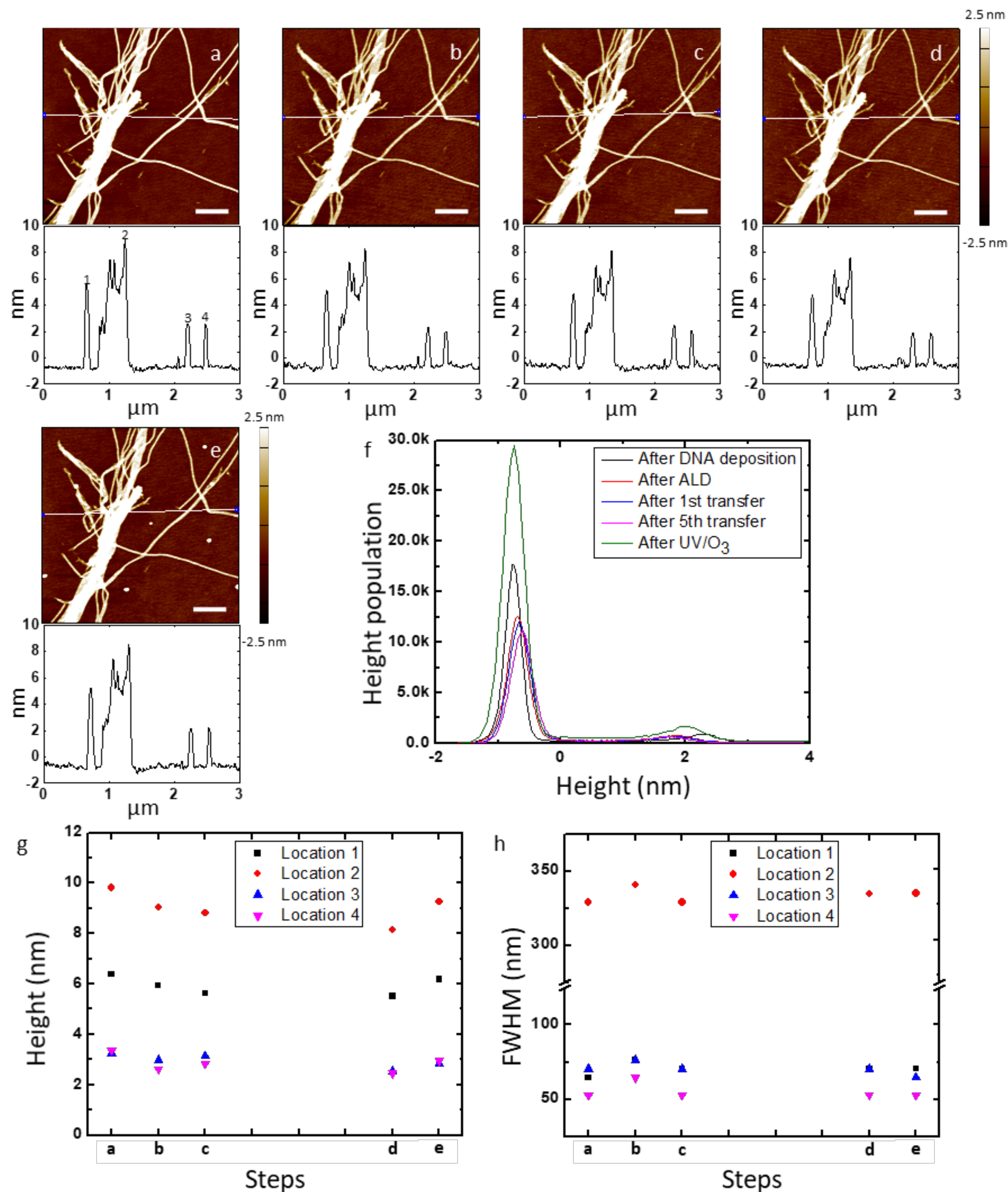

Figure 31. Stability of a DNA nanotube master template with a 5 nm Al_2O_3 film for multiple pattern replication process to polymer stamps and removal of polymer residues with UV/O_3 treatment. AFM height images with corresponding cross-sectional analysis of DNA nanotubes in the same location after (a) deposited on a silicon wafer, (b) 50 cycles of ALD of Al_2O_3, (c) 1st and (d) 5th pattern transfer to PLLA stamps, and (e) UV/O_3 treatment for 1 h and washing with deionized water. White lines on the AFM images indicate where the cross-sections were determined. (f) Histograms of the AFM height images from a to e. (g) Height and (h) FWHM of the DNA nanotubes in four different locations of the images from a to e. Locations 1, 2, 3, and 4 correspond to 1, 2, 3, and 4 in the cross-section of image a. Scale bars represent 500 nm.

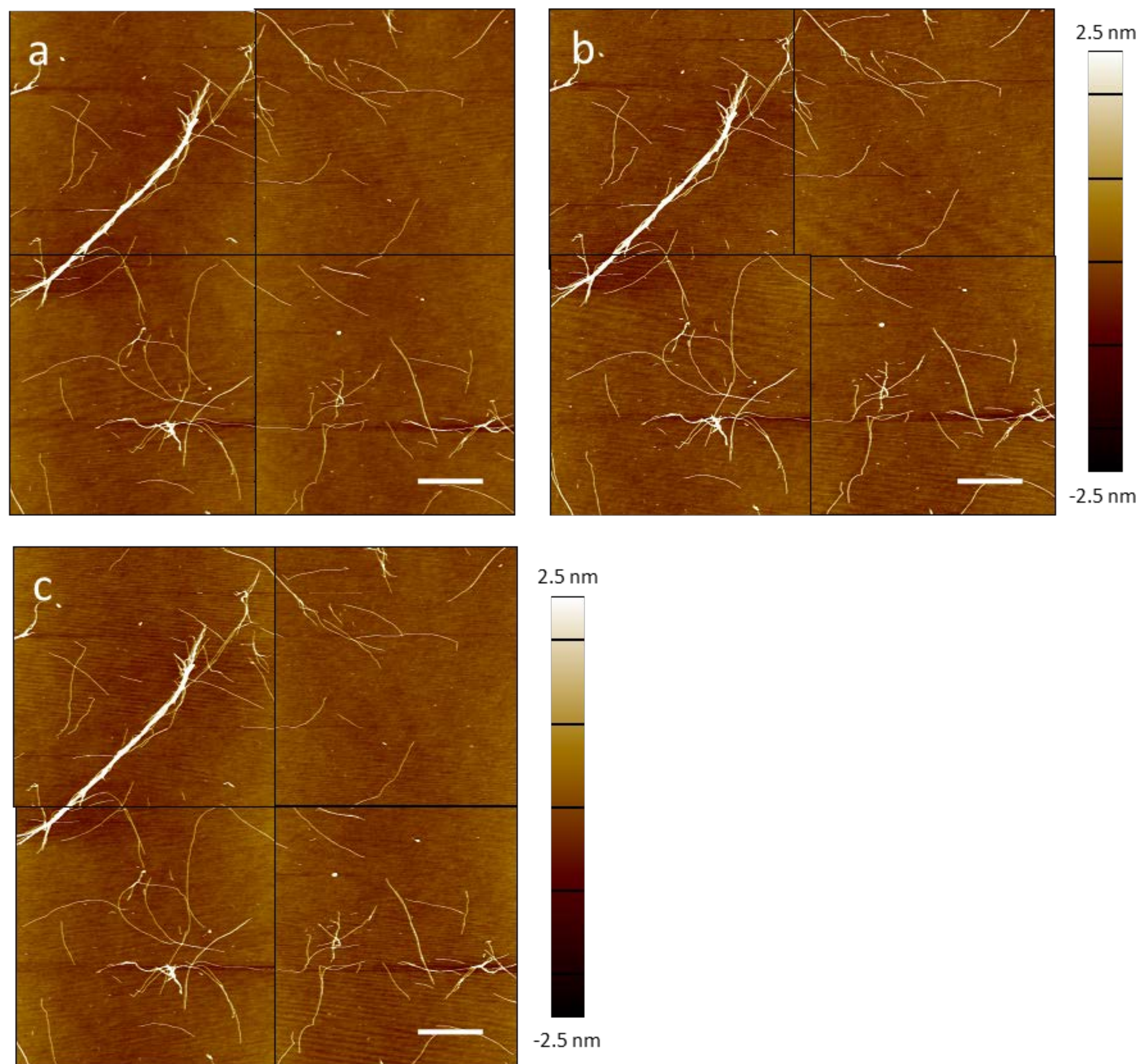

Figure 32. Stability of a DNA nanotube master template with a 5 nm Al_2O_3 film for multiple pattern replication process to polymer stamps over an area of 30 × 30 μm^2 and removal of polymer residues with UV/O_3 treatment. AFM height images of DNA nanotubes in the same location of a silicon wafer after (a) 50 cycles of ALD of Al_2O_3 and (b) 1st and (c) 5th pattern transfer to PLLA stamps. Scale bars represent 4 μm.

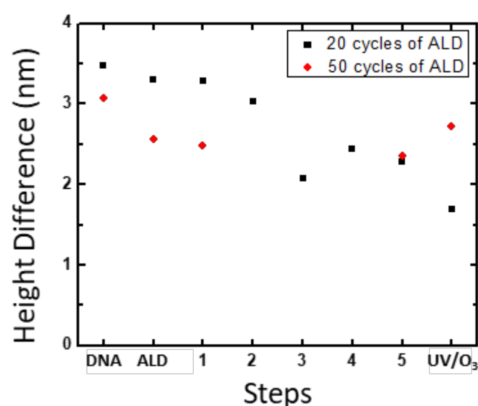

Figure 33. Comparison of the height differences between the maximum peaks of the histograms in Figures 28i and 31f.

3.4.3 Fabrication of a PLLA Stamp by Replication over a DNA Origami Triangle Master Template with a 2 nm or 5 nm Al_2O_3 Film

The DNA nanotubes tested above are simple one-dimensional linear structures. To evaluate the effectiveness of a protective conformational coating on complex patterns, DNA origami triangle nanostructures were employed as master templates for the pattern transfer to PLLA stamps. The DNA origami triangle is a single layer of DNA double strands and has a theoretical height of 2 nm (Figure 11a).[39] The triangle consists of three trapezoidal domains formed by folding an M13mp18 scaffold strand with short synthetic staple strands. Among the three trapezoidal domains, one has a dangling loop. These domains are further connected to each other by bridging the edges of the domains with the staple strands. There are three holes at each of the vertex and one large triangular hole in the center of the DNA origami triangle. The AFM images show that the three holes at the vertex, the central triangular hole, and the dangling loop were clearly visible before and after ALD, and after replication process with both *ca.* 2 nm and *ca.* 5 nm thick

Al_2O_3 layers (Figure 34a,b,d). Through these steps, the three holes at the vertex were frequently seen as a linear gap and the depth of the holes or the linear gap was much smaller than the height of the nanostructures due to the limited resolution of the AFM images. The vertex with the holes or the linear gap was highlighted by the blue dots (Figures 35d and 36d). The dangling loop was also highlighted by the yellow arrows (Figures 35a,d and 36a,d). The loop might not be seen in some DNA origami triangles if the loop was folded above or beneath the DNA structures. According to the cross-sectional analysis of the AFM images, the average height, FWHM, inner length and outer length of the DNA origami triangles remained comparable throughout the replication process including the ALD (Figure 37). All these results prove that the protective 2 nm and 5 nm of Al_2O_3 films successfully preserves the surface morphology of the complex DNA origami triangle nanostructures.

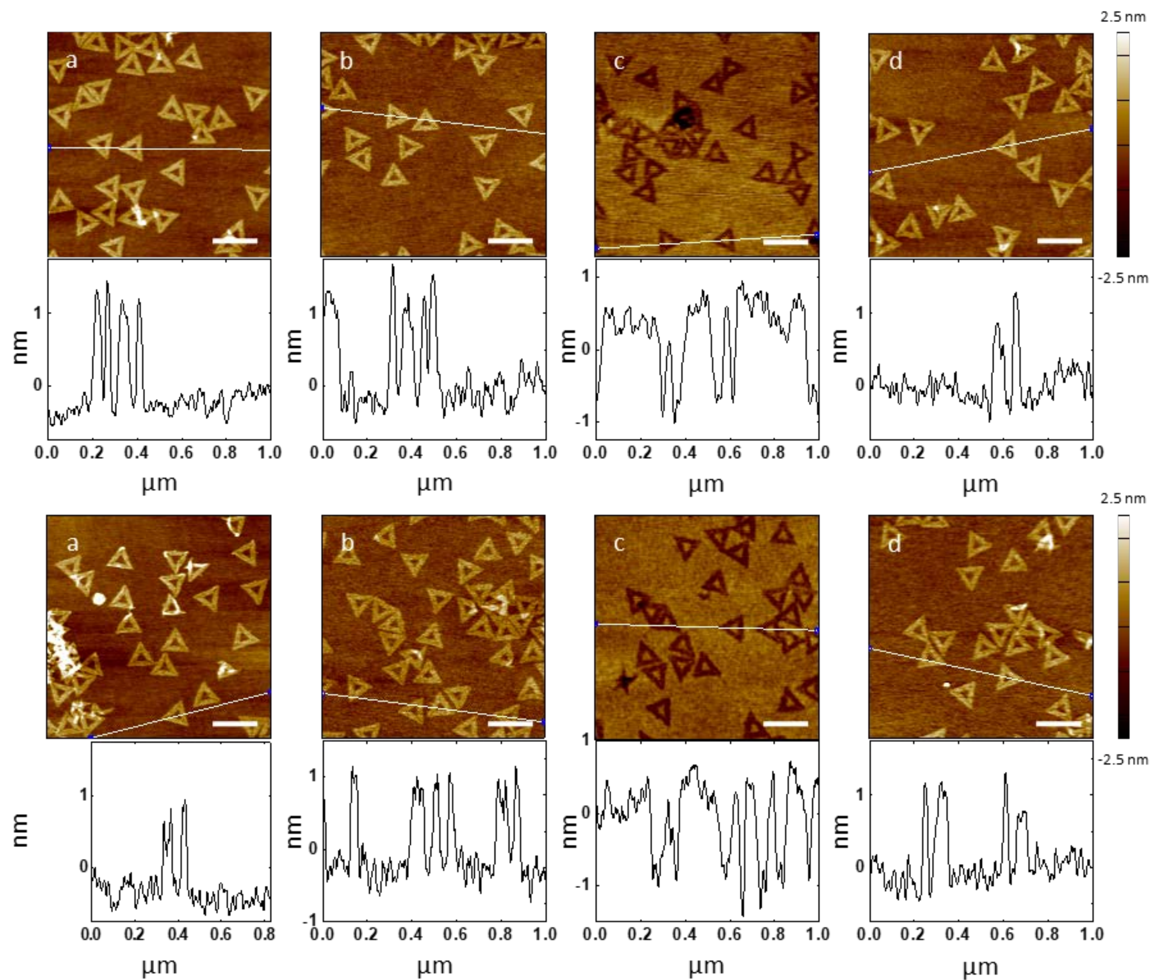

Figure 34. Fabrication of a PLLA Stamp by replication over a DNA origami triangle master templates with 2 nm and 5 nm Al_2O_3 films. AFM height images with corresponding cross-sectional analysis of DNA origami triangles after (a) deposited on silicon wafers, (b) 20 cycles (top) or 50 cycles (bottom) of ALD of Al_2O_3, and (d) pattern transfer to PLLA stamps, and (c) negative replicas of the DNA origami triangles on the PLLA stamps. White lines on the AFM images indicate where the cross-sections were determined. Scale bars represent 200 nm.

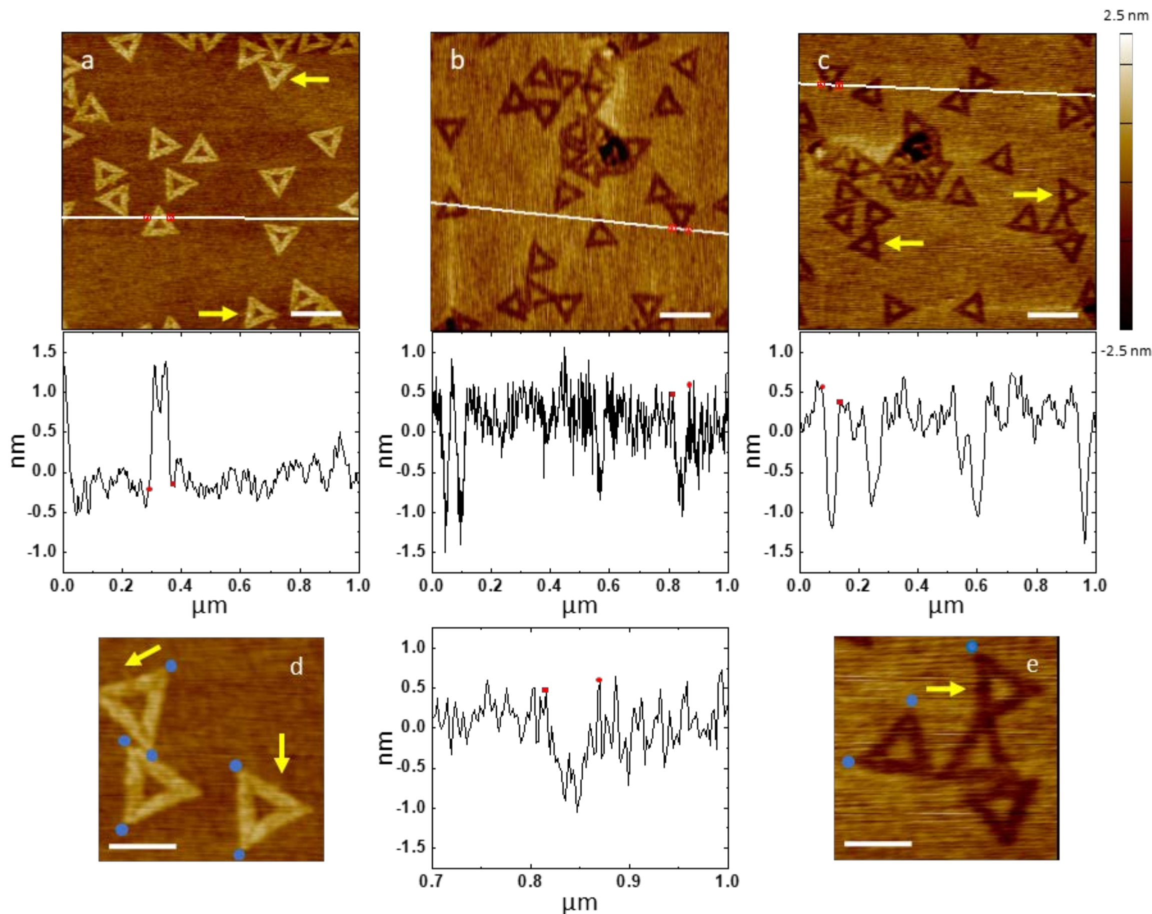

Figure 35. Analysis of dangling loops and vertices of a DNA origami triangle master template with a 2 nm Al_2O_3 film and a PLLA stamp. AFM height images with corresponding cross-sectional analysis of (a) DNA origami triangles deposited on a silica wafer after 20 cycles of ALD of Al_2O_3 and (b,c) negative replicas of the DNA origami triangles on a PLLA stamp. White lines on the AFM images indicate where the cross-sections were determined. The dangling loops are indicated by the yellow arrows. Red cursors in the AFM images and corresponding cross-sections define the outer sides of the vertices that are measured. In image b, the bump appears in the zoomed-in curve valley of the cross-section (bottom), confirming the presence of the bump at the vertex. In image c, the bump does not appear at the curve valley, indicating that no bump exists in the vertex. Zoomed-in AFM images of (d) DNA origami triangles and (e) their negative replicas. The dangling loops and vertices with the holes/bumps are indicated by the yellow arrows and blue dots, respectively. Scale bars represent (a–c) 200 nm and (d,e) 100 nm. Note: Images b and c are identical. Image b is rotated 90° clockwise to match the orientation of its corresponding cross-section. The images from a to c are also shown in Figure 34.

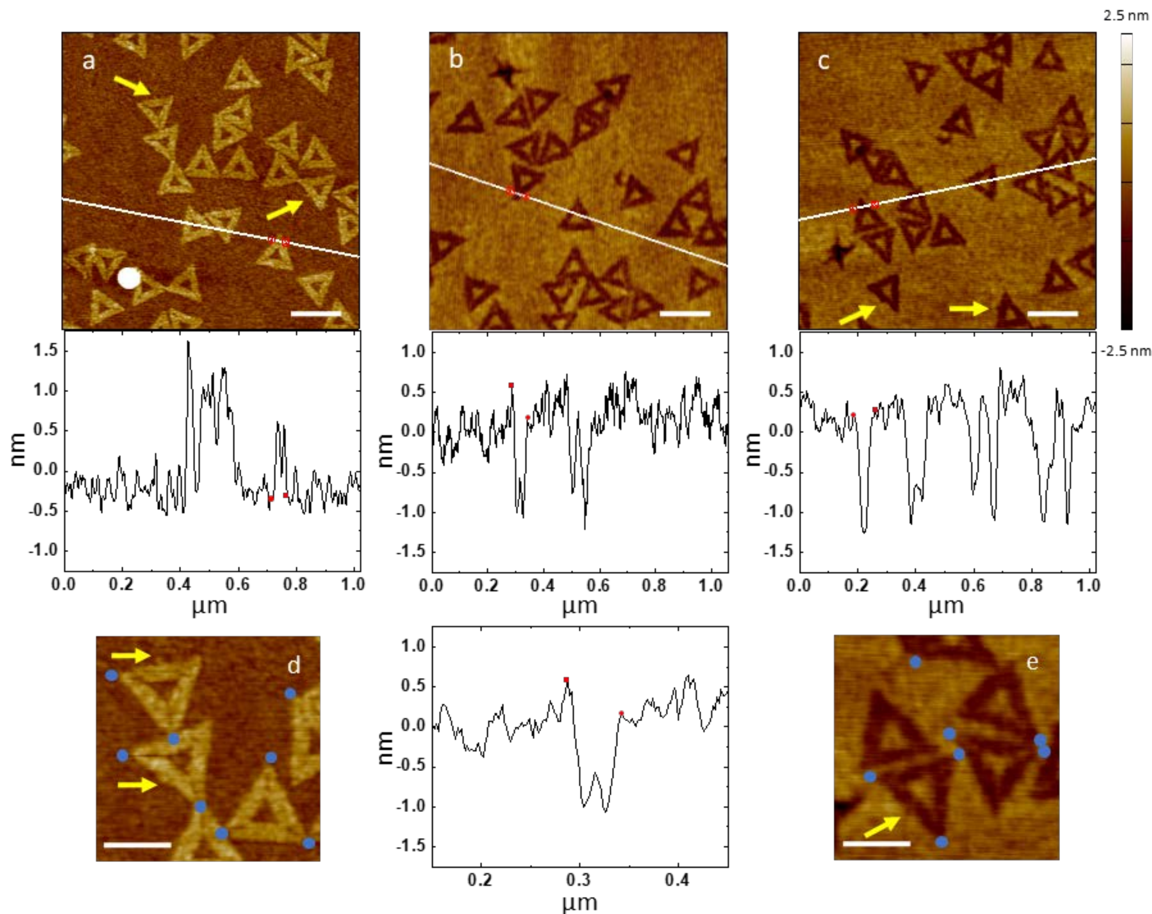

Figure 36. Analysis of dangling loops and vertices of a DNA origami triangle master template with a 5 nm Al_2O_3 film and a PLLA stamp. AFM height images with corresponding cross-sectional analysis of (a) DNA origami triangles deposited on a silica wafer after 50 cycles of ALD of Al_2O_3 and (b,c) negative replicas of the DNA origami triangles on a PLLA stamp. White lines on the AFM images indicate where the cross-sections were determined. The dangling loops are indicated by the yellow arrows. Red cursors in the AFM images and corresponding cross-sections define the outer sides of the vertices that are measured. In image b, the bump appears in the zoomed-in curve valley of the cross-section (bottom), confirming the presence of the bump at the vertex. In image c, the bump does not appear at the curve valley, indicating that no bump exists in the vertex. Zoomed-in AFM images of (d) DNA origami triangles and (e) their negative replicas. The dangling loops and vertices with the holes/bumps are indicated by the yellow arrows and blue dots, respectively. Scale bars represent (a–c) 200 nm and (d,e) 100 nm. Note: Images b and c are identical. Image b is rotated 90° clockwise to match the orientation of its corresponding cross-section. Images b and c are also shown in Figure 34.

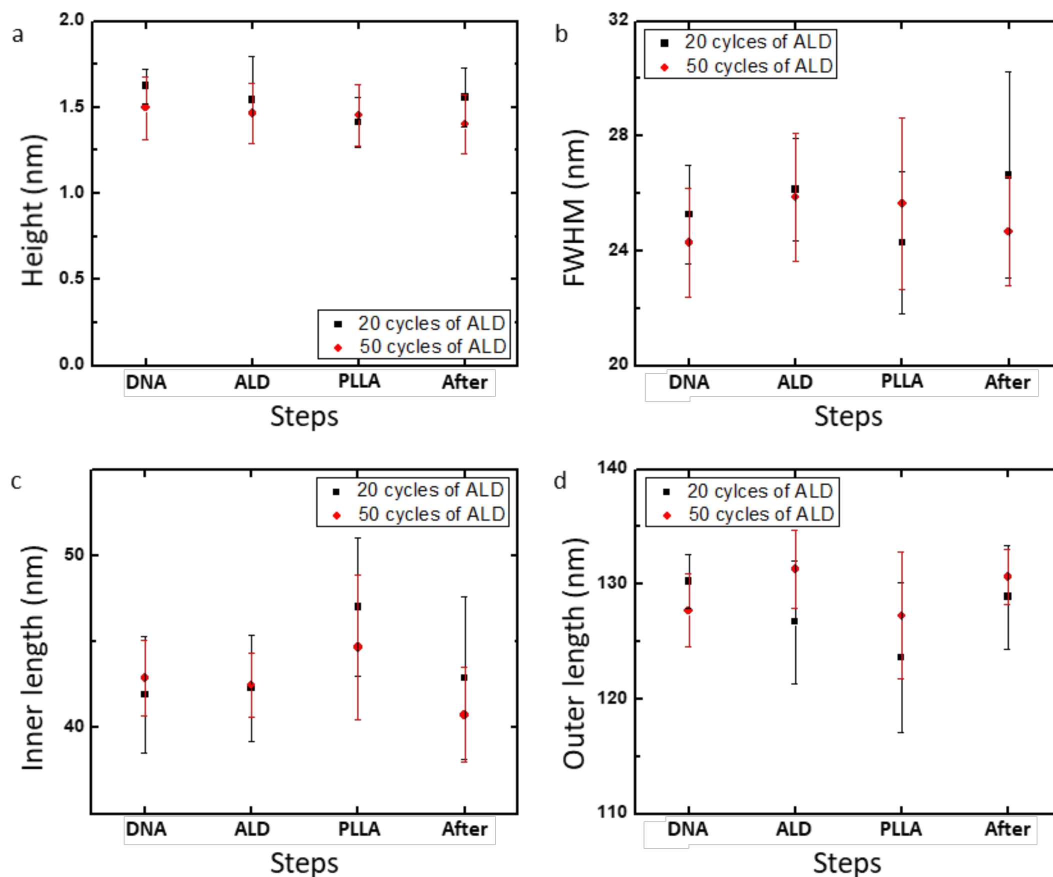

Figure 37. Yield of shape conservation process of a DNA origami triangle master template by ALD and pattern replication process to a PLLA stamp. Average (a) height, (b) FWHM, (c) inner length, and (d) outer length (n = 10) of features on DNA origami triangle master templates with 2 nm and 5 nm Al_2O_3 layers and PLLA stamps at each step of fabrication process, after (DNA) DNA origami triangles were deposited on silicon wafers, (ALD) ALD of Al_2O_3, and (After) pattern transfer to PLLA stamps, and (PLLA) their negative replicas on the PLLA stamps.

After the replication process, triangular trenches resembling the shape of the DNA origami triangles were formed on the PLLA films (Figure 34c). Compared to the dimensions of the DNA triangles with the protective layers on the templates, the average depth of the trenches remained consistent with the average height of the triangles (Figure 37a). Due to the AFM probe convolution, however, the average outer length (the edge length of the trench measured outside of the triangle) and FWHM of the triangular trenches decreased and the average inner length of the trenches increased (Figure 37b–d). Both of the patterns corresponding to the dangling loop and the three holes at the vertex were transferred to the PLLA stamps, but they were difficult to find in the trenches compared to the original features on the templates (Figures 35b,c,e and 36b,c,e). The parts of the trench responsible for the three holes at the vertex and the dangling loop were also highlighted by the blue dots and the yellow arrows, respectively (Figure 35c,e and 36c,e). On the PLLA stamps, the holes or the linear gap between the trapezoidal domains of the DNA origami triangles were replicated as a small bump at the vertex of the triangular trenches. The height of the bump, however, never reached the height of the DNA origami triangles and the bump was frequently not observed in some trenches, as the bump on the PLLA stamp peeled off from the DNA origami triangle master template without the protective film. We attribute these observations to the mechanical instability of the bumps during the scanning with AFM and/or the intrinsic limitation of the resolution of the pattern transfer.[154] In the latter case, a large PLLA molecule may not be able to completely fill the nanometer-sized holes in the DNA origami triangle during the spin-coating process. A decrease in the feature size of the DNA nanostructure appears to result in a height decrease and/or loss of features in the polymer stamp. Overall, the PLLA film is capable of replicating the overall features of the complex DNA origami triangles

with high fidelity and the local features below *ca.* 5 nm only to some extent even with the presence of the protective *ca.* 2 nm or *ca.* 5 nm thick Al_2O_3 layer.

3.4.4 Investigation of Surface Morphology of a DNA Nanostructure Master Template with a 20 nm Al_2O_3 Film

Finally, we investigated how the surface morphology of the DNA nanostructures was influenced as the thickness of the protective Al_2O_3 film was further increased. We coated both the DNA nanotube (Figure 38a,b) and the DNA origami triangle (Figure 38c,d) master templates with a *ca.* 20 nm thick Al_2O_3 layer and compared their AFM images before (Figure 38a,c) and after (Figure 38b,d) the 200 cycles of ALD. With the *ca.* 20 nm thick Al_2O_3 film, the DNA nanotubes were still visible and the FWHM stayed consistent (Figure 38b,f). The height of the DNA nanotubes, however, considerably decreased from 3.83 nm, 9.36 nm, 3.85 nm, and 3.94 nm to 1.54 nm, 2.81 nm, 1.66 nm, and 1.71 nm, respectively (Figure 38e). In case of the DNA origami triangles, the DNA nanostructures with average height of 1.68 nm (n = 10) were barely seen and the height profile along the individual DNA triangles also showed the significant increase of roughness (Figure 38d). These results indicate that there is a limit to the thickness of the protective Al_2O_3 film deposited by ALD to maintain the nanoscale features of the DNA nanostructures on the template.

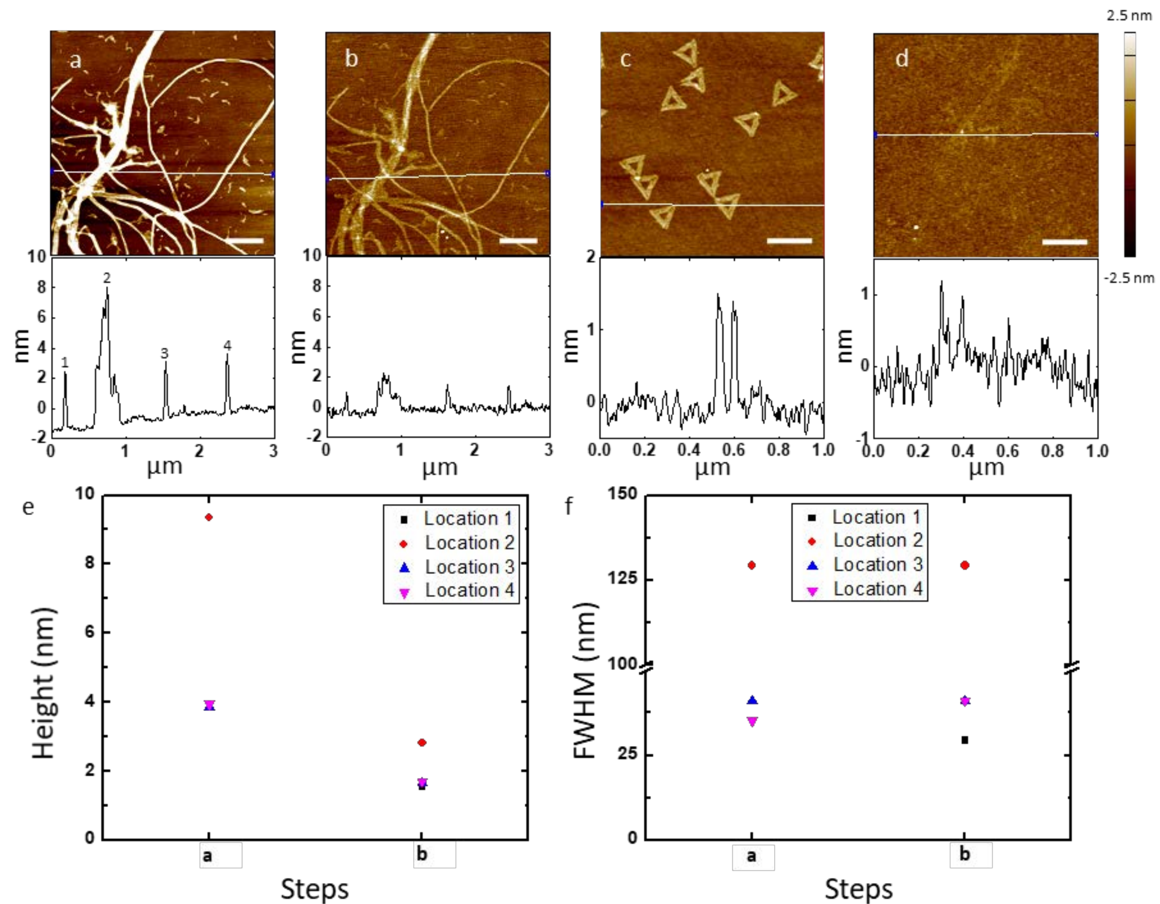

Figure 38. Investigation of surface morphology of a DNA nanostructure master template with a 20 nm Al_2O_3 Film. AFM height images with corresponding cross-sectional analysis of DNA (a,b) nanotubes and (c,d) origami triangles deposited on silica wafers (a,c) before and (b,d) after 200 cycles of ALD of Al_2O_3. White lines on the AFM images indicate where the cross-sections were determined. (e) Height and (f) FWHM of the DNA nanotubes in four different locations of the images from a to b. Locations 1, 2, 3, and 4 correspond to 1, 2, 3, and 4 in the cross-section of image a. Scale bars represent (a,b) 500 nm and (c,d) 200 nm.

3.5 CONCLUSIONS

We have reported a method to increase the stability of DNA nanostructure master templates through the conformal growth of an inorganic oxide film by ALD and demonstrated its usefulness in soft lithography patterning of polymer films. DNA nanotubes and origami triangles with a Al_2O_3 film of *ca.* 2 nm, *ca.* 5 nm or *ca.* 20 nm thickness have been tested as master templates to imprint their nanoscale features to PLLA films. As the thickness of the Al_2O_3 coating grows, the mechanical and/or chemical stability increases while some of the nanoscale features of the DNA nanostructures are lost. Based on our results, the conformational coating of the *ca.* 5 nm thick Al_2O_3 layer to the DNA nanostructures provides a good compromise between increasing the stability and maintaining the nanoscale feature of the master template for repeated use in soft lithography. In addition, the *ca.* 5 nm thick Al_2O_3 layer offered good protection to the underlying DNA nanostructures from exposure to UV/O_3. Although our study focused on the ALD of Al_2O_3, other metals, metal oxides, or inorganic oxides can also be used as long as they can be conformally coated at a temperature below 250 °C. Above 250 °C, the degradation of DNA nanostructures deposited onto silicon wafers starts to occur although the decomposition residues may still maintain their nanoscale features.[77, 139] A conformal protective film significantly improves the mechanical and chemical stabilities of DNA nanostructures, allowing them to be used in environments that are incompatible with pristine DNA nanostructures.

4.0 CALCIUM INTERFERENCE IN REACTIVE ION ETCHING FOR NANOSCALE PATTERNING OF HIGH ASPECT RATIO

4.1 CHAPTER PREFACE

Materials contained in this chapter were in preparation for publication as a research article.

List of Authors: Hyojeong Kim, Feng Zhou, Mitch Cholewinski, Muhammad Salim, Bin Chong and Haitao Liu

Author Contributions: H.K., F.Z., and H.L. designed and directed the experiments. H.K., F.Z., M.C., M.S., and B.C. conducted the experiments. All authors discussed the results. H.K., and H.L. wrote the manuscript with input from all authors.

4.2 INTRODUCTION

In 1982, a door was opened that began the era of DNA nanotechnology as Seeman introduced the idea of utilizing DNA to build a mechanically robust four-arm junction structure to the scientific community.[50] Since then, DNA has been not only a mere carrier for hereditary information but also a building block for nanofabrication. Programmable folding combined with hierarchical self-assembly based on Watson-Crick base pairing has led to an explosive growth in the field of structural DNA nanotechnology over the past decades.[51-52] A wide range of one-dimensional (1D),[61, 72, 119] two-dimensional (2D),[39-40, 44] and three-dimensional (3D)[41, 43, 73] nanostructures with arbitrarily shaped features have been fabricated.

DNA nanostructures have been considered to be promising templates for bottom-up nanofabrication due to their structural diversity and complexity with a theoretical resolution down to 2 nm.[39-44] A lot of effort has been devoted to directly assemble various nanomaterials intermittently or continuously onto DNA nanostructures as templates, such as proteins,[60, 81-83] carbon nanotubes,[84-87] and metal nanoparticles.[88-96, 158] Taking one step further in this direction, chemical vapor deposited graphene layers were patterned using metallized DNA nanostructures.[131] 3D gold nanoparticles were also fabricated by growing seed particles in 3D DNA nanostructure molds with high specificity.[98-99]

Furthermore, numerous strategies have been developed to transfer pattern to both hard and soft substrates from DNA nanostructures. Metal films were patterned by metal evaporation onto 1D DNA nanotubes and 2D DNA arrays followed by lift-off.[100] Both positive and negative tone patterns were replicated from DNA origami triangles into inorganic oxides through HF vapor-phase etching and chemical vapor deposition methods by exploiting the difference in adsorption of water on DNA nanostructures and on a SiO_2 substrate.[102-103] Likewise, the replicas

of DNA nanostructures in positive tone with sub-10 nm resolution were fabricated by treating DNA nanostructures on a SiO_2 substrate in anhydrous HF vapor etching.[104] Trenches with linewidths of sub-10 nm resolution were also generated though angled metal vapor deposition on aligned DNA molecular bundles as shadow masks and subsequent etching.[101] Patterning with DNA nanostructures also can be extended to fabricate polymer films with good fidelity. The patterns of a wide range of DNA nanostructures were faithfully replicated to various types of polymer stamps, from polyacrylamide gel to photocurable acryloxy perfluoropolyether.[106, 154] Carbon nanostructures were formed from DNA nanostructures by thermal annealing of Al_2O_3 coated DNA nanostructures.[105]

Herein we propose a new approach of direct pattern transfer from DNA nanostructures to a Si substrate by reactive ion etching (RIE). The effect of calcium, cobalt, and cadmium chlorides were investigated; the addition of calcium chloride to the DNA nanostructure in buffer solution resulted in a negative tone pattern transfer with minimal etching occurred in the background. We propose that as calcium chloride was added to the buffer solution with DNA nanotubes, certain calcium-containing compound (e.g., $Ca(OH)_2$) precipitated due to its low solubility. The adsorption of calcium-containing compound was modulated by the DNA nanotubes, which in turn locally changes the plasma etching rate of Si substrate to result in negative trenches with high aspect ratio.

4.3 EXPERIMENTAL

4.3.1 Materials

Silicon wafers [Si (110), with native oxide] were purchased from University Wafers (South Boston, MA) and Okmetic (Vantaa, Finland). Strand for DNA nanotubes was synthesized by Integrated DNA Technologies (Coralville, IA). 2-Amino-2-(hydroxymethyl)-1,3-propanediol (Trizma base), ethylenediaminetetraacetic acid (EDTA), magnesium acetate tetrahydrate, sulfuric acid, hydrogen peroxide solution (30% H_2O_2), and cobalt chloride hexahydrate were purchased from Sigma-Aldrich (St. Louis, MO). Acetic acid (glacial) and calcium chloride anhydrous were purchased from Fisher Scientific (Fair Lawn, NJ). Ethanol was purchased from Fisher Scientific and Decon Laboratories, Inc. (King of Prussia, PA). Cadmium chloride was purchased from Fluka Analytical (Mexico City, Mexico). All materials were used as received. Water (18.3 MΩ) was filtered by a Barnstead MicroPure Standard water purification system (Thermo Scientific, Waltham, MA) and used throughout the entire experiment.

4.3.2 Preparation of a Silicon Wafer

A silicon wafer with a native oxide layer was cleaned by immersing it into hot piranha solution [7:3 (v/v) concentrated H_2SO_4/30% H_2O_2]. To a glass petri dish containing a silicon wafer in concentrated H_2SO_4, H_2O_2 was slowly added and a glass cover was placed. A heating plate was set to 40 °C and turned off after 20 minutes. After additional 10 minutes of cooling the piranha solution, the wafer was thoroughly washed with deionized water and dried with N_2 gas.

Warning: Piranha is a strong oxidant solution and reacts violently with organic materials. It should be handled with proper protective equipment in a fume hood. Extra caution is required.

4.3.3 Preparation and Deposition of DNA Nanotubes on a Silicon Wafer with an Additional Divalent Cation

DNA nanotubes were synthesized following a previously published procedure.[119] Single strands of DNA nanotubes were diluted in 10 × TAE/Mg^{2+} (125 mM Mg^{2+}) buffer solution to a final concentration of 1 μM. The DNA solution was subject to an annealing process from 95 to 23 °C over 2 days and stored at 4 °C overnight.

The annealed DNA nanotube solution and divalent cationic chloride aqueous solution (62.5, 125, or 250 mM of $CaCl_2$, $CoCl_2$, or $CdCl_2$) were mixed in equal volume. Within 30 seconds, 20 μL of the mixed solution was deposited onto a clean silicon wafer with an area of 1×1 cm^2 and the wafer was incubated in a humid chamber to minimize the evaporation of the solution. After 15 minutes, the wafer with the solution was directly immersed in an ethanol/water [9:1 (v/v)] solution for 10 seconds to remove ionic salt residues from the solution, then dried with N_2 gas. After the deposition, the DNA nanotube substrate was processed with RIE within 24 hours.

4.3.4 Reactive Ion Etching (RIE) of a DNA Nanotube Substrate

RIE was conducted using a Phantom III LT RIE system (Trion Technology, Tempe, AZ). Power and pressure were set to 100 W and 20 mTorr, respectively. Total O_2 and SF_6 flows were at 8 sccm and 20 sccm, respectively. Although process time was set to 1 second, actual exposure time to plasma was *ca.* 9.5 seconds. After etching, the RIE system was cleaned and a DNA nanotube substrate was washed with deionized water and dried with N_2 gas.

4.3.5 UV/Ozone Treatment

A DNA nanotube substrate after etching was treated with UV/O_3 in a PSD Pro 4 Digital UV Ozone Cleaner (Novascan Technologies, Inc., Ames, IA). Before UV irradiation, the chamber was filled with O_2 at least for 3 minutes, and the substrate was processed with UV/O_3 treatment for 1 hour at room temperature.

4.3.6 Characterization

4.3.6.1 Atomic force microscopy (AFM)

A DNA nanotube substrate was imaged at each step of fabrication process using tapping-mode on an MFP-3D atomic force microscope with NSC15/Al BS or NSC15/Hard/AL BS AFM probe in air at room temperature to investigate the surface morphology (Oxford Instruments Asylum Research, Inc., Santa Barbara, CA). Both NSC15/AL BS (325 kHz, 40 N/m) and NSC15/Hard/AL BS (325 kHz, 40 N/m) AFM probes were purchased from MikroMasch (Lady's Island, SC). The NSC15/AL BS AFM probe was used to scan the DNA nanotube substrate before etching with RIE. After the etching, the NSC15/Hard/AL BS (325 kHz, 40 N/m) AFM probe was used to scan the DNA nanotube substrate.

4.3.6.2 X-ray photoelectron spectroscopy (XPS)

XPS elemental analysis for the presence of Ca on the surface of Si wafer was conducted using a Thermo ScientificTM Escalab 250Xi. The monochromatic X-Ray source used an Al anode with a spot size of 0.4 mm at a takeoff angle of 45˚. Each sample was scanned with XPS at five random locations for good signal to noise ratio. 10 scans for Ca were employed at each location. Measurements were analyzed using the Thermo ScientificTM Avantage Data System.

4.4 RESULTS AND DISCUSSION

4.4.1 General Preparation Process of a DNA Nanotube Substrate with an Additional Divalent Cation

In a typical experiment, a DNA nanotube substrate with an additional divalent cation was prepared and subjected to reactive ion etching (RIE) as illustrated in Figure 39. DNA nanotubes in 10 $\times$ TAE/Mg^{2+} buffer solution were mixed with an equivalent volume of divalent cationic chloride solution (Figure 39a). Within 30 seconds, the mixed DNA nanotube solution with the extra divalent cation was deposited onto a clean silicon wafer (Figure 39b). After incubating the wafer with the mixed solution in a humid environment for 15 minutes, the substrate was directly immersed into an ethanol/water [9:1 (v/v)] solution for 10 seconds, then dried with N_2 gas (Figure 39c). Within 24 hours of the sample preparation, the substrate was subjected to RIE (Figure 39d).

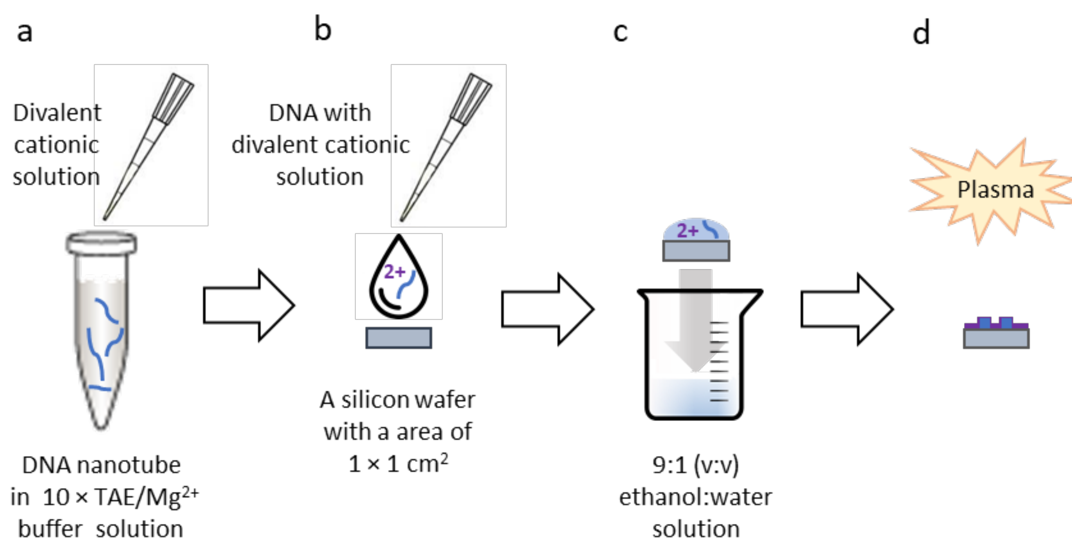

Figure 39. General preparation process of a DNA nanotube substrate with an additional divalent cation.

4.4.2 Pattern Transfer from DNA Nanotubes to a Silicon Substrate with RIE

First, we evaluate the pattern transfer process from DNA nanotubes to a silicon substrate with RIE. The width and length of the DNA nanotubes are 30–70 nm and up to 60 μm, respectively.[119] When deposited onto a silicon wafer, the nanotubes are generally collapsed, showing a height of 3.4 ± 0.1 nm.[154] To test the effect of divalent cationic ions, calcium, cobalt, and cadmium chloride were each added to the DNA solution. For a control substrate, deionized water was instead used. The surface topography of the DNA nanotube substrates before (Figure 40, top) and after (Figure 40, bottom) RIE was characterized by atomic force microscopy (AFM) at the same location. By addition of deionized water and cobalt and cadmium chloride solutions, patterns in positive tone resulted. The quality of the patterns, however, was poor enough such that the shape of the DNA nanotubes was transferred as an assembly of dots. Furthermore, the dots replicated from the single or double nanotubes were especially discontinuous and hard to

distinguish from the surrounding background. The dotted rough surface of the silica substrate was attributed to the intrinsic characteristic of RIE: a bare silicon wafer with a native oxide layer which was only cleaned with piranha solution showed similar surface features after RIE (Figure 41). We note that the positive tone pattern formed with cobalt salt was more continuous than those formed with deionized water and cadmium salt. Further study is needed to elucidate the difference resulted from adding cobalt chloride. Overall, these results are expected given the low chemical stability of DNA nanostructures under the harsh plasma etching conditions.

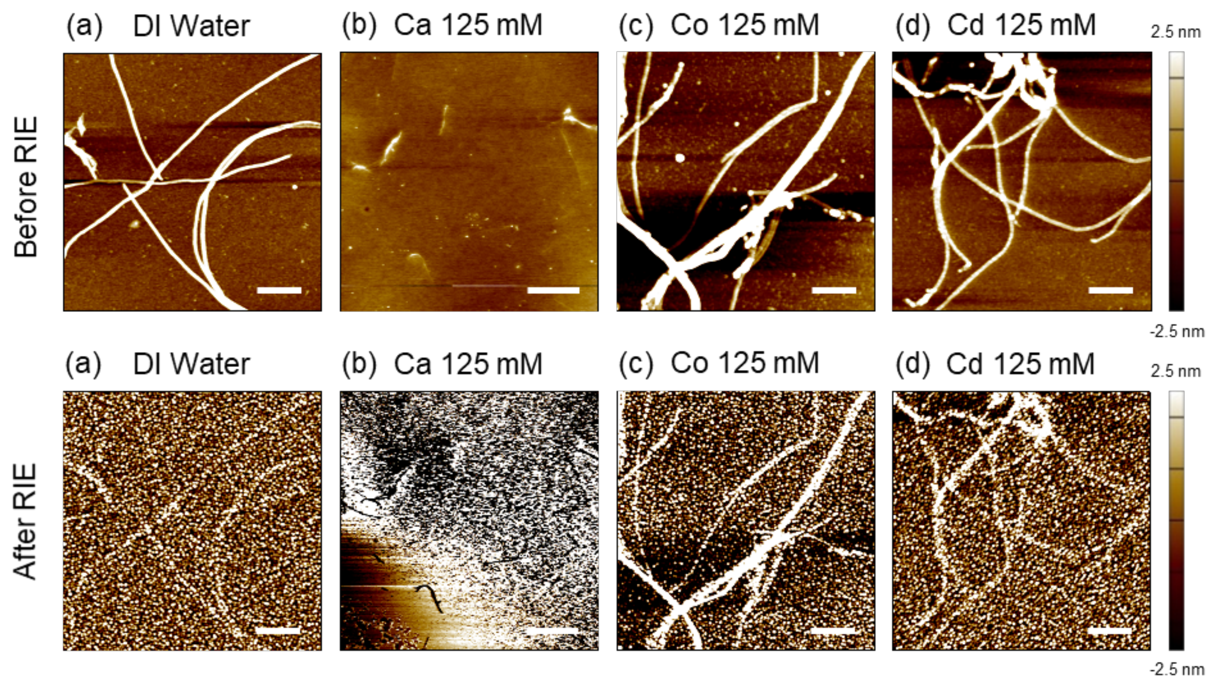

Figure 40. Pattern transfer from DNA nanotubes to a silicon wafer with RIE. AFM height images in the same location of DNA nanotubes deposited on a silicon wafer before (top) and replicas of the DNA nanotubes on the silicon wafer after (bottom) RIE. To DNA nanotube solutions, (a) deionized water, and 125 mM (b) $CaCl_2$, (c) $CoCl_2$, and (d) $CdCl_2$ aqueous solutions were added. Scale bars represent (a,c,d) 500 nm and (b) 3 µm.

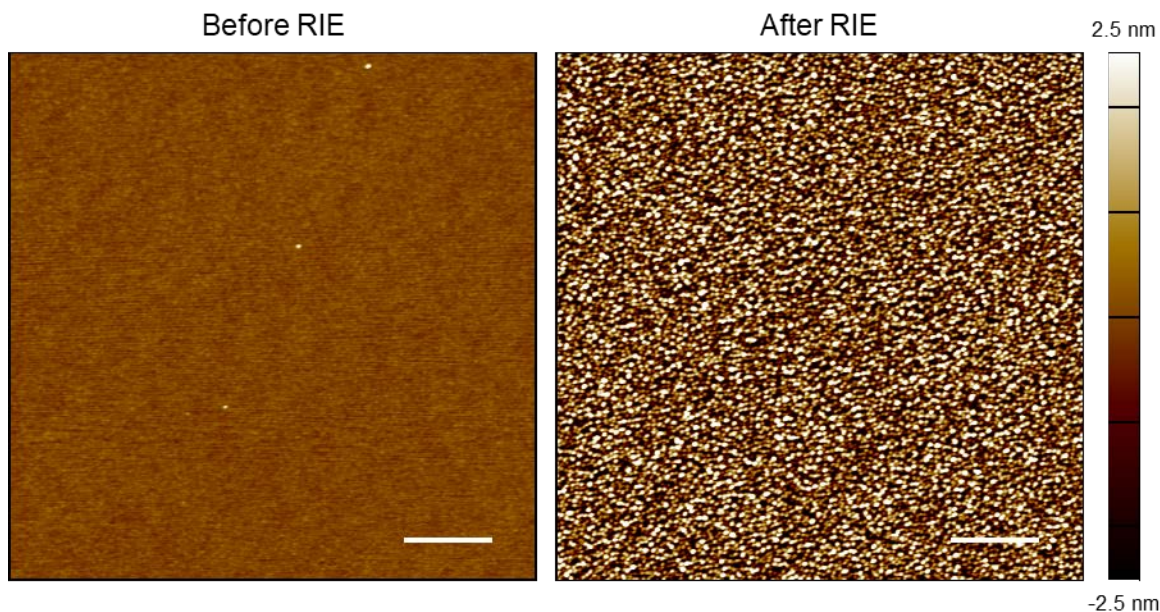

Figure 41. Intrinsic surface characteristic of a silicon wafer with RIE. AFM height images of a silicon wafer with a native oxide layer cleaned with piranha solution before (left) and after (right) RIE. Scale bars represent 500 nm.

An interesting and unexpected phenomenon was observed when calcium chloride was added to the DNA nanotubes in buffer solution (Figures 40c, 42, and 43); unlike the other cases, patterns in negative tone were observed after the etching in such cases. After deposition onto a silicon substrate, the DNA nanostructures were covered by a powdery layer which was unevenly distributed throughout the entire substrate as seen using AFM. The height of the DNA nanotubes substantially decreased in the presence of such a layer, suggesting that the thickness of the layer is greater on the background substrate than on the DNA nanotubes. Due to the presence of such a layer, it was difficult to precisely measure the height of the nanotube; the apparent height of the DNA nanotube was *ca.* 0.83 nm. After RIE, the patterns of the DNA nanotubes were transferred into negative tone. Trenches as deep as 26.87 nm were fabricated after RIE and surface cleaning by oxidation by O_3 (Figure 42). Also, the substrate surfaces were uneven from area to area. In some areas, the surface was very rough with a lot of holes or trenches which did not represent the

shape of the DNA nanostructures (Figure 43a, top and b). In contrast, the surface in other areas was entirely flat and appeared to be not etched during the RIE process (Figures 42 and 43a, bottom and c). All these results indicate that calcium chloride caused the difference in behavior from the other samples.

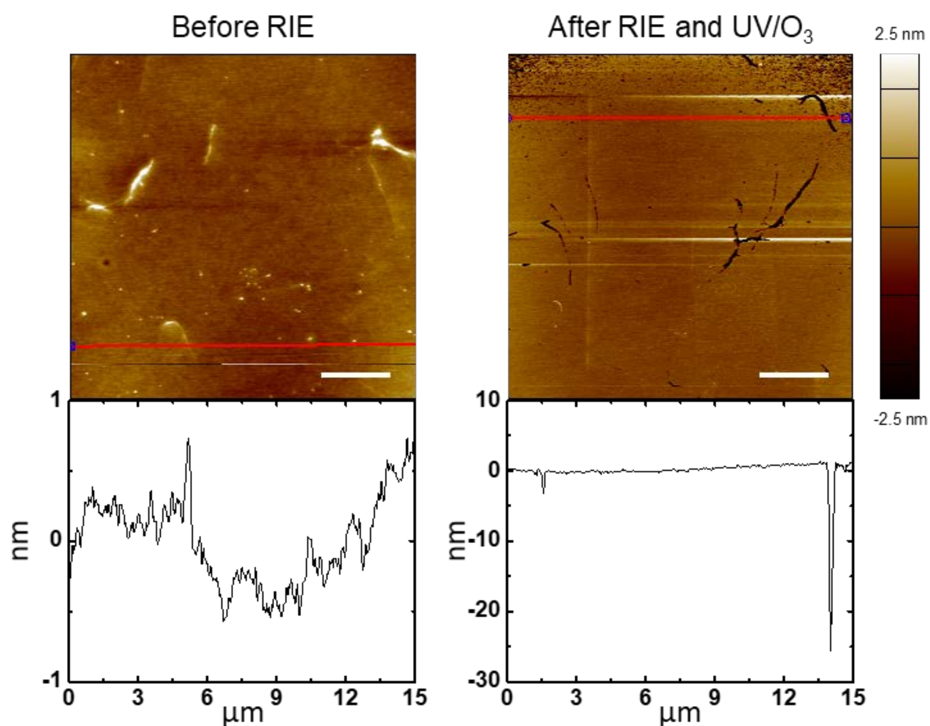

Figure 42. Negative tone pattern transfer from DNA nanotubes with addition of $CaCl_2$ to a silicon wafer with RIE. AFM height images with corresponding cross-sectional analysis in the same location of (a) DNA nanotubes deposited on a silicon wafer with 125 mM $CaCl_2$ and (b) negative replicas of the DNA nanotubes on the silicon wafer after RIE, UV/O_3 treatment for 1 h, and washing with deionized water. Red lines on the AFM images indicate where the cross-sections were determined. Scale bars represent 3 µm. The left (top) image is also shown in Figure 40.

4.4.3 Removal of Polymer Residues on an Etched DNA Nanotube Substrate with UV/O_3 Treatment

After RIE, a continuous layer of material with small globular clusters at the edges was found on some areas of the substrate (Figure 43). This layer of material was easily removed with an UV/O_3 treatment for 1 hour. Based on its removal with oxidation with O_3, we can conclude that this layer is made of organic materials. Another support for the presence of a layer coating comes from the fact that the depth of trenches decreased after the UV/O_3 treatment. At two different locations, the depth of the trenches decreased from 78.70 nm and 96.32 nm to 72.17 nm and 83.97 nm, respectively (Figure 43b).

Currently, we do not know the identity of this organic layer. The RIE system was cleaned between each run, therefore, the contaminant of the system is not likely to be the source of the layer. We thus attribute the layer to a fluorocarbon polymer which is known to form during etching process using CF_4 plasma.[159-160] We hypothesize that fluorocarbon polymer is formed from the reaction between the SF_6 plasma and the organic compounds from the buffer solution (*e.g.*, Trizma base). Further study is needed to understand the identity and deposition mechanism of this organic layer.

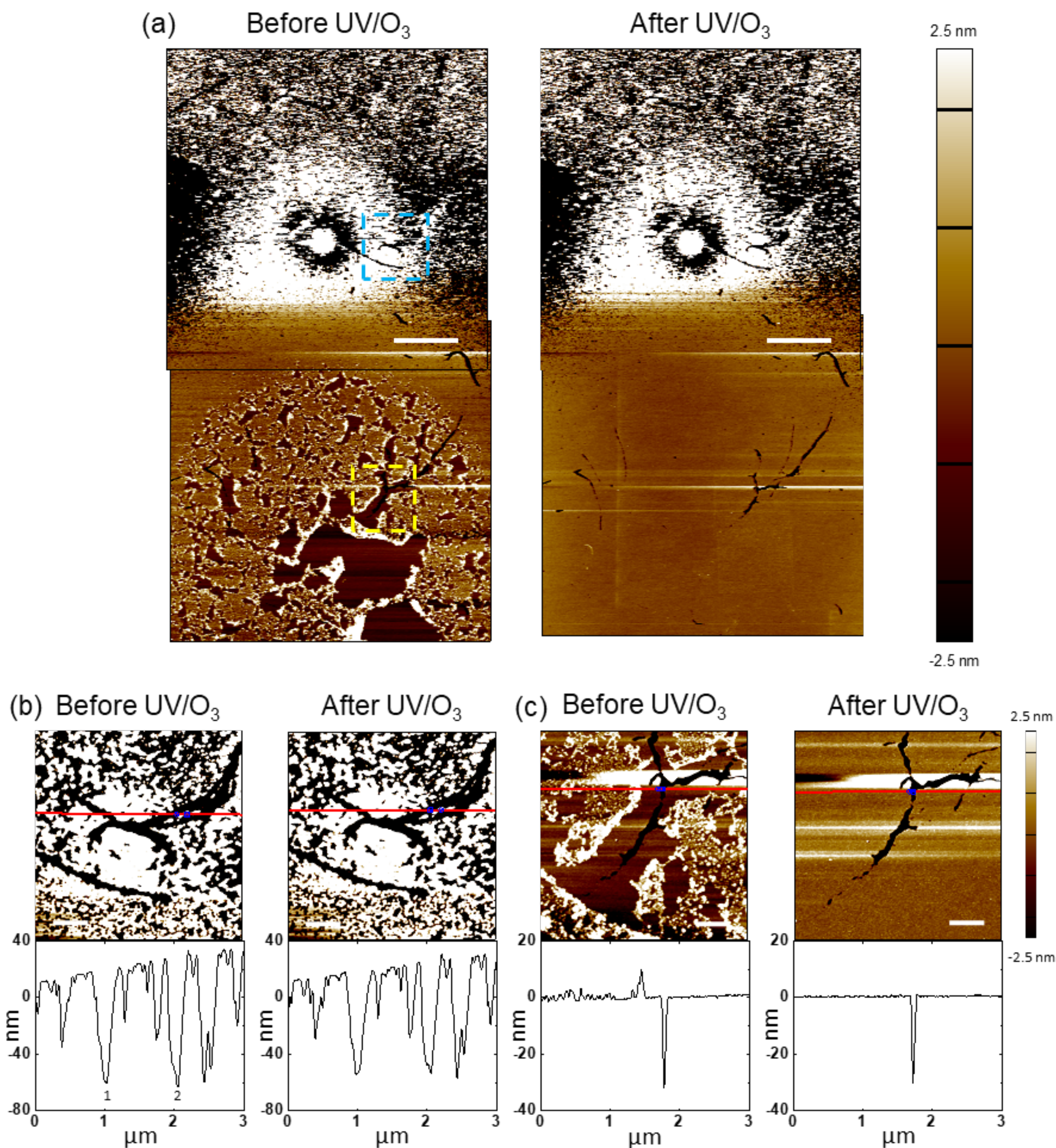

Figure 43. Removal of polymer residues on an etched DNA nanotube substrate with UV/O_3 treatment. (a) AFM height images with corresponding cross-sectional analysis in the same location of negative replicas of DNA nanotubes before (left) and after (right) UV/O_3 treatment for 1 h and washing with deionized water. AFM height images with corresponding cross-sectional analysis in the same location of the areas in the (b) blue and (c) yellow dashed boxes in image a. Red lines on the AFM images indicate where the cross-sections were determined. Locations 1 and 2 correspond to 1 and 2 in the cross-sections of image b. Scale bars represent (a) 3 µm and (b,c) 500 nm. Image a (right, lower) is also shown in Figure 42.

4.4.4 Effect of Calcium Concentration on a DNA Nanotube Substrate

As the shape of DNA nanotubes was replicated to a silicon substrate in negative tone with the addition of calcium chloride, the effect of calcium concentration was investigated within the range of 62.5 – 250 mM. Figure 44 shows that the degree of etching decreased with increasing concentration of calcium chloride. At the lowest concentration tested, 62.5 mM, an entire area of 15 x 15 μm^2 was completely etched as can be seen from the rough background (Figure 44a). Although trenches transferred from nanotubes were distinct from surrounding background, the depth of the trenches were not distinguishable from that of the background. At the medium concentration, 125 mM, islands with flat surfaces were fabricated (Figure 44b). The top of the islands was covered with organic residues and had a height of *ca.* 100 nm. At the highest concentration tested, 250 mM, most of areas were protected from the etching as can be seen in the low roughness of the background. The depth of trenches replicated from DNA was *ca.* 90 nm. This result confirms that calcium is essential to the successful pattern transfer from DNA to a silicon wafer with unetched background surface using RIE.

The thorough analysis of AFM images of the substrate prepared at the concentration of 125 mM gave us a clue of what caused this result. Direct comparison of the images before and after the RIE at the same location showed that the islands with flat surfaces formed at the locations where particles were found after DNA deposition but before RIE. Such areas were highlighted by the red circles and box in Figure 45. The presence of a large particle or a cluster of small particles before RIE correspond to the large islands after RIE, indicating that such particles protect the silicon substrate from being etched. We attribute this particle to calcium-containing precipitates (*e.g.*, $Ca(OH)_2$ crystal). In the 10 × TAE/Mg^{2+} buffer solution at a pH ~8.0, such calcium-containing compound could precipitate out when the calcium chloride

aqueous solution was added and then immersed into an ethanol:water [9:1 (v:v)] solution. The DNA nanotubes hold a lesser amount of calcium-containing precipitate than the silicon substrate and were etched away along with the underneath substrate while the surrounding substrate was protected by the precipitates.

Another interesting observation was the change that occurred on the surfaces of the silicon substrates after the RIE (Figure 46). Before the RIE, the surface of a silicon wafer with DNA nanotubes generally did not show any visual difference from a bare clean silicon wafer. After the RIE, however, the surface of the wafer became darkened with random patterns. These patterns did not disappear after washing with deionized water and oxidation by O_3. Such changes occurred on all samples subjected to the RIE regardless of the concentration of calcium chloride and were observable to both the optical microscope and the naked eye under white light.

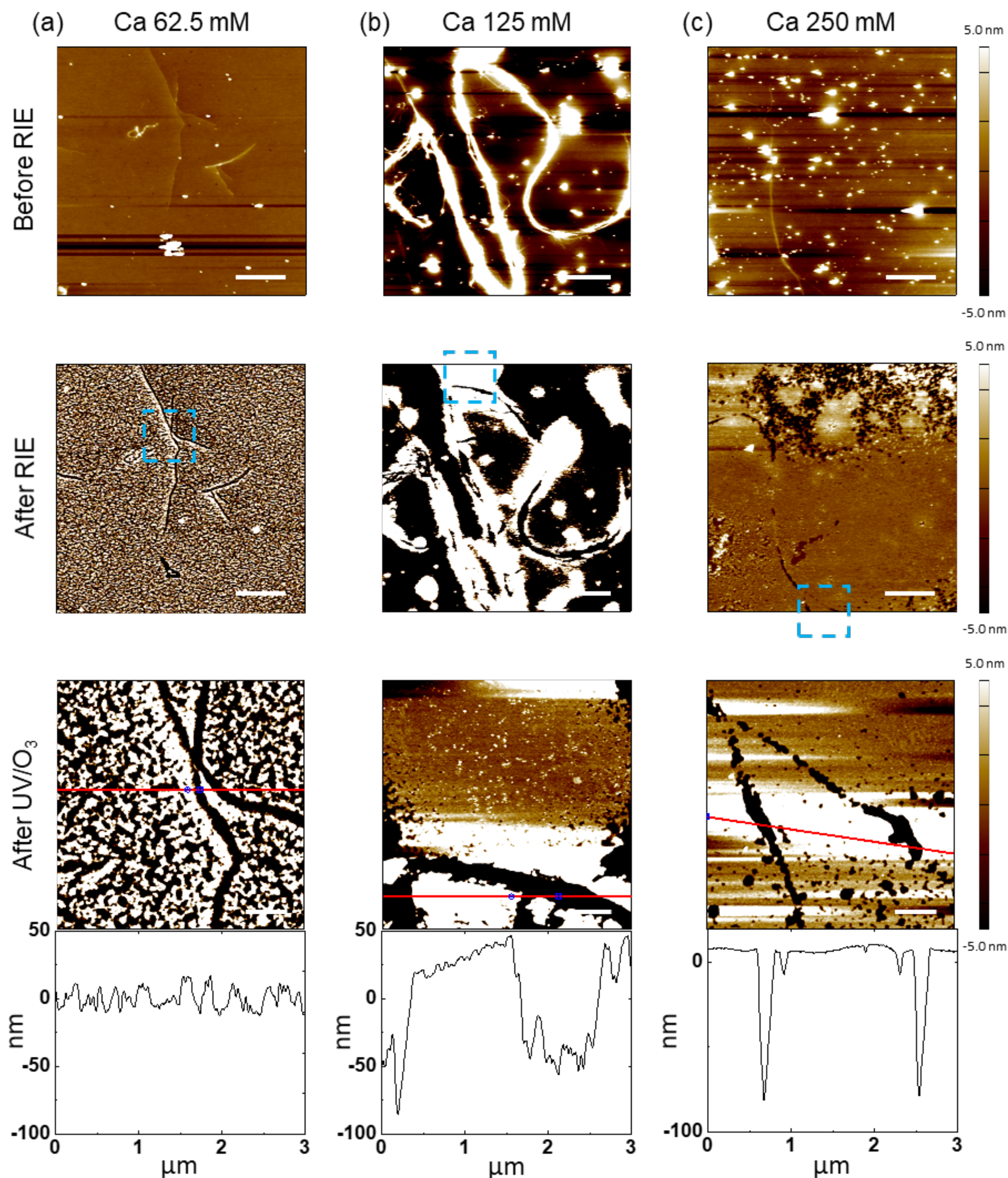

Figure 44. Effect of calcium concentration on a DNA nanotube substrate. AFM height images with corresponding cross-sectional analysis in the same location of silicon wafers after DNA nanotubes were deposited (top), RIE (middle), and UV/O_3 treatment for 1 h and washing with deionized water (bottom). To the DNA nanotubes in 10 × TAE/Mg^{2+} buffer solutions, (a) 62.5 mM, (b) 125 mM, and (c) 250 mM $CaCl_2$ solutions were added. The bottom row contains the zoomed-in views of the areas in the blue dashed boxes in the middle row. Red lines on the AFM images indicate where the cross-sections were determined. Scale bars represent 3 μm (top, middle) and 500 nm (bottom).

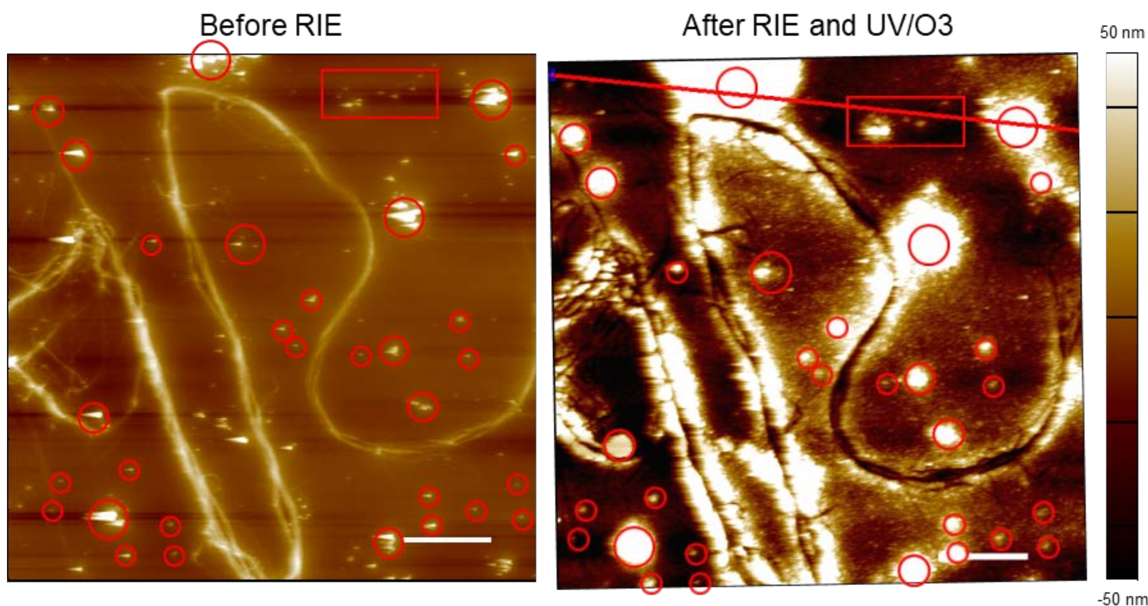

Figure 45. Direct comparison of a DNA nanotube substrate with 125 mM $CaCl_2$ before and after RIE and UV/O_3 treatment at the same location. AFM height images with corresponding cross-sectional analysis of a silicon wafer with DNA nanotubes (a) before and (b) after RIE, UV/O_3 treatment for 1 h, and washing with deionized water. To the DNA nanotubes in 10 × TAE/Mg^{2+} buffer solutions, 125 mM $CaCl_2$ solution was added. Red lines on the AFM images indicate where the cross-sections were determined. Scale bars represent 3 μm.

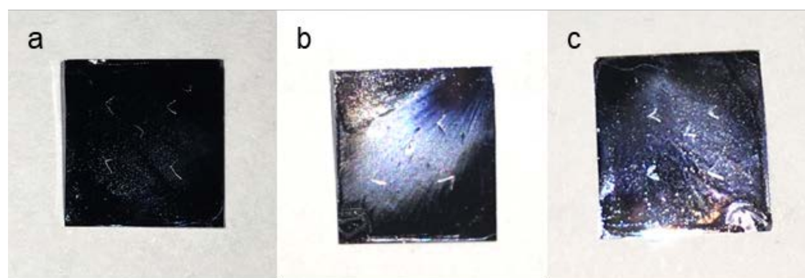

Figure 46. Surface analysis of a DNA nanotube substrate after RIE and UV/O_3 treatment. Photo image of DNA nanotube substrates after RIE and UV/O_3 treatment. To the DNA nanotubes in 10 × TAE/Mg^{2+} buffer solutions, (a) 62.5 mM, (b) 125 mM, and (c) 250 mM $CaCl_2$ solutions were added. Silicon wafers had an area of 1 × 1 cm^2. "<'" marks on the substrates were drawn with a diamond pen for AFM imaging at the same location.

4.4.5 Effects of Calcium-Containing Crystals and Their Concentration on a Silicon Substrate without DNA Nanotubes

Previously, we hypothesized that calcium-containing precipitate is a key to the protected background substrate from RIE. To verify this hypothesis, we compared silicon wafers treated with 250 mM calcium chloride solution to those treated with 62.5 – 250 mM calcium chloride solution mixed with 10 × TAE/Mg^{2+} buffer solution but without DNA nanotubes. For statistical analysis, each sample was imaged with AFM at 10 random locations twice, once after RIE and another time after oxidation by O_3. Each location was classified into one of four categories to evaluate the degree of etching: completely etched (E), islands with flat top (I), moderately etched (M), and completely flat, unetched (F) (Figure 47).

For the substrate incubated with only 250 mM $CaCl_2$ solution, most of the areas were completely etched with a few islands with flat top (Table 1). These islands were only observed at the edge of area where a small droplet of the solution evaporated (*e.g.*, from the tip of a tweezer) during the drying process with N_2 gas (Figure 48). At this edge, the concentration of calcium ions is expected to be higher due to evaporation (*i.e.*, coffee ring effect). The size and population of the islands rapidly decreased toward the center of the drop (the yellow arrow). Toward the opposite side (the blue arrow toward the center of the substrate), the entire area was completely etched. Furthermore, with increasing concentration of calcium chloride added to the buffer solution, the degree of etching progressively moved from completely etched to completely flat, unetched states. All these results suggest that calcium-containing crystals, or high concentration of calcium ions, at least, is the key to protect a silicon substrate from RIE.

The differences between the substrates with and without buffer were also observable with naked eyes. On the surface of all three samples with both calcium chloride and buffer solutions,

marks with random shapes appeared after the etching as mentioned previously. Within a sample, however, there is no direct relationship between clean and dirty areas with completely flat and totally etched surfaces. In contrast, for the sample only treated with calcium chloride aqueous solution, there was no visible difference before and after etching when inspected with naked eyes and an optical microscope. On this sample, only the evaporation mark became relatively darkened.

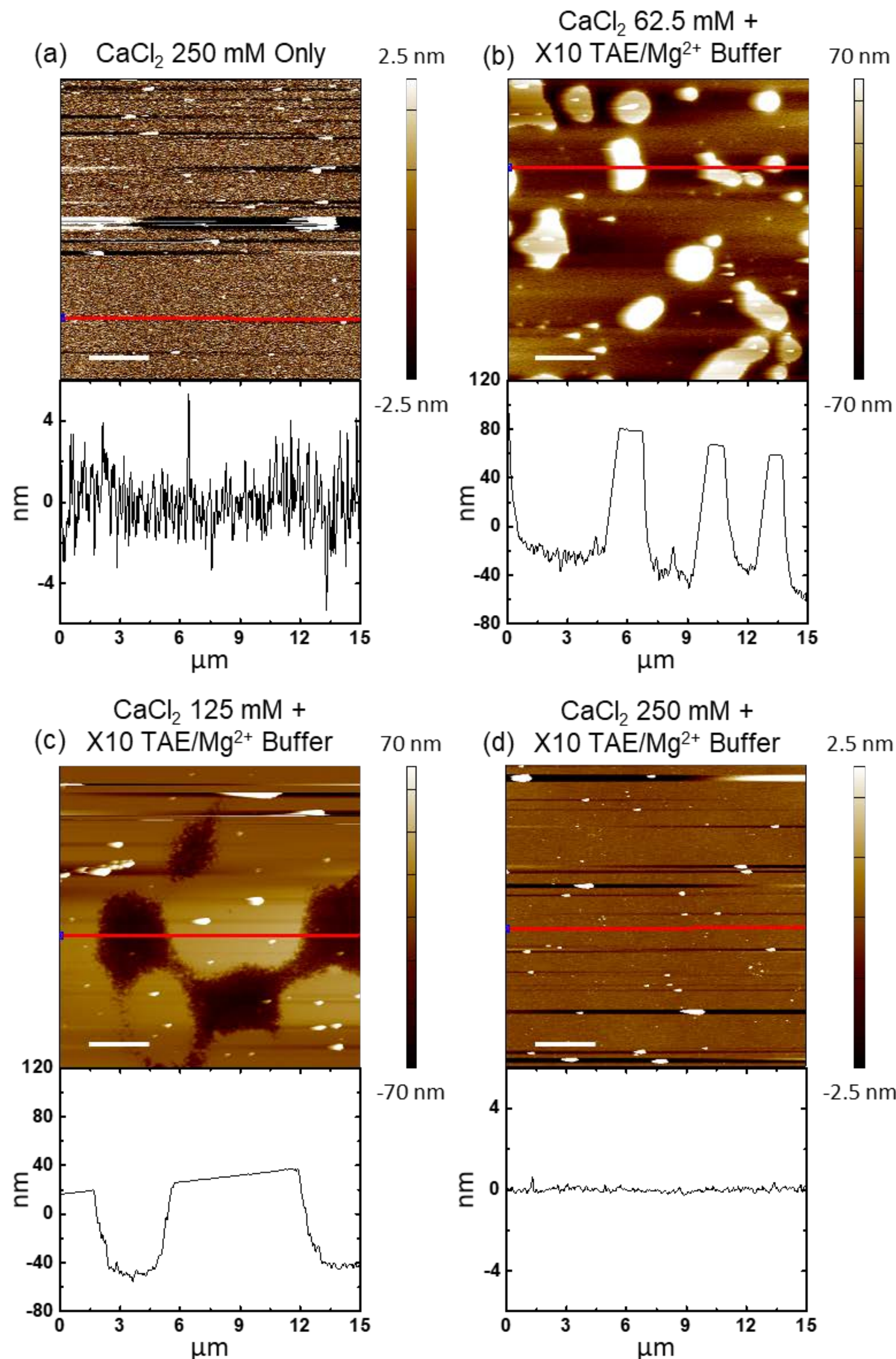

Figure 47. Representative images of degrees of etching. AFM height images with corresponding cross-sectional analysis of silicon wafers without DNA nanotubes after RIE, UV/O_3 treatment for 1 h, and washing with deionized water. The wafers were incubated with (a) 250 mM $CaCl_2$ and 10 × TAE/Mg^{2+} buffer solutions to which (b) 62.5 mM, (c) 125 mM, and (d) 250 mM $CaCl_2$ solutions were added. The AFM images were classified as (a) completely etched (E), (b) islands with flat top (I), (c) moderately etched (M), and (d) completely flat, unetched (F). Red lines on the AFM images indicate where the cross-sections were determined. Scale bars represent 3 µm.

Table 1. Statistical analysis of degrees of etching. Silicon wafers were incubated with 250 mM $CaCl_2$ and 10 × TAE/Mg^{2+} buffer solutions to which 62.5 mM, 125 mM, and 250 mM $CaCl_2$ solutions were added. The AFM images were classified as (a) completely etched (E), islands with flat top (I), moderately etched (M), and completely flat, unetched (F).

	250 mM $CaCl_2$				**10 × TAE/Mg^{2+} + 62.5 mM $CaCl_2$**				**10 × TAE/Mg^{2+} + 125 mM $CaCl_2$**				**10 × TAE/Mg^{2+} + 250 mM $CaCl_2$**			
	T	**I**	**M**	**N**	**T**	**I**	**M**	**N**	**T**	**I**	**M**	**N**	**T**	**I**	**M**	**N**
After RIE	9	1	0	0	0	8	1	1	2	4	1	3	3	0	4	3
After UV/O_3	8	2	0	0	0	9	0	1	1	5	3	1	1	1	5	3
Total	**17**	**3**	**0**	**0**	**0**	**17**	**1**	**2**	**3**	**9**	**4**	**4**	**4**	**1**	**9**	**6**

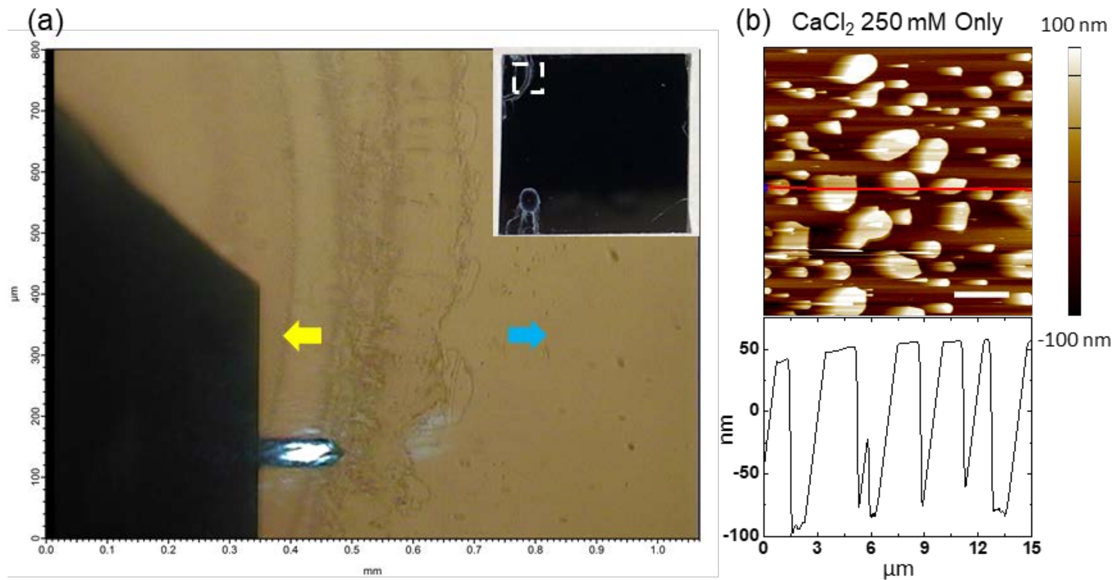

Figure 48. Analysis of a silicon substrate incubated with 250 mM $CaCl_2$ after RIE and UV/O_3 treatment. (a) Optical microscopic and (b) AFM height images with corresponding cross-sectional analysis of a silicon wafer incubated only with 250 mM $CaCl_2$ after RIE, UV/O_3 treatment for 1 h, and washing with deionized water. The optical image was taken while the AFM image was taken. The inset in image a is the photo image of the wafer. The silicon wafer had an area of 1 × 1 cm^2. White dashed box approximates the location of the optical microscopic and AFM images. The yellow arrow points toward the center of mark of the evaporation while the blue arrow points toward the center of the wafer. Red lines on the AFM images indicate where the cross-sections were determined. Scale bars represent 3 µm.

4.4.6 XPS Analysis of Calcium Coverage on a Silicon Substrate

To confirm the presence of Ca on the surface of Si wafer, XPS elemental analysis was conducted on a new set of samples. Each sample was scanned with XPS at five random locations (Table 2). The data confirms not only the presence of Ca on all samples but also that the surface Ca coverage (4.47 ± 0.68 atomic %) of a substrate treated with $CaCl_2$ only was substantially lower than those of substrates treated with both $CaCl_2$ and 10 × TAE/Mg^{2+} buffer (30.11 ± 23.42, 38.12 ± 20.24, and 35.11 ± 21.38 atomic % for 62.5, 125, and 250 mM $CaCl_2$ added to the buffer, respectively). Furthermore, the surface Ca coverage showed a large standard deviation, indicating that it is difficult to control the deposition of calcium on a silicon wafer (Table 2 and Figure 49).

Table 2. XPS analysis of calcium and silicon coverage on a silicon substrate. Silicon wafers were incubated with 250 mM $CaCl_2$ and 10 × TAE/Mg^{2+} buffer solutions to which 62.5 mM, 125 mM, and 250 mM $CaCl_2$ solutions were added. The silicon wafers used for XPS analysis were different from the wafers used for statistical analysis of degrees of etching in Table 1.

	250 mM $CaCl_2$		**10 × TAE/Mg^{2+} + 62.5 mM $CaCl_2$**		**10 × TAE/Mg^{2+} + 125 mM $CaCl_2$**		**10 × TAE/Mg^{2+} + 250 mM $CaCl_2$**	
	Ca Atomic %	**Si Atomic %**	**Ca Atomic %**	**Si Atomic %**	**Ca Atomic %**	**Si Atomic %**	**Ca Atomic %**	**Si Atomic %**
1	3.66	96.34	63.86	36.14	54.28	45.72	57.94	42.06
2	4.29	95.71	11.06	88.94	39.65	60.35	8.59	91.41
3	4.43	95.57	36.12	63.88	47.69	52.31	44.94	55.06
4	5.55	94.45	4.91	95.09	3.14	96.86	16.42	83.58
5	4.43	95.57	34.59	65.41	45.82	54.18	47.67	52.33
Ave.	**4.47**	**95.53**	**30.11**	**69.89**	**38.12**	**61.88**	**35.11**	**64.89**
St. dev.	**0.68**		**23.42**		**20.24**		**21.38**	

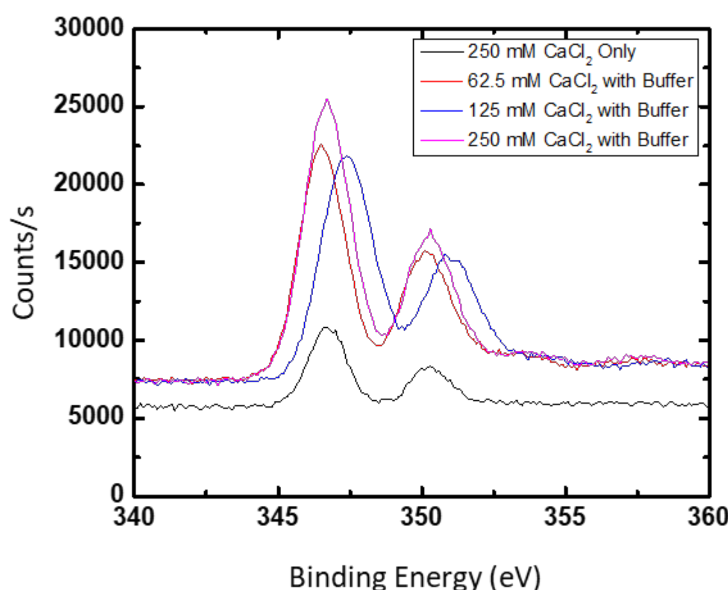

Figure 49. XPS analysis of calcium coverage on a silicon substrate. Out of five XPS measurements for each sample, that which had the highest calcium coverage was chosen.

4.4.7 Relationship between the Height of DNA Nanotubes to the Depth of Trenches

The relationship between the height of DNA nanotubes and the depth of trenches was also investigated. Between single/low and multiple/high DNA nanotubes, continuous and deeper trenches were formed from the multiple/high DNA nanotubes. This indicates that the high and/or multiple DNA nanotubes more effectively modulated the calcium deposition than the low and/or single nanotubes. However, there was not a precise correlation between the depth of the trenches and the height of the DNA nanotube structures. The DNA nanotubes with height of 1.81 nm and 2.10 nm resulted in the trenches with depth of 45.29 nm and 22.73 nm while the DNA nanotubes with height of 3.69 nm and 7.14 nm resulted in trenches with depth of 89.45 nm and 86.14 nm, respectively. Possible explanations for this observation are that it is difficult to precisely measure

the original height of DNA nanostructures due to uneven deposition of the calcium-containing materials on the surface.

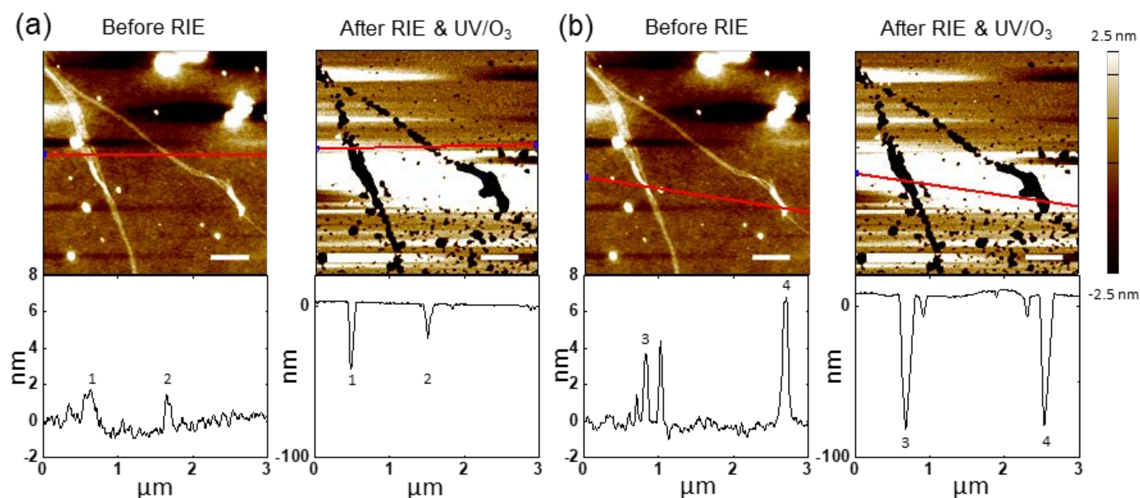

Figure 50. Relationship between height of DNA nanotubes to depth of trenches. AFM height images with corresponding cross-sectional analysis of (a) single/low and (b) multiple/high DNA nanotubes on a silicon wafer before (left) and after (right) RIE, UV/O_3 treatment for 1 h, and washing with deionized water. To the DNA nanotubes in 10 × TAE/Mg^{2+} buffer solutions, 125 mM $CaCl_2$ solutions were added. Red lines on the AFM images indicate where the cross-sections were determined. Scale bars represent 500 nm.

4.4.8 Proposed Mechanism

We attribute the negative tone pattern transfer from DNA nanostructures to a silicon wafer with protected surrounding surface to an interference of plasma with calcium-containing compound. We propose that after a calcium chloride solution is mixed with 10 × TAE/Mg^{2+} buffer solution (pH ~8.0), calcium-containing precipitate is formed when the wafer is immersed into an ethanol:water [9:1 (v:v)] solution.

The calcium-containing precipitates cover the surface of the DNA nanotube substrate (Figure 51a). Multiple/high DNA nanotubes modulate the calcium deposition more effectively between the nanotube and the background substrate than single/low nanotubes. During RIE, plasma interferes with calcium-containing compounds. While the background silicon substrate with the thicker layer of calcium is minimally influenced from plasma, the DNA nanostructures with the thinner layer of calcium are removed and the substrate underneath is etched away (Figure b). The role of the organic residues is not yet understood.

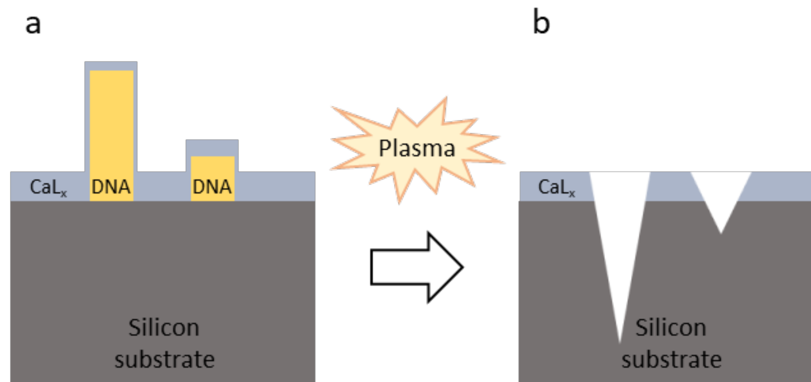

Figure 51. Proposed mechanism of negative tone pattern transfer from DNA nanostructures to a silicon wafer with protected surrounding surface. (a) The calcium-containing precipitates cover the surface of a DNA nanotube substrate. (b) The area of the silicon wafer underneath the DNA nanotubes is etched away while the surrounding silicon wafer is minimally influenced from plasma.

4.5 CONCLUSION

By using calcium to modulate plasma etching, negative tone pattern can be directly transferred from DNA nanostructures to a Si substrate with minimal etching of the background. To the best our knowledge, this result is the first to achieve a high contrast pattern transfer from unmodified DNA nanostructures to Si. A high concentration of Ca^{2+} is necessary although the buffer additionally played an important role that is not yet fully understood. This result is consistent with the idea that DNA nanostructures inhibit the adsorption of a calcium-containing solid, which in turn promotes the etching of Si underneath DNA. Given the weak chemical stability of DNA, the successful pattern transfer from DNA nanostructures to Si under such harsh conditions is unexpected. We hope this work will catalyze more work to reveal the true potential of DNA nanostructures in nanofabrication.

5.0 CONCLUSION

In this dissertation, my research focused on DNA based nanofabrication, most specifically, patterning soft and hard substrates at the nanoscale with DNA nanostructures. I developed a general fabrication method of a nano-structured polymeric thin film using a DNA nanostructure master template. In addition, this DNA master template can be repeatedly used to produce multiple copies of the polymeric film through conformal coating with a nanometer-thin protective inorganic oxide layer created using atomic layer deposition. A silicon substrate was also patterned at nanoscale in negative tones with DNA nanostructures with minimal etching of the background using reactive ion etching. Below, I summarize the main conclusions, and discuss the future directions of this dissertation.

5.1 DNA NANOSTRUCTURES-MEDIATED MOLECULAR IMPRINTING LITHOGRAPHY

In chapter two, I developed and demonstrated an advanced nanoimprint lithography method to construct poly(methyl methacrylate) (PMMA), poly-L-lactide (PLLA), and perfluoropolyether (PFPE) stamps with negative tone patterns using one- to three-dimensional DNA nanostructures to transfer patterns with high fidelity. DNA nanostructures including DNA nanotubes, stretched λ-DNA, two-dimensional (2D) DNA brick crystals with three-dimensional (3D) features, hexagonal DNA 2D arrays, and DNA origami triangles were used as master templates. The resulting negative imprints of the DNA nanostructures on the polymer stamps have diverse nanoscale features with dimensions ranging from several tens of nanometers to microns. The PMMA and PLLA stamps further served as molds to transfer the patterns to positive imprints on a-PFPE films. This work establishes an approach to using self-assembled DNA templates for applications in soft lithography.

Our method can enrich polymer stamps with enormously complex nanoscale features. Watson-Crick base pairing allows DNA nanostructures to be fabricated into multi-dimensional shapes that are not accessible by other self-assembly methods. The integration of DNA nanotechnology with soft lithography provides an alternative method to produce polymer stamps, which in turn can be potentially used in applications such as patterning small molecules and proteins through contact printing.[112-113, 147-148]

5.2 INCREASING THE STABILITY OF DNA NANOSTRUCTURE TEMPLATES BY ATOMIC LAYER DEPOSITION OF AL_2O_3 AND ITS APPLICATION IN IMPRINTING LITHGRAPHY

In chapter three, I presented a method to increase the stability of DNA nanostructure templates through conformal coating with a nanometer-thin protective inorganic oxide layer created using atomic layer deposition (ALD). DNA nanotubes and origami triangles were coated with *ca.* 2 nm, *ca.* 5 nm and *ca.* 20 nm of Al_2O_3. The ALD-coated DNA templates were used as master templates for a direct pattern transfer to poly(L-lactide) films. The mechanical and/or chemical stability increased with the growing thickness of the Al_2O_3 coating, but some of the nanoscale features of the DNA nanostructures were lost. The results indicated that the conformal coating of the *ca.* 5 nm of Al_2O_3 layer provided both the stability for repeated use in soft lithography and preserved nanoscale feature of the DNA master template. The *ca.* 5 nm of Al_2O_3 layer also protected the underlying DNA nanostructures from exposure to UV/O_3 and allowed the removal of polymeric residues from the master template.

In our method, the polymer stamps were fabricated by spin-coating of polymer in dichloromethane solution onto the ALD-coated DNA templates. The ALD-coated DNA templates can be used in the conventional nanoimprint lithography process to pattern the polymer film, by compressing down the template against the polymer which is heated above its glass transition temperature.[161] For example, the glass transition temperature of PMMA is 105 °C. Since DNA origami structures were still stable after 10 minutes of exposure to 250 °C temperatures,[139] both the DNA template and PMMA can be heated above 105 °C, compressed against each other, and separated after the temperature cools down below 105 °C, the PMMA's glass transition temperature.

The ALD-coated DNA templates can be further extended to other applications, such as the fabrication of nanoscale channels and bioinspired surfaces. In the first case, the ALD-coated DNA templates can be heated above 250 °C to remove the DNA nanostructures within the coating to form hollow channel. In the second case, biomimetic surface can be fabricated with DNA nanostructures to study its antifouling effect.[162-163]

5.3 CALCIUM INTERFERENCE IN REACTIVE ION ETCHING FOR NANOSCALE PATTERNING OF HIGH ASPECT RATIO

In chapter four, I demonstrated a new method of direct high contrast pattern transfer from DNA nanostructures to a Si substrate by reactive ion etching (RIE). By the addition of calcium chloride to 10 × TAE/Mg^{2+} buffer solution, calcium-containing compound precipitated due to its low solubility in an ethanol/water mixture. DNA nanostructures inhibit the adsorption of such calcium-containing compounds and locally enhance the plasma etching rate of a Si substrate. The Si substrate underneath DNA was etched away to result in negative trenches while the background substrate was minimally etched. Although the identity of the compound and the role of the buffer were not fully understood, a high concentration of Ca^{2+} was required to achieve high contrast pattern transfer from unmodified DNA nanostructures to silicon.

DNA is generally considered a soft material. However, DNA nanostructures were employed in hydrous[102] and anhydrous[104] HF vapor-phase etching for a direct pattern transfer from the DNA nanostructures to the SiO_2 substrate. In addition, the patterns of DNA nanostructures were intact during atomic layer deposition of Al_2O_3 at 200 °C.[105,164] Finally, DNA nanostructures were also employed in high contrast negative tone pattern transfer from the DNA nanostructures to the Si substrate using reactive ion etching. All these results suggest that the application window of DNA nanostructures is much wider than we had previously thought. We hope this work will promote others to further develop DNA-based nanofabrication.

5.4 FINAL REMARKS

Overall, my research provided new insight into nanoscale patterning of soft and hard materials using DNA nanostructures. I hope these results could catalyze future work to reveal the true potential of DNA nanostructures and their applications.

APPENDIX

LIST OF ABBREVIATIONS

AFM	Atomic force microscopy
ALD	Atomic layer deposition
a-PFPE	Acryloxy perfluoropolyether
DNA	Deoxyribonucleic acid
DUV	Deep ultraviolet lithography
EBL	Electron-beam lithography
EDTA	Ethylenediaminetetraacetic acid
EUV	Extreme ultraviolet lithography
FWHM	Full width at half maximum
IL	Immersion lithography
PLLA	Poly(L-lactide)
PMMA	Poly(methyl methacrylate)
PDMS	Polydimethylsiloxane
RIE	Reactive ion etching
TEM	Transmission electron microscopy

Trizma base	Amino-2-(hydroxymethyl)-1,3-propanediol
TMA	Trimethylaluminum
XPS	X-ray photoelectron spectroscopy

BIBLIOGRAPHY

1. Moore, E. Cramming More Components onto Integrated Circuits. Proc. IEEE 1998, 86, 82-84.

2. Mack, C. A., Fifty Years of Moore's Law. *Semiconductor Manufacturing, IEEE Transactions on* **2011,** *24* (2), 202-207.

3. Leggett, G. J., 8 - Photolithography beyond the diffraction limit. In *Nanolithography and Patterning Techniques in Microelectronics*, Bucknall, D. G., Ed. Woodhead Publishing: 2005; pp 238-266.

4. Rothschild, M.; Horn, M. W.; Keast, C. L.; Kunz, R. R.; Liberman, V.; Palmateer, S. C.; Doran, S. P.; Forte, A. R.; Goodman, R. B.; Sedlacek, J. H., Photolithography at 193 nm. *Lincoln Laboratory Journal* **1997,** *10* (1), 19-34.

5. Mistry, K.; Allen, C.; Auth, C.; Beattie, B.; Bergstrom, D.; Bost, M.; Brazier, M.; Buehler, M.; Cappellani, A.; Chau, R.; Choi, C. H.; Ding, G.; Fischer, K.; Ghani, T.; Grover, R.; Han, W.; Hanken, D.; Hattendorf, M.; He, J.; Hicks, J.; Huessner, R.; Ingerly, D.; Jain, P.; James, R.; Jong, L.; Joshi, S.; Kenyon, C.; Kuhn, K.; Lee, K.; Liu, H.; Maiz, J.; McIntyre, B.; Moon, P.; Neirynck, J.; Pae, S.; Parker, C.; Parsons, D.; Prasad, C.; Pipes, L.; Prince, M.; Ranade, P.; Reynolds, T.; Sandford, J.; Shifren, L.; Sebastian, J.; Seiple, J.; Simon, D.; Sivakumar, S.; Smith, P.; Thomas, C.; Troeger, T.; Vandervoorn, P.; Williams, S.; Zawadzki, K. In *A 45nm Logic Technology with High-k+Metal Gate Transistors, Strained Silicon, 9 Cu Interconnect Layers, 193nm Dry Patterning, and 100% Pb-free Packaging*, Electron Devices Meeting, 2007. IEDM 2007. IEEE International, 10-12 Dec. 2007; 2007; pp 247-250.

6. Lapedus, M. One-On-One: Mark Bohr | Semiconductor Engineering http://semiengineering.com/one-on-one-mark-bohr/ (accessed Feb 24, 2018).

7. Nalamalpu, A.; Kurd, N.; Deval, A.; Mozak, C.; Douglas, J.; Khanna, A.; Paillet, F.; Schrom, G.; Phelps, B. In *Broadwell: A family of IA 14nm processors*, 2015 Symposium on VLSI Circuits (VLSI Circuits), 17-19 June 2015; 2015; pp C314-C315.

8. Hruska, J. Intel delays Broadwell release date until 2014 because of defect density issues | ExremeTech http://www.extremetech.com/computing/168799-intel-delays-broadwell-2014 (accessed Feb 24, 2018).

9. Intel. Intel 14 nm Technology http://www.intel.com/content/www/us/en/silicon-innovations/intel-14nm-technology.html (accessed Feb 24, 2018).

10. Li, L.; Liu, X.; Pal, S.; Wang, S.; Ober, C. K.; Giannelis, E. P., Extreme ultraviolet resist materials for sub-7 nm patterning. *Chemical Society Reviews* **2017**.

11. Fujiwara, K. In *Novel EUV resist development for sub-14 nm half pitch*, 2017 China Semiconductor Technology International Conference (CSTIC), 12-13 March 2017; 2017; pp 1-2.

12. Chang, Y. W.; Ru-Gun, L.; Fang, S. Y. In *EUV and e-beam manufacturability: Challenges and solutions*, 2015 52nd ACM/EDAC/IEEE Design Automation Conference (DAC), 8-12 June 2015; 2015; pp 1-6.

13. Manfrinato, V. R.; Zhang, L.; Su, D.; Duan, H.; Hobbs, R. G.; Stach, E. A.; Berggren, K. K., Resolution Limits of Electron-Beam Lithography toward the Atomic Scale. *Nano Letters* **2013,** *13* (4), 1555-1558.

14. Manfrinato, V. R.; Stein, A.; Zhang, L.; Nam, C.-Y.; Yager, K. G.; Stach, E. A.; Black, C. T., Aberration-Corrected Electron Beam Lithography at the One Nanometer Length Scale. *Nano Letters* **2017,** *17* (8), 4562-4567.

15. Mohammad, M.A.; Muhammad, M. Fundamentals of Electron Beam Exposure and Development. In Nanofabrication; Stepanova, M., Dew, S., Eds.; Springer-Verlag Wien: Wien, 2012; Vol. 8, pp 11-41.

16. Ha, D.; Yang, C.; Lee, J.; Lee, S.; Lee, S. H.; Seo, K. I.; Oh, H. S.; Hwang, E. C.; Do, S. W.; Park, S. C.; Sun, M. C.; Kim, D. H.; Lee, J. H.; Kang, M. I.; Ha, S. S.; Choi, D. Y.; Jun, H.; Shin, H. J.; Kim, Y. J.; Lee, J.; Moon, C. W.; Cho, Y. W.; Park, S. H.; Son, Y.; Park, J. Y.; Lee, B. C.; Kim, C.; Oh, Y. M.; Park, J. S.; Kim, S. S.; Kim, M. C.; Hwang, K. H.; Nam, S. W.; Maeda, S.; Kim, D. W.; Lee, J. H.; Liang, M. S.; Jung, E. S. In *Highly manufacturable 7nm FinFET technology featuring EUV lithography for low power and high performance applications*, 2017 Symposium on VLSI Technology, 5-8 June 2017; 2017; pp T68-T69.

17. Jian, K.; Young, E. F. Y. In *An efficient layout decomposition approach for Triple Patterning Lithography*, Design Automation Conference (DAC), 2013 50th ACM / EDAC / IEEE, May 29 2013-June 7 2013; 2013; pp 1-6.

18. Ma, Q.; Zhang, H.; Wong, M. D. F., Triple patterning aware routing and its comparison with double patterning aware routing in 14nm technology. In *Proceedings of the 49th Annual Design Automation Conference*, ACM: San Francisco, California, 2012; pp 591-596.

19. Sivakumar, S. In *EUV lithography: Prospects and challenges*, Design Automation Conference (ASP-DAC), 2011 16th Asia and South Pacific, 25-28 Jan. 2011; 2011; pp 402-402.

20. Wagner, C.; Harned, N., Lithography gets extreme. *Nature Photonics* **2010,** *4*, 24.

21. Kelleher, A. Completing Fab 42 in Arizona Is a Statement of Our Belief in Our Ability to Continue to Progress Moore's Law | Intel Newsroom http://www.intel.com/content/www/us/en/silicon-innovations/intel-14nm-technology.html (accessed Feb 24, 2018).

22. Shim, W.; Braunschweig, A. B.; Liao, X.; Chai, J.; Lim, J. K.; Zheng, G.; Mirkin, C. A., Hard-tip, soft-spring lithography. *Nature* **2011,** *469* (7331), 516-521.

23. Gong, J.; Lipomi, D. J.; Deng, J.; Nie, Z.; Chen, X.; Randall, N. X.; Nair, R.; Whitesides, G. M., Micro- and Nanopatterning of Inorganic and Polymeric Substrates by Indentation Lithography. *Nano Lett.* **2010,** *10* (7), 2702-2708.

24. Haynes, C. L.; Van Duyne, R. P., Nanosphere Lithography: A Versatile Nanofabrication Tool for Studies of Size-Dependent Nanoparticle Optics. *J. Phys. Chem. B* **2001,** *105* (24), 5599-5611.

25. Hawker, C. J.; Russell, T. P., Block Copolymer Lithography: Merging "Bottom-Up" with "Top-Down" Processes. *MRS Bull.* **2005,** *30* (12), 952-966.

26. Stoykovich, M. P.; Muller, M.; Kim, S. O.; Solak, H. H.; Edwards, E. W.; de Pablo, J. J.; Nealey, P. F., Directed assembly of block copolymer blends into nonregular device-oriented structures. *Science* **2005,** *308* (5727), 1442-1446.

27. Ruiz, R.; Kang, H. M.; Detcheverry, F. A.; Dobisz, E.; Kercher, D. S.; Albrecht, T. R.; de Pablo, J. J.; Nealey, P. F., Density multiplication and improved lithography by directed block copolymer assembly. *Science* **2008,** *321* (5891), 936-939.

28. Jeong, S. J.; Kim, J. Y.; Kim, B. H.; Moon, H. S.; Kim, S. O., Directed self-assembly of block copolymers for next generation nanolithography. *Mater. Today* **2013,** *16* (12), 468-476.

29. Liao, W.-S.; Cheunkar, S.; Cao, H. H.; Bednar, H. R.; Weiss, P. S.; Andrews, A. M., Subtractive Patterning via Chemical Lift-Off Lithography. *Science* **2012,** *337* (6101), 1517-1521.

30. Cao, H. H.; Nakatsuka, N.; Liao, W.-S.; Serino, A. C.; Cheunkar, S.; Yang, H.; Weiss, P. S.; Andrews, A. M., Advancing Biocapture Substrates via Chemical Lift-Off Lithography. *Chemistry of Materials* **2017,** *29* (16), 6829-6839.

31. Xu, X.; Yang, Q.; Cheung, K. M.; Zhao, C.; Wattanatorn, N.; Belling, J. N.; Abendroth, J. M.; Slaughter, L. S.; Mirkin, C. A.; Andrews, A. M.; Weiss, P. S., Polymer-Pen Chemical Lift-Off Lithography. *Nano Letters* **2017,** *17* (5), 3302-3311.

32. Elhadj, S.; Rioux, R. M.; Dickey, M. D.; DeYoreo, J. J.; Whitesides, G. M., Subnanometer Replica Molding of Molecular Steps on Ionic Crystals. *Nano Lett.* **2010,** *10* (10), 4140-4145.

33. Xu, Q. B.; Mayers, B. T.; Lahav, M.; Vezenov, D. V.; Whitesides, G. M., Approaching zero: Using fractured crystals in metrology for replica molding. *J. Am. Chem. Soc.* **2005,** *127* (3), 854-855.

34. Hua, F.; Sun, Y. G.; Gaur, A.; Meitl, M. A.; Bilhaut, L.; Rotkina, L.; Wang, J. F.; Geil, P.; Shim, M.; Rogers, J. A., Polymer imprint lithography with molecular-scale resolution. *Nano Lett.* **2004,** *4* (12), 2467-2471.

35. Maynor, B. W.; LaRue, I.; Hu, Z.; Rolland, J. P.; Pandya, A.; Fu, Q.; Liu, J.; Spontak, R. J.; Sheiko, S. S.; Samulski, R. J.; Samulski, E. T.; DeSimone, J. M., Supramolecular Nanomimetics: Replication of Micelles, Viruses, and Other Naturally Occurring Nanoscale Objects. *Small* **2007,** *3* (5), 845-849.

36. Truong, T. T.; Lin, R.; Jeon, S.; Lee, H. H.; Maria, J.; Gaur, A.; Hua, F.; Meinel, I.; Rogers, J. A., Soft lithography using acryloxy perfluoropolyether composite stamps. *Langmuir* **2007,** *23* (5), 2898-2905.

37. Watson, J. D.; Crick, F. H. C., Molecular structure of nucleic acids. *Resonance* **2004,** *9* (11), 96-98.

38. Seeman, N. C., Nanotechnology and the Double Helix. *Scientific American* **2004,** *290* (6), 64-75.

39. Rothemund, P. W. K., Folding DNA to create nanoscale shapes and patterns. *Nature* **2006,** *440* (7082), 297-302.

40. Andersen, E. S.; Dong, M.; Nielsen, M. M.; Jahn, K.; Lind-Thomsen, A.; Mamdouh, W.; Gothelf, K. V.; Besenbacher, F.; Kjems, J., DNA origami design of dolphin-shaped structures with flexible tails. *ACS nano* **2008,** *2* (6), 1213-1218.

41. Andersen, E. S.; Dong, M.; Nielsen, M. M.; Jahn, K.; Subramani, R.; Mamdouh, W.; Golas, M. M.; Sander, B.; Stark, H.; Oliveira, C. L.; Pedersen, J. S.; Birkedal, V.; Besenbacher, F.; Gothelf, K. V.; Kjems, J., Self-assembly of a nanoscale DNA box with a controllable lid. *Nature* **2009,** *459* (7243), 73-76.

42. Douglas, S. M.; Dietz, H.; Liedl, T.; Hogberg, B.; Graf, F.; Shih, W. M., Self-assembly of DNA into nanoscale three-dimensional shapes. *Nature* **2009,** *459* (7245), 414-418.

43. Han, D. R.; Pal, S.; Nangreave, J.; Deng, Z. T.; Liu, Y.; Yan, H., DNA Origami with Complex Curvatures in Three-Dimensional Space. *Science* **2011,** *332* (6027), 342-346.

44. Wei, B.; Dai, M. J.; Yin, P., Complex Shapes Self-Assembled from Single-Stranded DNA Tiles. *Nature* **2012,** *485* (7400), 623-626.

45. Hawker, C. J.; Wooley, K. L., The convergence of synthetic organic and polymer chemistries. *Science* **2005,** *309* (5738), 1200-1205.

46. Yan, H.; Park, S. H.; Finkelstein, G.; Reif, J. H.; LaBean, T. H., DNA-templated self-assembly of protein arrays and highly conductive nanowires. *Science* **2003,** *301* (5641), 1882-1884.

47. Darling, S. B., Directing the self-assembly of block copolymers. *Progress in Polymer Science* **2007,** *32* (10), 1152-1204.

48. Tang, C.; Lennon, E. M.; Fredrickson, G. H.; Kramer, E. J.; Hawker, C. J., Evolution of block copolymer lithography to highly ordered square arrays. *Science* **2008,** *322* (5900), 429-432.

49. Integrated DNA technologies. http://www.idtdna.com. Accesssed Feb 24, 2018.

50. Seeman, N. C., Nucleic acid junctions and lattices. *Journal of Theoretical Biology* **1982,** *99* (2), 237-247.

51. Seeman, N. C., Nanomaterials Based on DNA. *Annual Review of Biochemistry* **2010,** *79* (1), 65-87.

52. Zhang, F.; Nangreave, J.; Liu, Y.; Yan, H., Structural DNA Nanotechnology: State of the Art and Future Perspective. *Journal of the American Chemical Society* **2014,** *136* (32), 11198-11211.

53. Fu, T.-J.; Tse-Dinh, Y.-C.; Seeman, N. C., Holliday Junction Crossover Topology. *Journal of Molecular Biology* **1994,** *236* (1), 91-105.

54. Ma, R. I.; Kallenbach, N. R.; Sheardy, R. D.; Petrillo, M. L.; Seeman, N. C., Three-arm nucleic acid junctions are flexible. *Nucleic Acids Research* **1986,** *14* (24), 9745-9753.

55. Petrillo, M. L.; Newton, C. J.; Cunningham, R. P.; Ma, R.-I.; Kallenbach, N. R.; Seeman, N. C., The ligation and flexibility of four-arm DNA junctions. *Biopolymers* **1988,** *27* (9), 1337-1352.

56. Fu, T. J.; Seeman, N. C., DNA double-crossover molecules. *Biochemistry* **1993,** *32* (13), 3211-3220.

57. Zhang, S.; Fu, T. J.; Seeman, N. C., Symmetric immobile DNA branched junctions. *Biochemistry* **1993,** *32* (32), 8062-8067.

58. Ding, B. Q.; Sha, R. J.; Seeman, N. C., Pseudohexagonal 2D DNA Crystals from Double Crossover Cohesion. *J. Am. Chem. Soc.* **2004,** *126* (33), 10230-10231.

59. He, Y.; Chen, Y.; Liu, H. P.; Ribbe, A. E.; Mao, C. D., Self-Assembly of Hexagonal DNA Two-Dimensional (2D) Arrays. *Journal of the American Chemical Society* **2005,** *127* (35), 12202-12203.

60. Yan, H.; Park, S. H.; Finkelstein, G.; Reif, J. H.; LaBean, T. H., DNA-Templated Self-Assembly of Protein Arrays and Highly Conductive Nanowires. *Science* **2003,** *301* (5641), 1882-1884.

61. Rothemund, P. W. K.; Ekani-Nkodo, A.; Papadakis, N.; Kumar, A.; Fygenson, D. K.; Winfree, E., Design and Characterization of Programmable DNA Nanotubes. *J. Am. Chem. Soc.* **2004,** *126* (50), 16344-16352.

62. Chen, J.; Seeman, N. C., Synthesis from DNA of a molecule with the connectivity of a cube. *Nature* **1991,** *350*, 631.

63. Zhang, C.; Su, M.; He, Y.; Zhao, X.; Fang, P.-a.; Ribbe, A. E.; Jiang, W.; Mao, C., Conformational flexibility facilitates self-assembly of complex DNA nanostructures. *Proceedings of the National Academy of Sciences of the United States of America* **2008,** *105* (31), 10665-10669.

64. Zheng, J.; Birktoft, J. J.; Chen, Y.; Wang, T.; Sha, R.; Constantinou, P. E.; Ginell, S. L.; Mao, C.; Seeman, N. C., From molecular to macroscopic via the rational design of a self-assembled 3D DNA crystal. *Nature* **2009,** *461*, 74.

65. He, Y.; Ye, T.; Su, M.; Zhang, C.; Ribbe, A. E.; Jiang, W.; Mao, C., Hierarchical self-assembly of DNA into symmetric supramolecular polyhedra. *Nature* **2008,** *452*, 198.

66. Han, D.; Pal, S.; Nangreave, J.; Deng, Z.; Liu, Y.; Yan, H., DNA origami with complex curvatures in three-dimensional space. *Science* **2011,** *332* (6027), 342-346.

67. Douglas, S. M.; Bachelet, I.; Church, G. M., A Logic-Gated Nanorobot for Targeted Transport of Molecular Payloads. *Science* **2012,** *335* (6070), 831-834.

68. Endo, M.; Sugita, T.; Katsuda, Y.; Hidaka, K.; Sugiyama, H., Programmed-Assembly System Using DNA Jigsaw Pieces. *Chemistry – A European Journal* **2010,** *16* (18), 5362-5368.

69. Rajendran, A.; Endo, M.; Katsuda, Y.; Hidaka, K.; Sugiyama, H., Programmed Two-Dimensional Self-Assembly of Multiple DNA Origami Jigsaw Pieces. *ACS Nano* **2011,** *5* (1), 665-671.

70. Woo, S.; Rothemund, P. W. K., Programmable molecular recognition based on the geometry of DNA nanostructures. *Nature Chemistry* **2011,** *3*, 620.

71. Woo, S.; Rothemund, P. W. K., Self-assembly of two-dimensional DNA origami lattices using cation-controlled surface diffusion. *Nature Communications* **2014,** *5*, 4889.

72. Yin, P.; Hariadi, R. F.; Sahu, S.; Choi, H. M. T.; Park, S. H.; LaBean, T. H.; Reif, J. H., Programming DNA Tube Circumferences. *Science* **2008,** *321* (5890), 824-826.

73. Ke, Y. G.; Ong, L. L.; Shih, W. M.; Yin, P., Three-Dimensional Structures Self-Assembled from DNA Bricks. *Science* **2012,** *338* (6111), 1177-1183.

74. Ke, Y.; Ong, L. L.; Sun, W.; Song, J.; Dong, M.; Shih, W. M.; Yin, P., DNA Brick Crystals with Prescribed Depths. *Nat. Chem.* **2014,** *6* (11), 994-1002.

75. Zhang, G.; Surwade, S. P.; Zhou, F.; Liu, H., DNA nanostructure meets nanofabrication. *Chemical Society Reviews* **2013,** *42* (7), 2488-2496.

76. Kim, H.; Surwade, S. P.; Powell, A.; O'Donnell, C.; Liu, H., Stability of DNA Origami Nanostructure under Diverse Chemical Environments. *Chemistry of Materials* **2014,** *26* (18), 5265-5273.

77. Pillers, M. A.; Lieberman, M., Thermal stability of DNA origami on mica. *Journal of Vacuum Science & Technology B, Nanotechnology and Microelectronics: Materials, Processing, Measurement, and Phenomena* **2014,** *32* (4), 040602.

78. Kershner, R. J.; Bozano, L. D.; Micheel, C. M.; Hung, A. M.; Fornof, A. R.; Cha, J. N.; Rettner, C. T.; Bersani, M.; Frommer, J.; Rothemund, P. W. K.; Wallraff, G. M., Placement and Orientation of Individual DNA Shapes on Lithographically Patterned Surfaces. *Nat. Nanotechnol.* **2009,** *4* (9), 557-561.

79. Yun, J. M.; Kim, K. N.; Kim, J. Y.; Shin, D. O.; Lee, W. J.; Lee, S. H.; Lieberman, M.; Kim, S. O., DNA origami nanopatterning on chemically modified graphene. *Angewandte Chemie (International ed.in English)* **2012,** *51* (4), 912.

80. Gopinath, A.; Rothemund, P. W. K., Optimized Assembly and Covalent Coupling of Single-Molecule DNA Origami Nanoarrays. *ACS Nano* **2014,** *8* (12), 12030-12040.

81. Becerril, H. A.; Ludtke, P.; Willardson, B. M.; Woolley, A. T., DNA-Templated Nickel Nanostructures and Protein Assemblies. *Langmuir* **2006,** *22* (24), 10140-10144.

82. Shimada, J.; Maruyama, T.; Kitaoka, M.; Yoshinaga, H.; Nakano, K.; Kamiya, N.; Goto, M., Programmable protein-protein conjugation via DNA-based self-assembly. *Chemical Communications* **2012,** *48* (50), 6226-6228.

83. Rahman, M.; Neff, D.; Norton, M. L., Rapid, high yield, directed addition of quantum dots onto surface bound linear DNA origami arrays. *Chemical Communications* **2014,** *50* (26), 3413-3416.

84. Chen, Y.; Liu, H.; Ye, T.; Kim, J.; Mao, C., DNA-Directed Assembly of Single-Wall Carbon Nanotubes. *Journal of the American Chemical Society* **2007,** *129* (28), 8696-8697.

85. Keren, K.; Berman, R. S.; Buchstab, E.; Sivan, U.; Braun, E., DNA-Templated Carbon Nanotube Field-Effect Transistor. *Science* **2003,** *302* (5649), 1380-1382.

86. Li, S.; He, P.; Dong, J.; Guo, Z.; Dai, L., DNA-Directed Self-Assembling of Carbon Nanotubes. *Journal of the American Chemical Society* **2005,** *127* (1), 14-15.

87. Mangalum, A.; Rahman, M.; Norton, M. L., Site-Specific Immobilization of Single-Walled Carbon Nanotubes onto Single and One-Dimensional DNA Origami. *Journal of the American Chemical Society* **2013,** *135* (7), 2451-2454.

88. Braun, E.; Eichen, Y.; Sivan, U.; Ben-Yoseph, G., DNA-templated assembly and electrode attachment of a conducting silver wire. *Nature* **1998,** *391* (6669), 775-778.

89. Gu, Q.; Cheng, C.; Haynie, D. T., Cobalt metallization of DNA: toward magnetic nanowires. *Nanotechnology* **2005,** *16* (8), 1358.

90. Mertig, M.; Colombi Ciacchi, L.; Seidel, R.; Pompe, W.; De Vita, A., DNA as a Selective Metallization Template. *Nano Lett* **2002,** *2* (8), 841-844.

91. Puchkova, A.; Sokolov, P.; Petrov, Y.; Kasyanenko, N., Metallization of DNA on silicon surface. *J Nanopart Res* **2011,** *13* (9), 3633-3641.

92. Geng, Y.; Liu, J.; Pound, E.; Gyawali, S.; Harb, J. N.; Woolley, A. T., Rapid metallization of lambda DNA and DNA origami using a Pd seeding method. *Journal of Materials Chemistry* **2011,** *21* (32), 12126-12131.

93. Liu, J.; Geng, Y.; Pound, E.; Gyawali, S.; Ashton, J. R.; Hickey, J.; Woolley, A. T.; Harb, J. N., Metallization of branched DNA origami for nanoelectronic circuit fabrication. *ACS Nano* **2011,** *5* (3), 2240-2247.

94. Pilo-Pais, M.; Goldberg, S.; Samano, E.; LaBean, T. H.; Finkelstein, G., Connecting the Nanodots: Programmable Nanofabrication of Fused Metal Shapes on DNA Templates. *Nano Letters* **2011,** *11* (8), 3489-3492.

95. Schreiber, R.; Kempter, S.; Holler, S.; Schuller, V.; Schiffels, D.; Simmel, S. S.; Nickels, P. C.; Liedl, T., DNA origami-templated growth of arbitrarily shaped metal nanoparticles. *Small* **2011,** *7* (13), 1795-1799.

96. Pearson, A. C.; Liu, J.; Pound, E.; Uprety, B.; Woolley, A. T.; Davis, R. C.; Harb, J. N., DNA Origami Metallized Site Specifically to Form Electrically Conductive Nanowires. *The Journal of Physical Chemistry B* **2012,** *116* (35), 10551-10560.

97. Jin, Z.; Sun, W.; Ke, Y.; Shih, C.-J.; Paulus, G. L. C.; Hua Wang, Q.; Mu, B.; Yin, P.; Strano, M. S., Metallized DNA nanolithography for encoding and transferring spatial information for graphene patterning. *Nat Commun* **2013,** *4*, 1663.

98. Sun, W.; Boulais, E.; Hakobyan, Y.; Wang, W. L.; Guan, A.; Bathe, M.; Yin, P., Casting inorganic structures with DNA molds. *Science* **2014,** *346* (6210), 1258361-1-1258361-8.

99. Helmi, S.; Ziegler, C.; Kauert, D. J.; Seidel, R., Shape-Controlled Synthesis of Gold Nanostructures Using DNA Origami Molds. *Nano Letters* **2014,** *14* (11), 6693-6698.

100. Deng, Z. X.; Mao, C. D., Molecular Lithography with DNA Nanostructures. *Angewandte Chemie-International Edition* **2004,** *43* (31), 4068-4070.

101. Becerril, H. A.; Woolley, A. T., DNA Shadow Nanolithography. *Small* **2007,** *3* (9), 1534-1538.

102. Surwade, S. P.; Zhao, S. C.; Liu, H. T., Molecular Lithography Through DNA-Mediated Etching and Masking of SiO2. *Journal of the American Chemical Society* **2011,** *133* (31), 11868-11871.

103. Surwade, S. P.; Zhou, F.; Wei, B.; Sun, W.; Powell, A.; O'Donnell, C.; Yin, P.; Liu, H. T., Nanoscale Growth and Patterning of Inorganic Oxides Using DNA Nanostructure Templates. *Journal of the American Chemical Society* **2013,** *135* (18), 6778-6781.

104. Diagne, C. T.; Brun, C.; Gasparutto, D.; Baillin, X.; Tiron, R., DNA Origami Mask for Sub-Ten-Nanometer Lithography. *ACS Nano* **2016,** *10* (7), 6458-6463.

105. Zhou, F.; Sun, W.; Ricardo, K. B.; Wang, D.; Shen, J.; Yin, P.; Liu, H., Programmably Shaped Carbon Nanostructure from Shape-Conserving Carbonization of DNA. *ACS Nano* **2016,** *10* (3), 3069-3077.

106. Qu, J. H.; Hou, X. L.; Fan, W. C.; Xi, G. H.; Diao, H. Y.; Liu, X. D., Scalable Lithography from Natural DNA Patterns via Polyacrylamide Gel. *Scientific Reports* **2015,** *5*.

107. Howland, R.; Benatar, L. In A Practical Guide to Scanning Probe Microscopy; Symanski, C., Emerson, L., Eds.; Park Scientific Instruments: 1993-1997; pp 5-14.

108. Torre, B.; Ricci, D.; Braga, P. C. How the Atomic Force Microscope Works? In Atomic Force Microscopy in Biomedical Research: Methods and Protocols; Braga, P. C., Ricci, D., Eds.; Methods in Molecular Biology; Springer Science+Business Media: Heidelberg, 2008; Vol. 736, pp 3-18.

109. Xia, Y. N.; Whitesides, G. M., Soft lithography. *Annu. Rev. Mater. Sci.* **1998,** *28*, 153-184.

110. Gates, B. D.; Xu, Q. B.; Stewart, M.; Ryan, D.; Willson, C. G.; Whitesides, G. M., New Approaches to Nanofabrication: Molding, Printing, and Other Techniques. *Chem. Rev.* **2005,** *105* (4), 1171-1196.

111. Rogers, J. A.; Nuzzo, R. G., Recent Progress in Soft Lithography. *Mater. Today* **2005,** *8* (2), 50-56.

112. Qin, D.; Xia, Y.; Whitesides, G. M., Soft Lithography for Micro- and Nanoscale Patterning. *Nat. Protoc.* **2010,** *5* (3), 491-502.

113. Lipomi, D. J.; Martinez, R. V.; Cademartiri, L.; Whitesides, G. M., Soft Lithographic Approaches to Nanofabrication. In *Polymer Science: A Comprehensive Reference*, Matyjaszewski, K.; Möller, M., Eds. Elsevier Science: Oxford, 2012; Vol. 7, pp 211-231.

114. Lipomi, D. J.; Martinez, R. V.; Whitesides, G. M., Use of Thin Sectioning (Nanoskiving) to Fabricate Nanostructures for Electronic and Optical Applications. *Angew. Chem. Int. Edit.* **2011,** *50* (37), 8566-8583.

115. Xia, Y. N.; Rogers, J. A.; Paul, K. E.; Whitesides, G. M., Unconventional Methods for Fabricating and Patterning Nanostructures. *Chem. Rev.* **1999,** *99* (7), 1823-1848.

116. Seeman, N. C., Nanomaterials Based on DNA. In *Annual Review of Biochemistry, Vol 79*, Kornberg, R. D.; Raetz, C. R. H.; Rothman, J. E.; Thorner, J. W., Eds. Annual Reviews: Palo Alto, 2010; Vol. 79, pp 65-87.

117. Lin, C. X.; Liu, Y.; Rinker, S.; Yan, H., DNA tile based self-assembly: Building complex nanoarchitectures. *Chemphyschem* **2006,** *7* (8), 1641-1647.

118. Aldaye, F. A.; Palmer, A. L.; Sleiman, H. F., Assembling Materials with DNA as the Guide. *Science* **2008,** *321* (5897), 1795-1799.

119. Liu, H. P.; Chen, Y.; He, Y.; Ribbe, A. E.; Mao, C. D., Approaching the limit: Can one DNA oligonucleotide assemble into large nanostructures? *Angew. Chem. Int. Edit.* **2006,** *45* (12), 1942-1945.

120. Tian, C.; Zhang, C.; Li, X.; Hao, C.; Ye, S.; Mao, C., Approaching the Limit: Can One DNA Strand Assemble into Defined Nanostructures? *Langmuir* **2014,** *30* (20), 5859-5862.

121. Zhang, F.; Jiang, S. X.; Wu, S. Y.; Li, Y. L.; Mao, C. D.; Liu, Y.; Yan, H., Complex wireframe DNA origami nanostructures with multi-arm junction vertices. *Nature Nanotechnology* **2015,** *10* (9), 779-784.

122. Wang, P.; Wu, S.; Tian, C.; Yu, G.; Jiang, W.; Wang, G.; Mao, C., Retrosynthetic Analysis-Guided Breaking Tile Symmetry for the Assembly of Complex DNA Nanostructures. *J. Am. Chem. Soc.* **2016,** *138* (41), 13579-13585.

123. Li, X.; Zhang, C.; Hao, C. H.; Tian, C.; Wang, G. S.; Mao, C. D., DNA Polyhedra with T-Linkage. *ACS Nano* **2012,** *6* (6), 5138-5142.

124. Tian, C.; Li, X.; Liu, Z. Y.; Jiang, W.; Wang, G. S.; Mao, C. D., Directed Self-Assembly of DNA Tiles into Complex Nanocages. *Angew. Chem. Int. Edit.* **2014,** *53* (31), 8041-8044.

125. Liu, Z.; Tian, C.; Yu, J.; Li, Y.; Jiang, W.; Mao, C., Self-Assembly of Responsive Multilayered DNA Nanocages. *J. Am. Chem. Soc.* **2015,** *137* (5), 1730-1733.

126. Li, Y.; Tian, C.; Liu, Z.; Jiang, W.; Mao, C., Structural Transformation: Assembly of an Otherwise Inaccessible DNA Nanocage. *Angew. Chem. Int. Edit.* **2015,** *54* (20), 5990-5993.

127. Braun, E.; Eichen, Y.; Sivan, U.; Ben-Yoseph, G., DNA-templated assembly and electrode attachment of a conducting silver wire. *Nature* **1998,** *391* (6669), 775-778.

128. Liu, J.; Geng, Y.; Pound, E.; Gyawali, S.; Ashton, J. R.; Hickey, J.; Woolley, A. T.; Harb, J. N., Metallization of Branched DNA Origami for Nanoelectronic Circuit Fabrication. *ACS Nano* **2011,** *5* (3), 2240-2247.

129. Uprety, B.; Gates, E. P.; Geng, Y.; Woolley, A. T.; Harb, J. N., Site-Specific Metallization of Multiple Metals on a Single DNA Origami Template. *Langmuir* **2014,** *30* (4), 1134-1141.

130. Uprety, B.; Westover, T.; Stoddard, M.; Brinkerhoff, K.; Jensen, J.; Davis, R. C.; Woolley, A. T.; Harb, J. N., Anisotropic Electroless Deposition on DNA Origami Templates To Form Small Diameter Conductive Nanowires. *Langmuir* **2017,** *33* (3), 726-735.

131. Jin, Z.; Sun, W.; Ke, Y.; Shih, C. J.; Paulus, G. L. C.; Wang, Q. H.; Mu, B.; Yin, P.; Strano, M. S., Metallized DNA Nanolithography for Encoding and Transferring Spatial Information for Graphene Patterning. *Nature Communications* **2013,** *4*, 1663.

132. Pinheiro, A. V.; Han, D. R.; Shih, W. M.; Yan, H., Challenges and opportunities for structural DNA nanotechnology. *Nat. Nanotechnol.* **2011,** *6* (12), 763-772.

133. Hung, A. M.; Micheel, C. M.; Bozano, L. D.; Osterbur, L. W.; Wallraff, G. M.; Cha, J. N., Large-Area Spatially Ordered Arrays of Gold Nanoparticles Directed by Lithographically Confined DNA Origami. *Nat. Nanotechnol.* **2010,** *5* (2), 121-126.

134. Gopinath, A.; Miyazono, E.; Faraon, A.; Rothemund, P. W. K., Engineering and mapping nanocavity emission via precision placement of DNA origami. *Nature* **2016,** *535* (7612), 401-405.

135. Sun, X. P.; Ko, S. H.; Zhang, C. A.; Ribbe, A. E.; Mao, C. D., Surface-Mediated DNA Self-Assembly. *J. Am. Chem. Soc.* **2009,** *131* (37), 13248-13249.

136. Lee, J.; Kim, S.; Kim, J.; Lee, C. W.; Roh, Y.; Park, S. H., Coverage Control of DNA Crystals Grown by Silica Assistance. *Angew. Chem. Int. Edit.* **2011,** *50* (39), 9145-9149.

137. Li, H.; Wu, J.; Huang, X.; Yin, Z.; Liu, J.; Zhang, H., A Universal, Rapid Method for Clean Transfer of Nanostructures onto Various Substrates. *ACS Nano* **2014,** *8* (7), 6563-6570.

138. Schneider, C. A.; Rasband, W. S.; Eliceiri, K. W., NIH Image to ImageJ: 25 Years of Image Analysis. *Nat. Methods* **2012,** *9* (7), 671-675.

139. Kim, H.; Surwade, S. P.; Powell, A.; O'Donnell, C.; Liu, H., Stability of DNA Origami Nanostructure Under Diverse Chemical Environments. *Chemistry of Materials* **2014,** *26* (18), 5265-5273.

140. Li, H. F.; Lin, J. M.; Su, R. G.; Cai, Z. W.; Uchiyama, K., A polymeric master replication technology for mass fabrication of poly(dimethylsiloxane) microfluidic devices. *Electrophoresis* **2005,** *26* (9), 1825-1833.

141. Martínez, E.; Pla-Roca, M.; Samitier, J., Micro/Nanopatterning of Proteins Using a Nanoimprint-Based Contact Printing Technique. In *Nanotechnology in Regenerative Medicine: Methods and Protocols*, Navarro, M.; Planell, J. A., Eds. Humana Press: Totowa, NJ, 2012; pp 79-87.

142. Gates, B. D.; Whitesides, G. M., Replication of vertical features smaller than 2 nm by soft lithography. *J. Am. Chem. Soc.* **2003,** *125* (49), 14986-14987.

143. Muhlberger, M.; Rohn, M.; Danzberger, J.; Sonntag, E.; Rank, A.; Schumm, L.; Kirchner, R.; Forsich, C.; Gorb, S.; Einwogerer, B.; Trappl, E.; Heim, D.; Schift, H.; Bergmair, I., UV-NIL fabricated bio-inspired inlays for injection molding to influence the friction behavior of ceramic surfaces. *Microelectron. Eng.* **2015,** *141*, 140-144.

144. Xia, Y. N.; McClelland, J. J.; Gupta, R.; Qin, D.; Zhao, X. M.; Sohn, L. L.; Celotta, R. J.; Whitesides, G. M., Replica molding using polymeric materials: A practical step toward nanomanufacturing. *Adv. Mater.* **1997,** *9* (2), 147-149.

145. Zhang, Y.; Lo, C. W.; Taylor, J. A.; Yang, S., Replica molding of high-aspect-ratio polymeric nanopillar arrays with high fidelity. *Langmuir* **2006,** *22* (20), 8595-8601.

146. Gilles, S.; Meier, M.; Prompers, M.; van der Hart, A.; Kugeler, C.; Offenhausser, A.; Mayer, D., UV nanoimprint lithography with rigid polymer molds. *Microelectron. Eng.* **2009,** *86* (4-6), 661-664.

147. Pla-Roca, M.; Fernandez, J. G.; Mills, C. A.; Martinez, E.; Samitier, J., Micro/nanopatterning of proteins via contact printing using high aspect ratio PMMA stamps and NanoImprint apparatus. *Langmuir* **2007,** *23* (16), 8614-8618.

148. Li, H. W.; Muir, B. V. O.; Fichet, G.; Huck, W. T. S., Nanocontact printing: A route to sub-50-nm-scale chemical and biological patterning. *Langmuir* **2003,** *19* (6), 1963-1965.

149. Wieland, M. J.; de Boer, G.; ten Berge, G. F.; van Kervinck, M.; Jager, R.; Peijster, J. J. M.; Slot, E.; Steenbrink, S.; Teepen, T. F.; Kampherbeek, B. J., MAPPER: High throughput maskless lithography. *Proc. SPIE* **2010,** *7637*.

150. Lin, B. J., Future of Multiple-E-Beam Direct-Write Systems. *Proc. SPIE* **2012,** *8323*.

151. Chandrasekaran, A. R.; Levchenko, O., DNA Nanocages. *Chemistry of Materials* **2016,** *28* (16), 5569-5581.

152. Totzeck, M.; Ulrich, W.; Gohnermeier, A.; Kaiser, W., Semiconductor fabrication: Pushing deep ultraviolet lithography to its limits. *Nat Photon* **2007,** *1* (11), 629-631.

153. Pease, R. F.; Chou, S. Y., Lithography and Other Patterning Techniques for Future Electronics. *Proceedings of the IEEE* **2008,** *96* (2), 248-270.

154. Tian, C.; Kim, H.; Sun, W.; Kim, Y.; Yin, P.; Liu, H., DNA Nanostructures-Mediated Molecular Imprinting Lithography. *ACS Nano* **2017,** *11* (1), 227-238.

155. Bonnet, J.; Colotte, M.; Coudy, D.; Couallier, V.; Portier, J.; Morin, B.; Tuffet, S., Chain and conformation stability of solid-state DNA: implications for room temperature storage. *Nucleic Acids Research* **2010,** *38* (5), 1531-1546.

156. Colotte, M.; Coudy, D.; Tuffet, S.; Bonnet, J., Adverse effect of air exposure on the stability of DNA stored at room temperature. *Biopreservation and biobanking* **2011,** *9* (1), 47-50.

157. Elam, J. W.; Sechrist, Z. A.; George, S. M., ZnO/Al2O3 nanolaminates fabricated by atomic layer deposition: growth and surface roughness measurements. *Thin Solid Films* **2002,** *414* (1), 43-55.

158. Tian, C.; Cordeiro, M. A. L.; Lhermitte, J.; Xin, H. L.; Shani, L.; Liu, M.; Ma, C.; Yeshurun, Y.; DiMarzio, D.; Gang, O., Supra-Nanoparticle Functional Assemblies through Programmable Stacking. *ACS Nano* **2017,** *11* (7), 7036-7048.

159. Stoffels, W. W.; Stoffels, E.; Tachibana, K., Polymerization of fluorocarbons in reactive ion etching plasmas. *Journal of Vacuum Science & Technology A: Vacuum, Surfaces, and Films* **1998,** *16* (1), 87-95.

160. Cunge, G.; Booth, J. P., CF2 production and loss mechanisms in fluorocarbon discharges: Fluorine-poor conditions and polymerization. *Journal of Applied Physics* **1999,** *85* (8), 3952-3959.

161. Chou, S. Y.; Krauss, P. R.; Renstrom, P. J., Imprint of sub-25 nm vias and trenches in polymers. *Applied Physics Letters* **1995,** *67* (21), 3114-3116.

162. Magin, C. M.; Cooper, S. P.; Brennan, A. B., Non-toxic antifouling strategies. *Materials Today* **2010,** *13* (4), 36-44.

163. Bixler, G. D.; Bhushan, B., Rice- and butterfly-wing effect inspired self-cleaning and low drag micro/nanopatterned surfaces in water, oil, and air flow. *Nanoscale* **2014,** *6* (1), 76-96.

164. Kim, H.; Arbutina, K.; Xu, A.; Liu, H. Beilstein J. Nanotechnol. **2017,** 8, 2363–2375. doi:10.3762/bjnano.8.236